UNIVERSITÄTSKLINIKUM HAMBURG-EPPENDORF

Klinik und Poliklinik für Diagnostische und Interventionelle Radiologie und Nuklearmedizin

Direktor: Prof. Dr. med. Gerhard Adam

Application of cardiac magnetic resonance imaging: the value in assessment of cardiac function, myocardial deformation, and tissue characterization

Dissertation

zur Erlangung des Doktorgrades PhD
an der Medizinischen Fakultät der Universität Hamburg

vorgelegt von:

Hang Chen
aus Sichuan, China

Hamburg 2023

(wird von der Medizinischen Fakultät ausgefüllt)

Angenommen von der
Medizinischen Fakultät der Universität Hamburg am: 12.09.2023

Veröffentlicht mit Genehmigung der
Medizinischen Fakultät der Universität Hamburg.

Prüfungsausschuss, der/die Vorsitzende: **PD Dr. Enver Tahir**

Prüfungsausschuss, zweite/r Gutachter/in: **PD Dr. Fabian Flottmann**

Drittgutachter: **PD Dr. Julian A. Luetkens**

Table of Contents

1 Chapter 1: Introduction

1.1 Basic principles magnetic resonance imaging

1.1.1 Magnetic properties of hydrogen nuclei

Magnetic resonance imaging (MRI) is grounded on the magnetic properties of hydrogen nuclei (protons). One magnetic property of hydrogen proton is positively charged and spins about its axis, thus spinning protons act like tiny magnets (Pooley, 2005). All of these tiny magnets form the net (macroscopic) magnetization. Normally, magnetic moments cancel with each other due to the random distribution of these tiny magnets, results in a null net magnetic vector (van Geuns *et al.*, 1999). However when placed in a strong external magnetic field (B_0), spinning protons wobble around the axis of external field like spinning-tops in a parallel or antiparallel direction, this motion is called precession. The frequency of precession is determined by the Larmor equation (van Geuns *et al*., 1999):

$$\omega_0 = \gamma \cdot B_0$$

where ω_0 is the precessional frequency (also called Larmor frequency), B_0 is the strength of the external magnetic field, and γ is the gyromagnetic ratio of the nucleus.

1.1.2 Nuclear magnetic resonance phenomenon

The net magnetic vector of spinning protons is decomposed into two orthogonal components: the transverse magnetic vector (M_{xy}) and the longitudinal magnetic vector (M_z). Due to the different phase of the precession for each individual proton, the transverse magnetic vector of protons cancel each other, and thus net magnetic field is generated from longitudinal magnetization. The longitudinal magnetization within the external field is determined by the proportion of the parallel and antiparallel protons. Since parallel alignment is the lower energy state than that in antiparallel alignment, a

few more spinning protons parallelly wobble around the B_0, which leads to the net magnetic field parallel to the main field B_0 (van Geuns *et al.*, 1999).

The protons within the main magnetic field reemit the absorbed energy in the form of radio signals after stimulated by a radiofrequency (RF) pulse at Larmor frequency, this phenomenon is referred to as nuclear magnetic resonance (NMR) (Pykett *et al*., 1982). To obtain the signals from the spins, the spin equilibrium needs to be altered through excited by RF pulse at resonance frequency. The net magnetization rotates away from the longitudinal direction to transverse plane as energy is absorbed from the RF pulse, the flip angle depends on the strength and duration of the RF pulse (Pooley, 2005). Applying a 90° RF pulse will rotate the longitudinal magnetization into the transverse plane and null longitudinal magnetization, whereas a 180° RF pulse will rotate the longitudinal magnetization over to the opposite direction.

1.1.3 T1 and T2 relaxation time

Relaxation refers to the process of net magnetization returning to equilibrium (from high energy to low energy) after the RF pulse is switched off. During this process, the transverse magnetization begins to decay, and the previously absorbed energy has to be released to the environment at the meantime, thus generating a free-induction decay (FID) signal (Pykett *et al.*, 1982, van Geuns *et al.*, 1999). Relaxation has two mechanisms including longitudinal (spin-lattice) relaxation and transverse (spin-spin) relaxation, the former involves the energy interaction between the spins and surrounding lattice and the latter results from spins getting out of phase with each other (Dixon and Ekstrand, 1982). Longitudinal relaxation refers to longitudinal magnetization recovery and transverse relaxation corresponds to transverse magnetization decay. Bloch proposed two relaxation time constants known as the longitudinal relaxation time (T1) and the transverse relaxation time (T2) (Bloch, 1946). T1 is defined as the time required for longitudinal magnetization to recover to 63% of its final value, and T2 represents the time required for transverse magnetization to decay down to 37% of its original value.

1.1.4 Spatial encoding

To reconstruct images from signals, spatial information needs to be added to the NMR signal, allowing the signals from tissue in one location to be differentiated from those in another location. This spatial encoding is achieved through the application of slice-encoding (selection), phase-encoding, and frequency-encoding gradient magnetic fields. Although these gradients produce similar effects but used for different purposes (Paschal and Morris, 2004).

Slice selection is achieved through gradient magnetic fields (G) applied perpendicular to the target slice plane. G can mildly distort the main magnetic field B_0 in a predictable pattern, causing tissue signals to have frequencies that vary linearly as a function of position (Paschal and Morris, 2004), according to the following Larmor equation:

$$\omega_p = \gamma \cdot (B_0 + G \cdot p)$$

where B_0 is the strength of the main magnetic field, γ is the gyromagnetic ratio of the nucleus, and G is the gradient magnetic field applied along the position axis (p). The selective RF pulse will only excite the spins in the desired slice, where the adapted frequency of RF pulse matches the local Larmor frequency, spins outside the desired slice do not resonate and emit signal (van Geuns *et al.*, 1999).

The frequency and phase encoding are used to specify position within the selective slice. A phase-encoding gradient is used to change the frequency of precession. These protons will return to the original frequency but accumulate a permanent phase shift after the gradient field is switched off. For encoding with linear gradients only, the accumulative phase shift (Φ), at location (x) and time (t) can be written according to the following formula of the gradient history (Gallichan *et al.*, 2011):

$$\Phi\,(x,t) = \gamma \int_0^t x \cdot G(t')dt'$$

where G is the linear gradient field applied to phase encoding at time t. By applying phase-encoding gradients with different strengths, different phase shifts are produced

each time. The amplitude plotted against each phase shift results in a phase-shift curve that corresponds to a specific frequency. Fourier transform will be applied to separate out the frequencies, which enables the acquisition of phase-encoding information.

The last step of spatial encoding involves the application of a frequency-encoding gradient to differentiate pixels with the same phase encoding. The basic principle is similar to slice selection (van Geuns *et al*., 1999). After obtaining all the spatial information, the processor fills in the corresponding k-space.

1.1.5 Pulse sequences

The essential components for pulse sequences are RF excitation pulse and gradients for spatial encoding (2D or 3D) (Brown and Semelka, 1999). The spin-echo (SE) and gradient-echo (GRE) are two fundamental types of pulse sequences, all other variations have been developed based on these two sequences with adding different parameters to accelerate image acquisition (Bitar *et al*., 2006).

1) Spin-echo pulse sequence

The simplest form of SE pulse sequence consists of 90° pulse, 180° rephasing pulse and signal reading. A SE sequence has two key parameters, namely the echo time (TE) and the repetition time (TR), which are essential to control image contrast. The time between the middle of the first RF pulse and the peak of the echo detected is called TE, and TR is the time between the application of an RF excitation pulse and the start of the next RF pulse (Brown and Semelka, 1999). In SE sequence, a 90° pulse flips the longitudinal magnetization vector into the transverse plane and results in a signal, but which will rapidly dephase due to local magnetic field inhomogeneities (T2* effects). A 180° pulse is applied at TE/2 to compensate for field inhomogeneities and rephase these spins whose phases have been scattered, then forming an echo at TE (Bitar *et al*., 2006, Pooley, 2005).

2) Inversion-recovery sequence

The inversion recovery (IR) sequence is a conventional SE sequence preceded by a 180° preparatory pulse, which is used to flip longitudinal magnetization vector in the

opposite direction. It is useful for nulling the unwanted signal from a particular tissue (e.g., water and fat) (Bitar *et al*., 2006). In detail, after initial inversion of the longitudinal magnetization, the spins begin to relax and the suppressed signal pass through the null point, a 90° pulse is applied to flip all other signals into the transverse plane for image formation as previous conventional SE sequence (Pooley, 2005). The time between the 180° preparatory pulse and the following 90° pulse is called the inversion time (TI) (Bydder and Young, 1985).

3) Gradient-echo pulse sequence

The GRE pulse sequence is based on only a single RF pulse, typically below 90°, in conjunction with readout gradient reversal. In GRE sequence, a flip angle less than 90° pulse partly flips the longitudinal magnetization vector into the transverse plane, a readout gradient is required to dephase and rephase transverse magnetization and then form an echo (Bitar *et al.*, 2006). As a result, TE is generally shorter for GRE sequence than for SE sequence (Markl and Leupold, 2012). Additionally, the smaller flip angle and the absence of rephasing 180° pulse allow the TR to be much shorter (Pooley, 2005). The combination of shorter TE and TR allows a very fast imaging acquisition, thus numerous GRE-based variants are applied in the clinical setting especially in cardiac MRI (Waterton *et al.*, 1985) and MR angiography (Dumoulin and Hart, 1986).

MRI techniques and systems have evolved dramatically over recent years overcoming many engineering, physical, and technical issues, which has become a widely used clinical imaging modality. Increased temporal resolution has been enabling the development of applications in the field of cardiovascular disease, including the creation of cardiac magnetic resonance (CMR) imaging.

1.2 Cardiac magnetic resonance imaging

Despite facing with numerous challenges posed by mobile structures, CMR imaging has been recognized as the gold standard for assessing the heart due to its high reproducibility and spatial resolution (Salerno *et al.*, 2017). With the ongoing

improvements of advanced techniques, CMR imaging has been facilitating a wide range of cardiac applications in research and clinical practice (see Table 1).

Table 1. Main applications of cardiac magnetic resonance imaging.

Applications	**Sequences**
Cardiac anatomy and morphology	Black-blood imaging and bright-blood static imaging
Cardiac function	Bright blood cine imaging
Flow	Phase-contrast, Q-flow, 4D flow
Myocardial perfusion	First-pass perfusion (rest and stress)
Myocardial viability	Late gadolinium enhancement imaging
Myocardial tissue quantification	T1 mapping, T2 mapping, and T2*mapping

1.2.1 Electrocardiographic gating

To acquire acceptable heart images, signal acquisition is required to be unaffected by the rapid and complex motion of the heart and cardiovascular normal contractility. Thereof the image acquisition needs to be synchronized with the phasic motion of the heart and rely on accurate detection of the R-wave, also known as electrocardiographic (ECG) gating (Chia *et al*., 2000). This can be achieved in two methods including prospective and retrospective gating.

Prospective gating involves initiating image acquisition using R-wave triggering (Ginat *et al.*, 2011). This method requires only the necessary data to be collected but is susceptible to the influence of heart rate and artifacts (Scott *et al*., 2009). Retrospective gating involves continuous image acquisition throughout the cardiac cycle, followed by post-processing of selected data according to the phase of cardiac cycle. Thus it is more time-consuming but not sensitive to heart rate (Ginat *et al*., 2011). Since the data can be acquired throughout the entire cardiac cycle, retrospective gating is typically used for cine sequences (Scott *et al.*, 2009).

1.2.2 Black-blood imaging

Black-blood imaging allows fast-flowing blood through the image slice to appear as low signal, while the myocardium appears as a relatively higher signal. This facilitates the observation of the anatomical structures (*e.g.*, large vessels of the heart, normal or diseased myocardium, pericardium, and pericardial cavity). The SE pulse sequences are conventionally used to generate black-blood imaging, consisting of the 90° and 180° pulses (Ginat *et al*., 2011). The 90° pulse excites all the tissue within the slice, but the signal is only generated when the same tissue and blood receive the 180° refocusing pulse. The tissue within the slice can receive the 180° pulse and generate a spin signal, while fast-flowing blood experiences the 90° pulse but misses the 180° rephasing pulse, resulting in signal loss due to the flow void effect (Ridgway, 2010). However, the application of the flow void effect alone cannot completely guarantee the black-blood appearance, the dual-inversion black-blood preparation pulse scheme using two 180° inversion pulses to null signal from flowing blood is applied to achieve consistent imaging (Edelman *et al.*, 1991). The first non-selective inversion 180° pulse inverts the magnetization of all tissue, the second slice-selective inversion 180° pulse restores the magnetization of the tissue within the intended image slices. The net effect of these two pulses is to invert the longitudinal magnetization vector of all tissue outside the selective slices (Ridgway, 2010). After the inversion delay, the signal is collected when the longitudinal magnetization of the inverted blood outside the slice recovers towards zero. The non-inverted blood within the slice also cannot generate signal due to the flow void effect at the same time. An additional selective pulse can be added in the interval between the dual-inversion preparation and SE readout to suppress the signal from fat.

1.2.3 Cine imaging

The cine imaging is conventionally used to quantify morphological and functional indices. Cine acquisition is performed at multiple time points within each cardiac cycle, requiring a very short TR as imaging data needs to be acquired at each time point. Therefore, cine imaging normally applied in clinical practice is based on GRE pulse sequences. There are basically two types of GRE pulse sequences including spoiled

and steady state sequences. One type of steady state sequences is fully refocused steady state sequence, also called as balanced-steady state-free precession (bSSFP) sequence, since gradients applied in all three axes (slice-selection, phase-encoding, and readout) are balanced (Chavhan *et al*., 2008). Key characteristics of the spoiled and bSSFP GRE sequences are summarized in Table 2.

Table 2. Key characteristics between the spoiled and bSSFP GRE sequences.
This table was adapted from John P Ridgway (Ridgway, 2010).

Characteristics	**Spoiled GRE**	**bSSFP GRE**
Flip angle (excitation pulse)	Variable 5°-40°	Variable 50°-70°
180° refocusing pulse	No	No
Contrast weighting	T1, T2*	T2/T1 ratio
Short repetition time (T1-weighting)	3-400 ms (depends on flip angle)	3-5 ms
Short echo time (minimize T2 or T2* weighting)	1-3 ms	1-3 ms
Long echo time (for T2 or T2* weighting)	7-15 ms	Not applicable
Long repetition time (minimize T1 weighting)	100 ms - (depends on flip angle)	Not applicable
Shortest practical TR	2-5 ms	2-5 ms
Intra-voxel signal loss (susceptibility, iron)	Yes	Yes
Signal from blood flowing through the slice	Bright (inflow enhancement)	Bright (intrinsic T2/T1 contrast)
Cardiac applications	Function, contrast-enhanced MR angiography, qualitative flow assessment (jets, regurgitation), T2*-weighted imaging for iron loading	Function, volumetric measurements
Vendor-specific names • Siemens • Philips • GE	 TFL: Turbo FLASH T1-TFE: T1-weighted Turbo Field Echo FSPGR: Fast Spoiled GRASS	 True FISP BTFE: Balanced Turbo Field Echo FIESTA: Fast Imaging Employing Steady sTate Acquisition

The GRE sequences typically require a very short TR, usually shorter than the T2 relaxation times of the blood or myocardium. Hence there is not enough time for the transverse magnetization to decay completely before the next RF pulse excitation, leading to a residual portion of the transverse magnetization vector at the end of each TR that can affect the next RF excitation (Chavhan *et al*., 2008). With bSSFP sequence, the residual transverse magnetization vector is refocused and aligns over several TR periods to converge towards a dynamic equilibrium (steady state), generating an intensive signal detected by the receiver coil (often stronger than with spoiled GRE sequence), but this can cause the banding artifacts characterized by strong signal drops due to field inhomogeneity (Scheffler and Lehnhardt, 2003). This dynamic equilibrium in bSSFP means that the use of balanced (symmetrical) gradient fields applied in all three gradient axes within TR (Figure 1). Because gradient-induced dephasing within the TR interval is exactly zero, the signal is at the center of the TR interval, making bSSFP relatively insensitive to motion (Chavhan *et al.*, 2008).

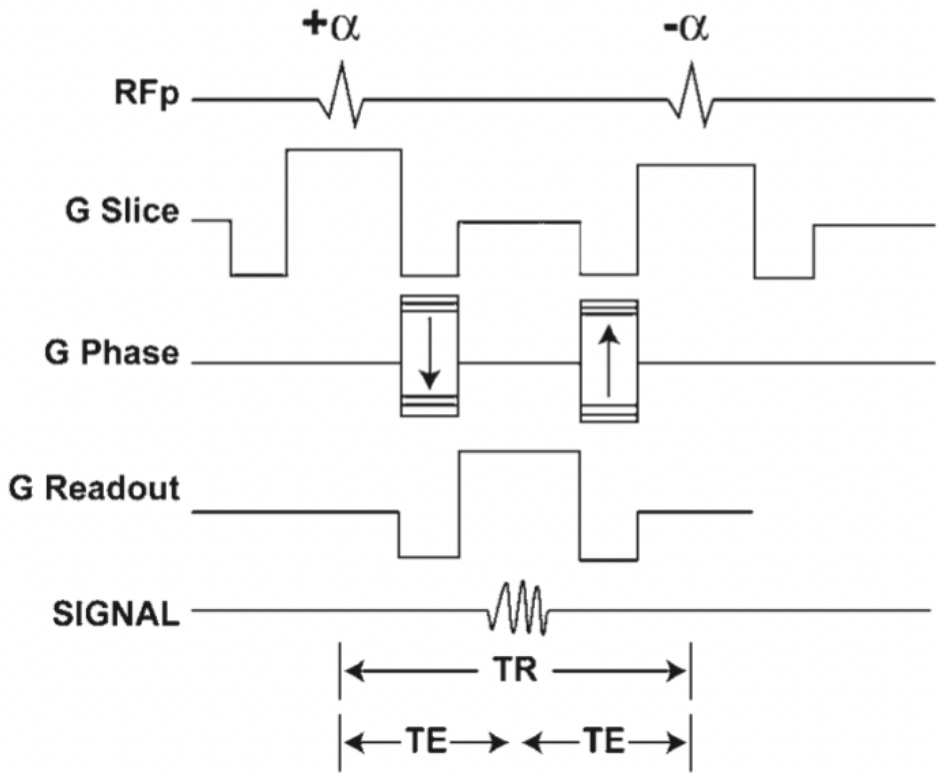

Figure 1. Balanced steady state free precession sequence.
α = flip angle, G = gradient, TE = echo time, TR = repetition time, RFp = radiofrequency pulse. This figure was adapted from Govind B. Chavhan (Chavhan et al., 2008).

Contrast in bSSFP is dependent on the T2/T1 ratio. The especially high contrast between the transient signal of inflowing blood and the steady-state signal of the myocardium, which is low due to a low T2/T1 ratio, makes bSSFP particularly useful for cardiac imaging (Scheffler and Lehnhardt, 2003).

1.2.4 Feature-tracking

In routine clinical practice, traditional indices including left ventricular (LV) ejection fraction (EF) cannot evaluate regional contractility and lack sensitivity to detect subtle alterations of cardiac function (Kalam *et al.*, 2014).

The novel feature-tracking (FT) technique allows the quantification of myocardial strain through a block-matching approach that identifies anatomical features on cine images tracking myocardial boundaries. Myocardial strain (ε_L) is a sensitive measurement of myocardial deformation and defined as the change in fiber length relative to a reference state (Taylor *et al.*, 2015):

$$\varepsilon_L = \frac{dL}{L_0}$$

where dL is the change in fiber length, L_0 is typically the fiber length at end-diastole.

LV myocardial strain is a multidimensional tensor and consists of three components (longitudinal, radial, and circumferential directions) when it is projected into an LV-centered cylinder system (Taylor *et al*., 2015) (Figure 2). Long-axis cine images are tracked to derive longitudinal strain, while short-axis cine images are evaluated to derive circumferential and radial strain. Systolic global longitudinal strain (GLS) represents the motion of the LV base toward the apex and global circumferential strain (GCS) reflects “hoop” shortening (Chitiboi and Axel, 2017). Systolic global radial stain (GRS) is primarily associated with wall thickening and regarded as the greatest principal stretch in all three directions (Young *et al.*, 1994). By convention, systolic longitudinal strain and circumferential strain are negative. Thus, fewer negative values indicate decreased wall contractility. Systolic radial strain on the contrary has positive values.

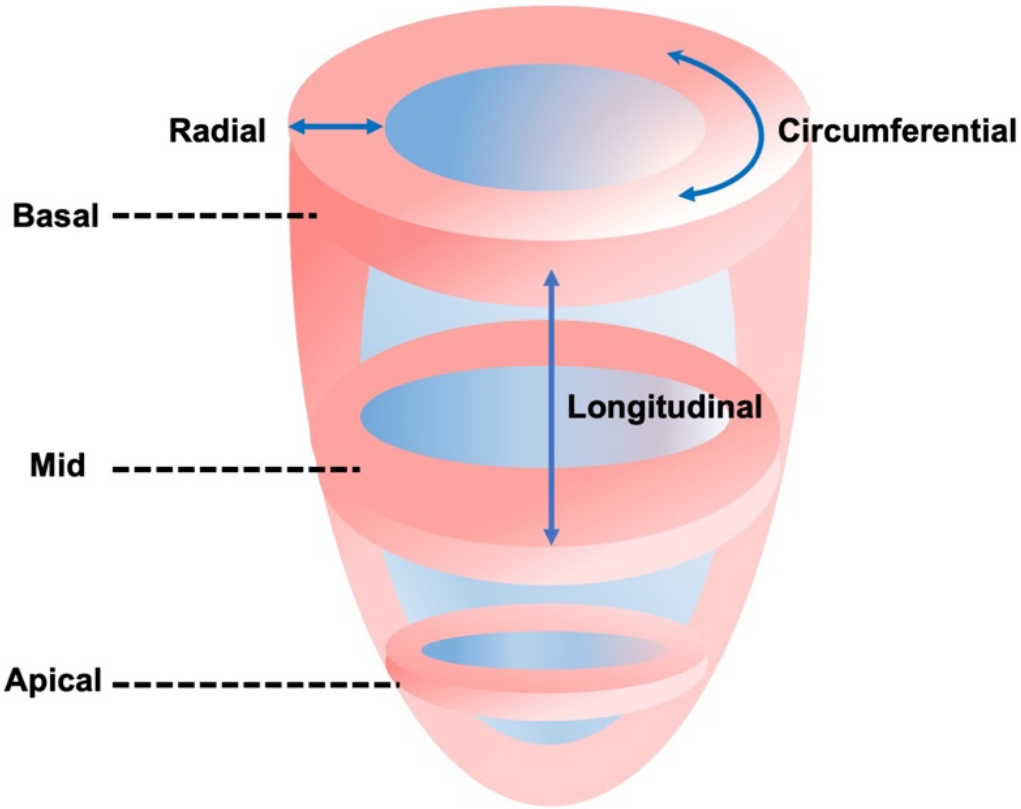

Figure 2. Schematic of left ventricular myocardial strain.
The basal slice is located at a distance equivalent to the systolic excursion of the mitral annular plane from the atrioventricular annulus at end-diastole. The mid slice is located at the mid-cavity at end-diastole. The apical slice is located at the midpoint between the apical tip and the mid-cavity at end-diastole. This figure was adapted from Teodora Chitiboi (Chitiboi et al., 2017).

Long-axis 4-chamber and short-axis cine images are used to calculate right ventricular (RV) longitudinal and circumferential strain (Lam *et al.*, 2021), endocardial RV contours are traced in the long-axis 4-chamber cine view to derive free wall (FW) longitudinal strain (Romano *et al.*, 2021). For atrial strain measurement, left atrial (LA) longitudinal strain is measured in 2- and 4- chamber views excluding the appendage and pulmonary veins (Leng *et al.*, 2018), and the right atrial (RA) longitudinal strain is measured tracking the endocardium in the 4-chamber cine view.

1.2.5 First-pass perfusion

Myocardial perfusion imaging is often referred by the first-pass perfusion, which represents the phase of contrast enhancement most sensitive to changes in blood flow (Jerosch-Herold, 2010). This technique is predominantly based on T1-weighted imaging after injection of a bolus of gadolinium-based contrast agent (GBCA) to observe the contrast agent through the cardiac chambers and myocardium, and is generally acquired at rest and stress. The basic requirements of a first-pass myocardial perfusion imaging pulse sequence are strong T1 contrast, coverage of relevant myocardial segments and adequate spatial resolution (Gerber *et al*., 2008). To achieve high temporal resolution, perfusion imaging requires an ultra-fast acquisition usually based on spoiled GRE, gradient echo-planar-imaging (EPI) or bSSFP sequences. Spoiled GRE sequence is the slowest but least susceptible to artifacts from off-resonance shifts (*i.e.* field inhomogeneities). In addition, although bSSFP sequence has a higher signal-to-noise ratio than spoiled GRE sequence, it is currently not ideal for perfusion imaging at 3 Tesla or higher field strengths due to the potential for image artifacts. GRE-EPI is mostly used in a hybrid form, where the echo-train length is limited to approximately 3-6 echoes, depending on the field strength and T2* (Jerosch-Herold, 2010).

Perfusion imaging relies on the relationship between signal intensity and contrast concentration, which can be analyzed through quantitative, semiquantitative, or qualitative observation for the signal intensity changes of the contrast agent bolus to pass through the myocardium. Normally, first-pass perfusion scan is followed by a late gadolinium enhancement (LGE) imaging with IR gradient pulse sequences 10-15 minutes after injection of contrast agent (Hendel *et al.*, 2016). The time between first-pass perfusion and LGE imaging can be utilized to acquire functional cine imaging (Gerber *et al*., 2008).

1.2.6 Late gadolinium enhancement

LGE imaging provides excellent depiction of acute myocardial injury and chronic myocardial scar (Kim *et al*., 1999), and is also commonly used to noninvasively

visualize and quantify focal areas of dense extracellular matrix deposition regarded as replacement fibrosis (Ambale-Venkatesh and Lima, 2015).

1) Fundamental principles of LGE

LGE imaging usually requires the intravenous bolus administration of GBCAs which is routinely applied in the MRI examination setting based on the strong T1 shortening effect and tissue dependent distribution (Holtackers *et al*., 2022). After the administration of GBCAs, gadolinium-ion bonded to a chelating agent that plays the role as a carrier to transport molecule and govern gadolinium distribution within the body, gadolinium spreads through the extracellular matrix, but does not infiltrate the myocytes (Judd *et al*., 1995). However, in the event of rupture of cell membrane due to necrosis, GBCAs enter the extracellular space and previously intact intracellular space (Kellman and Arai, 2012), which will affect contrast agent wash-in and wash-out kinetics within the infarcted area compared to normal myocardium. GBCAs need longer time to diffuse in and out of isolated breaks in the cellular membrane (Kim *et al.*, 1999). For chronic myocardial scar, the extracellular space is substantially increased because of replacement by a matrix of collagen. Due to the excessive deposition of collagenous tissue and the lack of vascularity, GBCAs penetrate scar at a much slower rate or even fail to penetrate at all, and scar will have retained more contrast. As a result, GBCAs generally take a longer time to wash-in and wash-out of the infarcted myocardium or scar than normal myocardium (Kellman and Arai, 2012). The difference in contrast deposition at the 10-15-minute time point, allowing the delayed enhancement.

There is a linear relationship between the relaxation rate of longitudinal magnetization and the change in contrast agent concentration ($[\mathrm{Gd}]$) can explain the reason for abnormal myocardial representing delayed enhancement (Kellman and Arai, 2012). The formula is as follows:

$$\Delta R1 = R1_{post} - R1_{pre} = \gamma[\mathrm{Gd}]$$

where $R1$ is the relaxation rate of longitudinal magnetization ($R1 = 1/\mathrm{T1}$), and γ = 4.5 $L\,mmol^{-1}s^{-1}$. Regions with a greater extracellular space or infarct have a higher concentration of contrast agent at steady state and suffer greater T1-shortening.

Accordingly, these regions appear brighter on T1-weighted images (Kellman and Arai, 2012). Figure 3 shows the illustration of first-pass perfusion and LGE imaging.

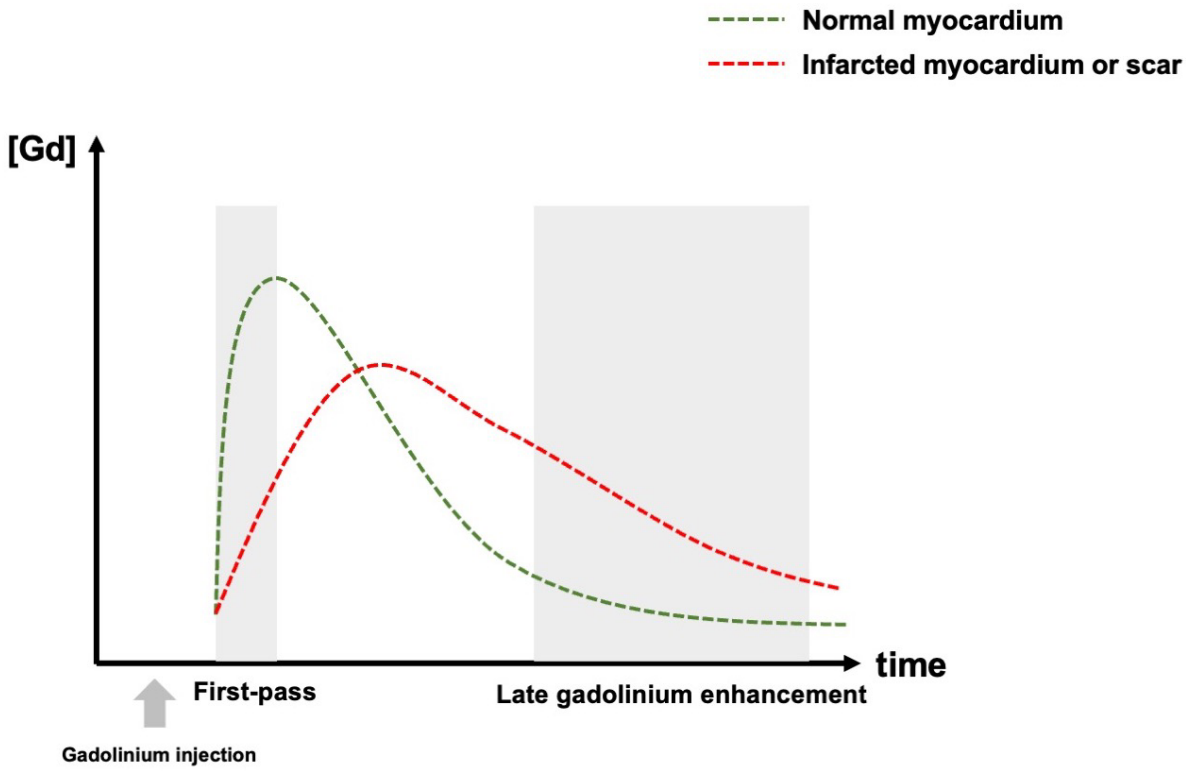

Figure 3. Illustration of first-pass perfusion and LGE imaging of the myocardium.

2) Phase-sensitive inversion-recovery

Previous literature has demonstrated that the strongly T1-weighted segmented IR GRE sequence has very good performance in differentiating injured from normal myocardium after the administration of gadolinium (Kim *et al.*, 2003). The IR sequence begins with a non-selective 180° inversion pulse that reverses the longitudinal magnetization of all tissues and is typically followed by an inversion time delay, which enables all tissues to return to the magnetization equilibrium at a rate depended on the tissue-specific T1 relaxation time. Afterwards, a spoiled GRE readout is used to acquire the IR-prepared signal (Holtackers *et al.*, 2022). The phase-sensitive inversion-recovery (PSIR) sequence is an alternative to conventional IR sequence, which removes the background phase while preserving the sign of the desired magnetization during IR. PSIR has become the most widely used sequence for acquiring LGE images (Kellman *et al.*, 2002). In order to maximize the contrast between the normal and

injured myocardium, the 180° inversion pulse is followed by two image acquisitions at every two cardiac cycles (R-R interval), thus PSIR is also known as “two-beat” sequence. The first IR image is acquired using multiple 20° flip angle pulses, whereas the reference image uses 5° flip angle pulses. During the reference acquisition, the longitudinal magnetization has nearly fully recovered. The phase of the reference image is used to correct the first IR image, followed by reconstruction of a corrected real image, which ensures that the signal from normal myocardium is nulled (Kellman *et al*., 2002). The PSIR sequence will be better if an optimal estimate by “Look-Locker” scan is first made (Look and Locker, 1970). Figure 4 is the schematic diagram of PSIR sequence.

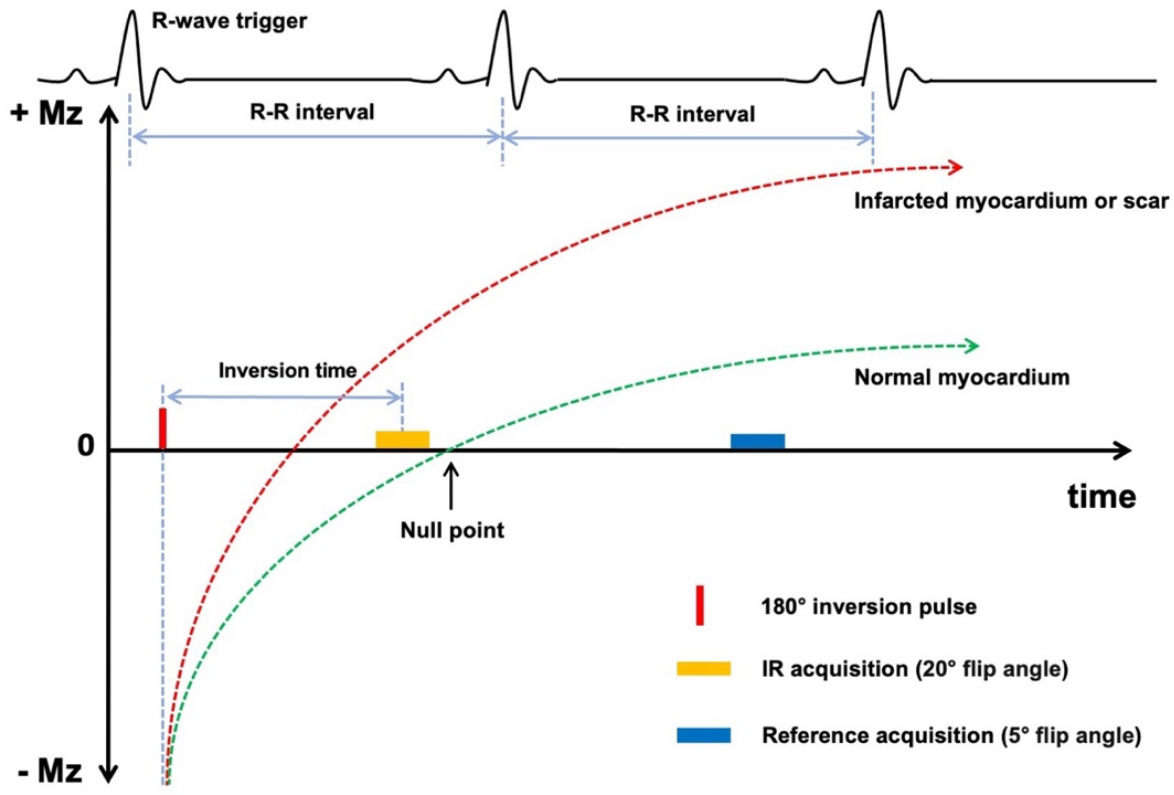

Figure 4. Schematic diagram of a phase-sensitive inversion-recovery (PSIR) sequence used for LGE imaging.
IR = inversion recovery. This figure was adapted from Robert J. Holtackers (Holtackers et al., 2022).

1.2.7 Myocardial quantification

Parametric mapping permits both visualization and quantification of alterations in myocardial characterization based on changes in mapping parameters of T1, T2, T2* relaxation times and extracellular volume (ECV), which facilitates the quantitative diagnostics and optimal treatment for focal and diffuse myocardial disease (Messroghli *et al*., 2017). Changes of mapping parameters are often associated with pathological process in the myocardium (Table 3).

Table 3. Myocardial pathological process revealed by T1, T2, T2* and ECV changes.
This table was adapted from Daniel R. Messroghli (Messroghli et al., 2017).

Mapping parameters	**Mid increase**	**Moderate-severe increase**	**Decrease**
Native T1	Diffuse fibrosis and scar, subacute inflammation	Amyloid, necrosis acute inflammation and ischemia	Fabry disease, iron and lipid overload, hemorrhage, athlete's heart
ECV	Diffuse fibrosis	Amyloid, necrosis, scar	
T2	Subacute inflammation	Acute inflammation, acute ischemia, necrosis	Iron overload, hemorrhage
T2*			Iron overload, hemorrhage, stress-induced ischemia

1) T1 Mapping

T1 mapping measures the T1 relaxation time determined by how rapidly the nuclear spin magnetization returns its equilibrium state after being excited by a RF pulse (Haaf *et al*., 2016), the general principle of which is to acquire multiple T1-weighted images at different times after an inversion pulse and to fit the signal intensities of these images to the equation for T1 relaxation time (Taylor *et al.*, 2016). The fitted T1 values for each pixel can be used to generate a T1 map, which represents arguably the most succinct and informative summary of the spatial and temporal changes during an IR pulse (Taylor *et al*., 2016). The initial T1 measurement based the Look-Locker pulse sequence involved multiple breath-holds, Messroghli subsequently proposed the modified Look-Locker inversion recovery (MOLLI) sequence to overcome the

limitations of Look-Locker. MOLLI allows acquisition within a single breath-hold over 17 successive heartbeats and has become the most widely used T1 mapping method (Messroghli *et al.*, 2004). Other pulse sequences are also applied to acquire T1 mapping, including saturation recovery single-shot acquisition (SASHA), shortened MOLLI (shMOLLI), saturation pulse prepared heart rate independent inversion recovery (SAPPHIRE) (Roujol *et al.*, 2014).

The original MOLLI is a 3(3)3(3)5 scheme, which indicates the number of inversion pulses and samples and the recovery period: the unbracketed numbers are the numbers of image acquisitions after the inversion and the bracketed numbers are the R-R intervals for T1 recovery (Kim *et al.*, 2017). However, it requires a long breath-hold duration and sufficient time to recover magnetization, a number of modifications have been proposed to shorten the acquisition time or to improve accuracy and precision (Kellman and Hansen, 2014). As illustrated in Figure 5, now one popular MOLLI protocol is 5(3)3 scheme, indicating that there are 2 inversion pulses, acquiring 5 images after the first inversion, followed by a recovery period (3 heart beats) and then 3 images are acquired after the second inversion (Kellman *et al.*, 2012b, Kim *et al.*, 2017). This protocol was used in our publications for T1 mapping.

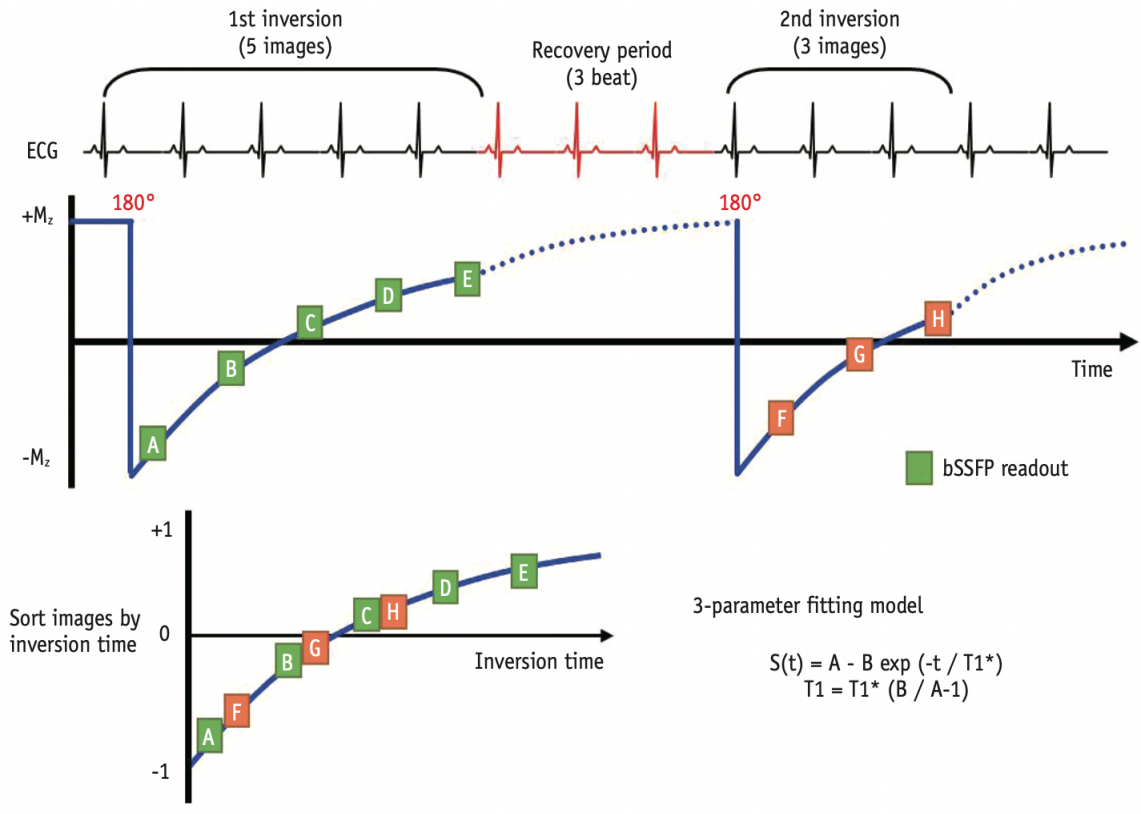

Figure 5. Modified Look-Locker inversion recovery (MOLLI) sequence with 5(3)3 scheme.
This scheme involves two inversion pulses and a recovery period of three heart beats, with five and three images acquired after the first and second inversions respectively. ECG = electrocardiogram, SSFP = steady-state free-precession. Adapted from Pan Ki Kim (Kim et al., 2017).

Since pathological processes change the water composition or focal molecular environment in the lesions, which usually are regarded to be associated with the alterations in T1 values, T1 mapping without the administration of contrast agent (native T1 mapping) has been reported to detect a variety of myocardial abnormalities. Myocardial alterations can be detected in the setting of myocardial edema (Ferreira *et al.*, 2012), myocarditis (Bohnen *et al.*, 2017), iron overload (Krittayaphong *et al.*, 2017), Fabry disease (Sado *et al*., 2013), myocardial infarct (Tahir *et al.*, 2017) and fibrosis (Bull *et al*., 2013). The two main determinants of an increase in native T1 values are myocardial edema and increased interstitial space (diffuse interstitial fibrosis or amyloid deposition), conversely, a decrease in native T1 values is typically associated with iron or lipid overload (Radenkovic *et al.*, 2017). Previous study reported that the reference native T1 values are 950±21 ms at 1.5 Tesla and 1052±23 ms at 3 Tesla in healthy volunteers acquiring by MOLLI sequence with 3(3)3(3)5 scheme (Dabir *et al.*, 2014), and myocardial T1 values are also gender and age dependent (Roy *et al*., 2017). Therefore, a local reference range is also recommended to be primarily used (Messroghli *et al.*, 2017).

2) Extracellular volume

After administration of contrast agents, the post-contrast T1 mapping is used to measure the ECV fraction. ECV dichotomizes the myocardium into its cellular and interstitial components with estimates expressed as volume fractions, which represents the size of the extracellular space (Moon *et al.*, 2013). Unlike native T1, post-contrast T1 values are known to vary due to various confounders, including gadolinium dosing and clearance rate, acquisition time, body composition, and hematocrit, but as a ratio ECV may offset the variations caused by different vendors, fields, and sequences (Haaf *et al.*, 2016). Estimation of the ECV requires measurement of native and post-contrast myocardial and blood T1 values and adjustment for hematocrit according to the following formula (Haaf *et al.*, 2016):

$$ECV = (1 - hematocrit)\ \frac{\left(\frac{1}{T1_{myo\ post}} - \frac{1}{T1_{myo\ native}}\right)}{\left(\frac{1}{T1_{blood\ post}} - \frac{1}{T1_{blood\ native}}\right)}$$

According to the consensus statement by the Society for Cardiovascular Magnetic Resonance (SCMR), hematocrit for the calculation of ECV should be obtained immediately before scanning, otherwise within 24 hours. For ECV measurements, post-contrast T1 mapping should be performed 10-30 minutes after the administration of contrast agents with doses of 0.1-0.2 mmol/kg (Messroghli *et al.*, 2017). In healthy subjects, myocardial ECV values are reported to be gender and age dependent and averaged 26.6±3.2% at 3 Tesla, which are significantly greater in age-matched women than in men (28±3% *vs.* 25±2%) and increase with age (Roy *et al*., 2017). The ECV can increase with diffuse interstitial remodeling and expansion, and has a great potential for visualizing and quantifying myocardial edema, fibrosis, necrosis, and amyloid accumulation.

3) T2 mapping

Conventional T2-weighted (T2w) imaging is commonly used to assess myocardial inflammation and edema, however a set of challenges limit its widespread clinical acceptance. T2 mapping, as an alternative technique, has been established to detect edematous myocardium accurately and reliably overcomes the limitations of T2w imaging (Giri *et al.*, 2009, Fernandez-Jimenez *et al.*, 2015). Changes in the myocardial water state can induce elevation in myocardial T2 relaxation time, making it a versatile parameter for assessing a range of myocardial pathologies (O'Brien *et al.*, 2022). Myocardial T2 relaxation time is thought to be helpful in the detection of myocardial edema in patients with acute inflammatory cardiomyopathies (Thavendiranathan *et al.*, 2012), myocardial infarct (Tahir *et al*., 2017), sarcoidosis (Crouser *et al.*, 2014) and athlete's heart (Tahir *et al.*, 2020). Female sex and aging correlate with increased myocardial T2 times (Bonner et al., 2015), field strength, pulse sequence and vendor may also account for heterogeneities. The reference range of T2 relaxation time is recommended to be defined as the mean±2 standard deviations of the local reference cohort (Messroghli *et al.*, 2017). T2 mapping is mainly acquired using turbo-spin-echo (TSE), T2-prepared bSSFP or gradient-spin-echo (GraSE) sequences (Messroghli *et al.*, 2017). GraSE-based T2 mapping combines a fast-spin-echo pulse sequence

together with echo-planar-imaging (O'Brien *et al*., 2022). In this sequence a train of spin-echoes is generated by several refocusing 180° pulses and gradient echoes are sampled before and after each spin echo with an echo-planar-imaging readout (Sprinkart *et al.*, 2015, O'Brien *et al*., 2022). In our publications, we applied GraSE sequences for acquiring T2 mapping imaging.

To summarize, this section introduced the main applications and corresponding primary principles of CMR imaging in this thesis, as well as the pathological alterations in cardiac function and myocardial tissue characterization revealed by conventional and multiparametric mapping techniques. Detailed descriptions of image acquisition and post-processing can be found in the Methods section of chapter 2, 3, 4 and 5, respectively. CMR imaging provides further insights into cardiac alterations, the next section will introduce the representative cardiac alterations discussed in the thesis.

1.3 Cardiac alterations

1.3.1 Athlete's heart

Athlete's heart is the term used for functional and structural adaptation to long-term and frequent physical training (Scharf *et al.*, 2010), which was first studied by Morganroth *et al*. by echocardiography (Morganroth *et al.*, 1975). This adaptation is categorized into two main morphologic types including LV eccentric and concentric hypertrophy. Eccentric hypertrophy refers to the increased ventricular wall and cavity dilatation due to volume load, whereas concentric hypertrophy reflects an increased wall thickness and myocardial mass but without cavity dilatation in response to pressure load (Scharf *et al.*, 2010, George *et al.*, 2012). In addition to the LV adaptation, RV function may be more profoundly altered by intense endurance exercise (La Gerche *et al.*, 2012). There is speculation that the thin-walled RV experiences a greater increase in workload than the thick-walled LV during endurance exercise and volume overload, leading to distinct remodeling patterns (Ector *et al.*, 2007). Regular exercise is generally recognized as beneficial to the cardiovascular system, but also associated with sudden cardiac death during or after physical exertion in a minority of athletes

(Maron *et al.*, 2009). Although there is hard evidence supporting the cardiac adaptations to physical exercise, the upper physiological limit remains controversial.

More importantly, due to the overlap features between physiology and pathology, differentiation of athlete's heart from other cardiomyopathies is still challenging (Kubler *et al.*, 2021). Now advanced cardiac imaging techniques are providing further insights into the phenotype of athlete's heart by delineating morphological and functional adaptation as well as evaluating tissue characterization. More data is required to evaluate the value of CMR imaging in assisting diagnostic decision-making and investigating the underlying mechanisms of athlete's heart within various athlete subtypes.

The adaptive alterations of athlete's heart have been investigated by recent CMR studies (Bohm *et al.*, 2016, Kramer *et al.*, 2013). The incidence of focal myocardial fibrosis detected by LGE-CMR is reported to occur in 0% to 50% of asymptomatic athletes (Domenech-Ximenos *et al.*, 2020, Breuckmann *et al.*, 2009, Bohm *et al.*, 2016). Diffuse myocardial fibrosis may occur in asymptomatic triathletes manifested by an elevated ECV based on T1 mapping, which is often not detected by LGE (Tahir *et al.*, 2018). Moreover, myocardial fibrosis has a measurable impact on LV systolic function in triathletes, even in those with normal LVEF (Tahir *et al.*, 2019). Although the effect of endurance exercise on LV diastolic function among athletes has been assessed in several echocardiographic studies (Teske *et al.*, 2009, Hoffmann *et al.*, 2021), CMR data focused on the effect of endurance exercise on LV diastolic function is still limited. In addition, the presence of myocardial fibrosis might impact the patterns of LV diastolic filling. To understand the impact of myocardial fibrosis on LV diastolic function, it is essential to compare diastolic filling parameters between athletes with and without myocardial fibrosis.

The chronic alterations might be the cumulative result of repeated bouts of intense exercise, an acute injury of exercise is equally noteworthy. Understanding the acute changes after an endurance exercise bout, is fundamental to elucidate the mechanisms of how intensive exercise triggers the development of cardiac adaptation in athletes. After an endurance race, biomarkers of cardiac injury increase in triathletes and post-race cardiac dysfunction can be observed in triathletes with myocardial fibrosis (Tahir *et al.*, 2020). Nevertheless, a more recent study has shown that

biomarkers of myocardial injury are not associated with cardiac dysfunction following endurance exercise (Wilson et al., 2011b). Conventional parameters may not always reflect preclinical cardiac alterations in certain cases (*e.g.*, biomarkers or LVEF). CMR-FT is a sensitive method for quantifying myocardial deformation and could detect subtle acute changes in cardiac function in triathletes following an endurance race.

1.3.2 Resistant hypertension

The global prevalence of hypertensive heart disease has risen steadily over the past three decades, maintaining a high burden of mortality in cardiovascular disease (Roth *et al.*, 2020). According to the European Society of Cardiology Guidelines, resistant hypertension is defined as above-goal elevated blood pressure despite the concurrent use of three different antihypertensive drugs, which should include a diuretic (Williams *et al.*, 2018). Furthermore, patients with resistant hypertension are at higher risk for adverse cardiovascular events compared to those without resistant hypertension (Daugherty *et al.*, 2012). It emphasizes the need for greater efforts towards monitoring the cardiac alterations during disease progression and improving outcome in these patients who are a potentially higher-risk subset.

Hypertension is considered as the most common risk factor of LV hypertrophy (Koren *et al.*, 1991). Pressure overload of the left ventricle primarily results in adaptive wall thickening and increase in mass leading to concentric hypertrophy (Grossman *et al.*, 1975), while some hypertensive patients also exhibit an eccentric hypertrophy pattern characterized by normal relative wall thickness despite increased ventricular mass (Koren *et al.*, 1991). However, concentric hypertrophy is more closely associated with poor prognosis than eccentric hypertrophy (Koren *et al.*, 1991). Due to the uncontrolled blood pressure, patients with resistant hypertension may experience longer-term pressure overload compared to those with controlled hypertension. The severity and duration of hypertension contribute to the development of hypertrophic remodeling (Hill and Olson, 2008). Hence, it might be speculated that patients with resistant hypertension are at a higher risk of adverse outcome.

Hypertensive heart disease generally results in concentric LV hypertrophy first, then it affects myocardial contractility (Frohlich *et al.*, 1992). In addition, subtle abnormalities

in systolic function occur in hypertensive patients with concentric hypertrophy, it is possible that these subtle abnormalities in systolic function may be related to adverse outcome (Sadler *et al.*, 1997). Numerous previous studies focused on myocardial strain in resistant hypertension using echocardiology, demonstrating that speckle tracking technique is a promising tool to evaluate early-stage LV dysfunction in patients with hypertension (Alsharari *et al*., 2021).

Myocardial fibrosis is a common end point of many cellular and noncellular pathological processes in hypertension (Kuruvilla *et al*., 2015). Recent studies reported the incidence of focal myocardial fibrosis detected by LGE in hypertensive patients ranges between 18% and 30% (Iyer *et al.*, 2022, Wang *et al.*, 2017). Furthermore, hypertensive patients with LV hypertrophy have greater diffuse myocardial fibrosis as measured by ECV (Kuruvilla *et al.*, 2015). CMR-derived measurement of myocardial fibrosis and function is related in patients with hypertension (Pichler *et al.*, 2020). Utilizing the advantages of CMR for assessing myocardial function and tissue characteristics, the analysis of the relationship between subtle functional alterations and the degree of myocardial impairment in resistant hypertension would be a viable research direction.

1.3.3 Platinum-related chemotherapeutic cardiotoxicity

Over the past three decades, significant advancements have been made in the treatment outcomes of cancer patients due to a better understanding of cancer biology and the development of more effective therapies. Despite the ability of current oncologic therapies to promote long-term survival, many of these treatments have both short- and long-term cardiotoxic effects. There has been a renewed focus on better characterization of the underlying myocardial impairment (Harries *et al*., 2020).

Platinum-based chemotherapy is known to be highly effective in treating a variety of cancers, with the cisplatin or carboplatin as the representative regimen. Cisplatin is the most frequently used platinum-based chemotherapy, and carboplatin is used as an alternative for its ototoxicity and nephrotoxicity. Nevertheless, it is important to note

that platinum-based treatments can cause severe side effects due to their poor selectivity (Oun *et al.*, 2018).

Platinum-containing chemotherapy can cause acute cardiovascular injury and long-term cardiotoxicities. Specifically, during the early phase of treatment, cisplatin can induce acute endothelial dysfunction and increase the risk of cardiovascular complications (Cameron *et al*., 2020), diastolic function decreases accompanied by an unfavorable change in metabolic profile (van Schinkel *et al*., 2013). Subtle impairment in systolic function is also detected by echocardiographic strain imaging (Altin *et al.*, 2015). In long-term survivors of testicular cancer treated with cisplatin-containing chemotherapy, cardiac events increase (Meinardi *et al.*, 2000), diastolic cardiac function progressively deteriorates (Altena *et al.*, 2011). Platinum-based chemotherapy is associated with impaired RV function and LV diastolic function in female survivors with germ cell cancer (Murbraech *et al.*, 2015). A recent study also confirms the worse diastolic function, but reports no signs of reduction in biventricular systolic function (Bjerring *et al.*, 2021). Further research is needed to clarify the long-term effects of platinum-based chemotherapy on systolic function, as well as the extent of platinum-induced impairment on myocardial tissue based on CMR quantification techniques.

In summary, this section briefly introduced the representative cardiac alterations investigated in this thesis, including athlete's heart, myocardial impairment of resistant hypertension, and platinum-related cardiotoxicity. There are still some controversies about the intrinsic mechanisms of the above cardiac alterations, lacking of adequate quantitative analysis for myocardial deformation and tissue impairment. The combined application of conventional and advanced CMR techniques can yield more clues. In the following chapters, the different publications will demonstrate how we applied multiparametric CMR imaging to assess cardiac function, myocardial deformation, and tissue characterization in competitive triathletes, patients with resistant hypertension, and long-term germ cell cancer survivors, who received platinum-based chemotherapy.

2 Chapter 2: Publication in *European Radiology*, December 2021

Acute impact of an endurance race on biventricular and biatrial myocardial strain in competitive male and female triathletes evaluated by feature-tracking CMR

Hang Chen*, Malte L. Warncke*, Kai Muellerleile, Dennis Saering, Antonia Beitzen-Heineke, Anna Kisters, Monika Swiderska, Ersin Cavus, Charlotte M. Jahnke, Gerhard Adam, Gunnar K. Lund, Enver Tahir

*contributed equally

Personal contribution:

The following research article has been published in ***European Radiology***. I am the shared first author of the paper. I post-processed the image data (strain analysis) and analyzed the results (analysis of raw data and statistical analysis). I contributed to writing the manuscript draft and editing during the revisions.

https://doi.org/10.1007/s00330-021-08401-y

CARDIAC

Acute impact of an endurance race on biventricular and biatrial myocardial strain in competitive male and female triathletes evaluated by feature-tracking CMR

Hang Chen[1] · Malte L. Warncke[1] · Kai Muellerleile[2] · Dennis Saering[3] · Antonia Beitzen-Heineke[4] · Anna Kisters[1] · Monika Swiderska[1] · Ersin Cavus[2] · Charlotte M. Jahnke[2] · Gerhard Adam[1] · Gunnar K. Lund[1] · Enver Tahir[1]

Received: 27 June 2021 / Revised: 2 September 2021 / Accepted: 11 October 2021

Abstract

Objectives Cardiac adaptation in endurance athletes is a well-known phenomenon, but the acute impact of strenuous exercise is rarely reported on. The aim of this study was to analyze the alterations in biventricular and biatrial function in triathletes after an endurance race using novel feature-tracking cardiac magnetic resonance (FT-CMR).

Methods Fifty consecutive triathletes (45 ± 10 years; 80% men) and twenty-eight controls were prospectively recruited, and underwent 1.5-T CMR. Biventricular and biatrial volumes, left ventricular ejection fraction (LVEF), FT-CMR analysis, and late gadolinium imaging (LGE) were performed. Global systolic longitudinal (GLS), circumferential (GCS), and radial strain (GRS) were assessed. CMR was performed at baseline and following an endurance race. High-sensitive troponin T and NT-proBNP were determined. The time interval between race completion and CMR was 2.3 ± 1.1 h (range 1–5 h).

Results Post-race troponin T ($p < 0.0001$) and NT-proBNP ($p < 0.0001$) were elevated. LVEF remained constant (62 ± 6 vs. 63 ± 7%, $p = 0.607$). Post-race LV GLS decreased by tendency (− 18 ± 2 vs. − 17 ± 2%, $p = 0.054$), whereas GCS (− 16 ± 4 vs. − 18 ± 4%, $p < 0.05$) and GRS increased (39 ± 11 vs. 44 ± 11%, $p < 0.01$). Post-race right ventricular GLS (− 19 ± 3 vs. − 19 ± 3%, $p = 0.668$) remained constant and GCS increased (− 7 ± 2 vs. − 8 ± 3%, $p < 0.001$). Post-race left atrial GLS (30 ± 8 vs. 24 ± 6%, $p < 0.0001$) decreased while right atrial GLS remained constant (25 ± 6 vs. 24 ± 6%, $p = 0.519$).

Conclusions The different alterations of post-race biventricular and biatrial strain might constitute an intrinsic compensatory mechanism following an acute bout of endurance exercise. The combined use of strain parameters may allow a better characterization of ventricular and atrial function in endurance athletes.

Key Points

- *Triathletes demonstrate a decrease of LV global longitudinal strain by tendency and constant RV global longitudinal strain following an endurance race.*
- *Post-race LV and RV global circumferential and radial strains increase, possibly indicating a compensatory mechanism after an acute endurance exercise bout.*
- *Subgroup analyses of male triathletes with focal myocardial fibrosis did not demonstrate alterations in biventricular and biatrial strain after an endurance race.*

Keywords Cardiac · Magnetic resonance imaging, Cine · Cardiac imaging techniques · Athletes

Hang Chen and Malte L. Warncke contributed equally to this work.

✉ Enver Tahir
e.tahir@uke.de

[1] Department of Diagnostic and Interventional Radiology and Nuclear Medicine, University Hospital Hamburg Eppendorf, Martinistr. 52, 20246 Hamburg, Germany

[2] Department of General and Interventional Cardiology, University Heart Center, Hamburg, Germany

[3] Information Technology and Image Processing, University of Applied Sciences, Wedel, Germany

[4] Department of Oncology, Hematology, BMT With Department of Pneumology, University Medical Center Hamburg, Hamburg, Germany

Abbreviations

CMR	Cardiovascular magnetic resonance
ECV	Extracellular volume
EF	Ejection fraction
FT-CMR	Feature-tracking cardiac magnetic resonance
FW	Free wall
GCS	Global circumferential strain
GLS	Global longitudinal strain
GRS	Global radial strain
LA	Left atrial
LGE	Late gadolinium enhancement
LV	Left ventricle
MOLLI	Modified look-locker inversion recovery
NT-proBNP	N-terminal pro-brain natriuretic peptide
RA	Right atrial
RV	Right ventricle
STE	Speckle tracking echocardiography

Introduction

Numerous studies have reported on cardiac adaptations in endurance athletes [1–3], yet standard parameters of systolic function such as left ventricular ejection fraction (LVEF) might not detect subtle functional alterations of the athlete's heart. Feature-tracking cardiac magnetic resonance (FT-CMR) imaging is an advanced technique for quantification of myocardial strain using conventional cine images [4]. Myocardial strain is defined as the relative change in fiber length from end diastole and can be a sensitive measure of myocardial deformation [5].

While normal values of ventricular and atrial strain in endurance athletes at rest are largely undefined, echocardiographic and CMR studies report that prolonged endurance training is associated with attenuated myocardial strain compared with sedentary controls, whereas biventricular ejection fractions are similar [6–10]. However, the acute changes of myocardial strain in response to an endurance race are less well studied. Previous echocardiographic studies have described differences in myocardial strain before and after a high-intensity exercise [11, 12]. Further, Christou et al showed that the absolute values of both ventricular longitudinal strains decreased after a race, but were still within normal range for the vast majority of athletes [13].

We hypothesized that triathletes develop acute cardiac alterations after an endurance race, which are directly or indirectly reflected by changes in myocardial function and increased cardiac biomarkers. The aim of this study was to analyze the alterations in biventricular and biatrial function in triathletes after an endurance race using novel FT-CMR.

Methods and materials

Triathletes and controls

The local ethics committee approved the study and all participants gave written informed consent. Triathletes were contacted through advertisements at triathlon clubs and were included if a minimum of 10 h weekly training and regular participation in official competitions in the last 3 years were given [14]. Control subjects were eligible with a weekly exercise of less than 3 h [14]. Study exclusion criteria were CMR contraindications, systemic disease, or cardiovascular diseases. No intake of any cardiac or illicit medication was reported [14]. Fifty consecutive male (80%; age: 44 ± 9 years, range 18–61 years) and female triathletes (age: 46 ± 11 years, range 29–62 years) underwent baseline and post-race CMR. Baseline CMR was acquired at least 30 days after the last race and subjects were instructed to refrain from any exercise in the preceding 72 h [14]. The interval between baseline and post-race CMR was more than a month. Baseline and post-race CMR findings of this cohort were partly reported previously and details are provided in the Supplementary Material [14–16]. This study expands the previous post-race cohort by nine male and eleven female triathletes. Blood samples were drawn immediately before each CMR from an antecubital vein in supine position for 5 min to obtain hematocrit, creatine kinase, high-sensitive troponin T, and N-terminal pro-brain natriuretic peptide (NT-proBNP) [14].

Post-race CMR

All triathletes successfully finished their endurance races with a total cumulative race distance of 58 ± 62 km. Details on the endurance races are provided in the Supplementary Material. Post-race CMR was performed at 2.3 ± 1.1 h (range 1–5 h).

CMR protocol

Studies were performed on a 1.5-T Achieva scanner with a 5-channel cardiac phased array receiver coil (Phillips, Healthcare). ECG-triggered steady-state free-precession (SSFP) cine sequences were acquired in short axis and 2-, 3-, and 4-chamber views. Native T1 mapping was performed using a 5 s(3 s)3 s modified look-locker inversion recovery (MOLLI) sequence on three short-axes slices [14]. A gradient (echo planar imaging) and spin-echo multi-echo sequence was applied to acquire native T2 mapping images in three short-axis slices. Ten minutes after injection of 0.15 mmol/kg gadoterate meglumine (Dotarem®, Guerbet),

end-diastolic late gadolinium enhancement (LGE) images were acquired using end-diastolic phase-sensitive inversion recovery (PSIR) sequences in short-axis and 2-, 3-, and 4-chamber views. Additional details are given in the Supplementary Material.

CMR data analysis

Two investigators (H.C. and M.W.) independently and blindly analyzed each CMR in random order using a commercially available software (CVi42, Circle Cardiovascular Imaging Inc.). CMR parameters were indexed to the body surface area (BSA). Additional details are provided in the Supplementary Material.

Myocardial strain analysis

Myocardial strain was analyzed on cine images using feature-tracking software (Segment, version 2.1.R.6108, Medviso) as previously reported [15]. In short, this software analyzes myocardial strain by computing interframe deformation fields using an endocardial tracking strategy based on non-rigid image registration. LV global longitudinal strain (GLS) was measured on 3 long-axis cine series using 2-, 3-, and 4-chamber views (Fig. 1a), whereas LV global circumferential strain (GCS) and radial strain (GRS) were measured on three short-axis cine series (apical, midventricular, and basal) (Fig. 1b) [17]. Long-axis 4-chamber and three short-axis series were used to calculate RV GLS and GCS (Fig. 1c, d); long-axis 4-chamber series were applied for RV free wall (FW) GLS [17]. LA and RA endocardial contours were manually delineated on end-diastolic images and propagated throughout the cardiac cycle generating longitudinal strain (Fig. 1c) [18].

Statistical analysis

Statistical analysis was performed with commercially available software (GraphPad Prism, version 9.00) and SPSS for Windows (version 21.0, IBM SPSS Inc.). All CMR data are given as the mean of two observers (H.C. and M.W.). Continuous variables were checked for normality using the D'Agostino-Pearson omnibus normality test. Normally distributed data are presented as mean ± SD and categorical data are presented as absolute numbers and percentage. Normally distributed data were compared using the unpaired or paired Student's *t*-test. If normal distribution was not given, the Mann–Whitney or the Wilcoxon matched-pairs signed rank tests were used. Categorical variables were compared using the χ^2 test or Fischer's exact test as appropriate. Statistical significance was defined as $p < 0.05$.

Results

Baseline characteristics of triathletes compared to controls

There were no differences in age, sex distribution, body surface area, blood biomarkers, and blood pressure (BP) between controls and triathletes (Table 1). Triathletes had a lower heart rate ($p < 0.0001$), but LV cardiac index ($p = 0.927$), LVEF ($p = 0.766$), and RVEF ($p = 0.606$) were similar. LV mass ($p < 0.0001$), ventricular, and atrial volumes were higher in triathletes (Table 1). LV GLS ($p < 0.05$), GCS ($p < 0.01$), and GRS ($p < 0.05$) as well as RV GLS ($p < 0.0001$) and GCS ($p < 0.0001$), RV FW GLS ($p < 0.05$), and RA GLS ($p < 0.0001$) were lower in triathletes (Table 1). LA GLS ($p = 0.288$) was similar between triathletes and controls. Triathletes had a lower native T1 value ($p < 0.0001$), but there were no differences in T2 and ECV values. Baseline CMR revealed LGE indicative of focal myocardial fibrosis in 11 of 40 (28%) male triathletes, but in none of the male controls ($p < 0.01$). None of the female triathletes had LGE.

Post-race changes in all triathletes

Cardiac biomarkers increased in all triathletes including troponin T, NT-proBNP, and creatine kinase MB (Table 1). There was no correlation between troponin T and the race distance ($r = -0.06$, $p = 0.69$; Fig. 2a), but NT-proBNP showed a positive correlation ($r = 0.41$, $p < 0.01$; Fig. 2b). CMR revealed post-race volume decrease in all cardiac chambers, whereas heart rate and cardiac index increased (Table 1). LV ($p = 0.607$) and RV ejection fractions ($p = 0.552$) remained constant.

For clarity, systolic GLS and GCS values are negative by convention; thus, fewer negative values indicate decreased contractility. Systolic GRS on the other hand has positive values. In this study, post-race LV GLS decreased by tendency (-18 ± 2 vs. $-17 \pm 2\%$, $p = 0.054$), whereas GCS (-16 ± 4 vs. $-18 \pm 4\%$, $p < 0.05$) and GRS increased (39 ± 11 vs. $44 \pm 11\%$, $p < 0.01$; Table 1, Fig. 3). Post-race RV GLS ($p = 0.668$) and FW GLS ($p = 0.309$) remained constant, RV GCS increased (-7 ± 2 vs. $-8 \pm 3\%$, $p < 0.001$; Table 1, Fig. 4), and LA GLS decreased (30 ± 8 vs. $24 \pm 6\%$, $p < 0.0001$; Table 1, Fig. 5). Post-race RA GLS ($p = 0.519$), native T1 ($p = 0.486$), and T2 ($p = 0.458$) were stable.

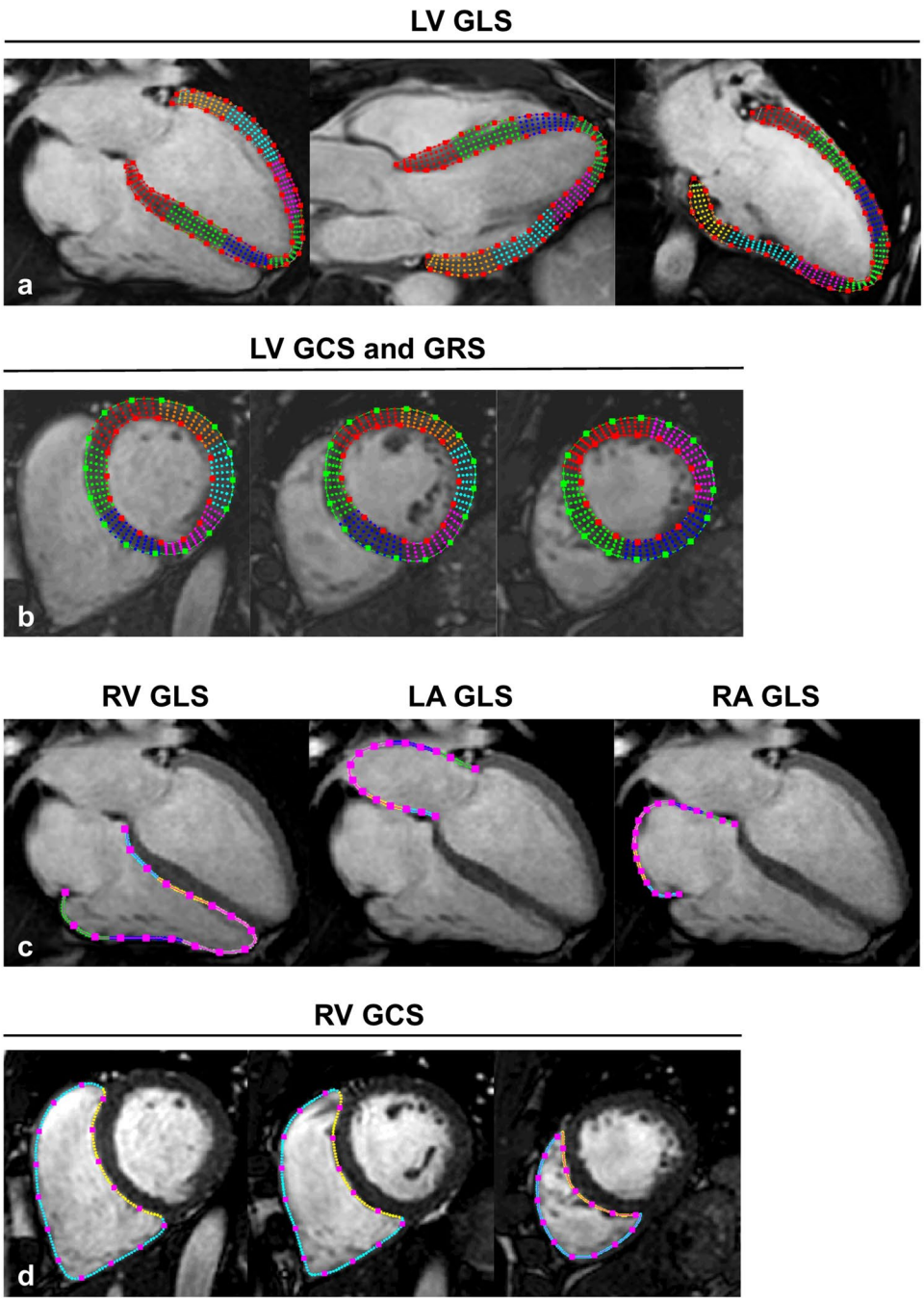

Fig. 1 Depiction of LV endo- and epicardial, and RV, LA, and RA endocardial contours to determine LV GLS (**a**); LV GCS and GRS (**b**); RV, LA, and RA GLS (**c**); as well as RV GCS (**d**). Strain values were generated by feature-tracking CMR using the Segment software, which automatically propagates the manually drawn contours through all cardiac phases of the long- and short-axis cardiac cine series

Post-race correlations between blood biomarkers and myocardial strain

Post-race troponin T correlated with LV GLS ($r = 0.30$, $p < 0.05$), LV GCS ($r = 0.37$, $p < 0.01$), and LV GRS ($r = -0.39$, $p < 0.01$), indicating decrease of myocardial contractility with increasing post-race troponin T. There were no correlations with LA GLS ($r = -0.20$, $p = 0.155$), RA GLS ($r = 0.10$, $p = 0.506$), T1 ($r = -0.11$, $p = 0.451$), and T2 ($r = -0.26$, $p = 0.069$). Post-race NT-proBNP did not correlate with any of the strain parameters.

Post-race changes of myocardial strain in male triathletes

Post-race LV ($p = 0.476$) and RV EF ($p = 0.499$) were unchanged. Post-race LV GLS decreased (-17 ± 2 vs. $-16 \pm 2\%$, $p < 0.05$), whereas GCS (-15 ± 3 vs. $-17 \pm 3\%$, $p < 0.01$) and GRS increased (36 ± 10 vs. $41 \pm 9\%$, $p < 0.05$; Table 2). Post-race RV GLS ($p = 0.724$) and FW GLS ($p = 0.331$) remained constant and GCS increased (-6 ± 3 vs. $-7 \pm 2\%$, $p < 0.001$). LA GLS

Table 1 Demographics and CMR parameters of all triathletes at baseline compared to sedentary controls and post-race alterations in triathletes

	Controls ($n=28$)	Baseline All triathletes ($n=50$)	Post-race All triathletes ($n=50$)	p value
Clinical parameters				
Age, years	42 ± 11	45 ± 10	-	-
Female, %	6 (21)	10 (20)	-	-
Body surface area, m^2	1.94 ± 0.19	1.94 ± 0.19	1.93 ± 0.19	< 0.01
Troponin T, pg/ml	5 ± 3	6 ± 4	51 ± 77	< 0.0001
NT-proBNP, pg/ml	41 ± 24	45 ± 73	116 ± 99	< 0.0001
CK, U/l	182 ± 179	188 ± 145	478 ± 316	< 0.0001
CK-MB, U/l	4 ± 8	10 ± 14	32 ± 19	< 0.0001
Systolic BP at rest, mmHg	121 ± 15	126 ± 15	-	-
Diastolic BP at rest, mmHg	80 ± 18	84 ± 9	-	-
CMR—left heart				
Heart rate, bpm	66 ± 11	54 ± 8‡	68 ± 10	< 0.0001
LV cardiac index, l/min/m^2	3.20 ± 0.82	3.30 ± 0.66	3.91 ± 0.60	< 0.0001
LVEF, %	63 ± 8	62 ± 6	63 ± 7	0.607
LV mass index, g/m^2	65 ± 11	78 ± 11‡	78 ± 12	0.499
LVEDVi, ml/m^2	79 ± 13	98 ± 17‡	93 ± 15	< 0.001
LVESVi, ml/m^2	30 ± 10	37 ± 9†	35 ± 11	0.084
LVSVi, ml/m^2	49 ± 8	61 ± 10‡	58 ± 10	0.100
LAEDVi, ml/m^2	13 ± 4	20 ± 8‡	16 ± 6	< 0.01
LAESVi, ml/m^2	33 ± 7	47 ± 12‡	37 ± 10	< 0.0001
CMR—right heart				
RVEF, %	60 ± 7	59 ± 9	60 ± 8	0.552
RVEDVi, ml/m^2	80 ± 14	101 ± 19‡	97 ± 18	< 0.05
RVESVi, ml/m^2	32 ± 10	41 ± 14†	40 ± 14	0.065
RVSVi, ml/m^2	48 ± 7	60 ± 10‡	57 ± 9	0.296
RAEDVi, ml/m^2	19 ± 5	28 ± 10‡	28 ± 10	0.460
RAESVi, ml/ m^2	36 ± 7	52 ± 14‡	47 ± 12	< 0.01
CMR—strain				
LV GLS, %	− 19 ± 2	− 18 ± 2*	− 17 ± 2	0.054
LV GCS, %	− 19 ± 4	− 16 ± 4†	− 18 ± 4	< 0.05
LV GRS, %	45 ± 11	39 ± 11*	44 ± 11	< 0.01
RV GLS, %	− 22 ± 3	− 19 ± 3‡	− 19 ± 3	0.668
RV GCS, %	− 10 ± 3	− 7 ± 2‡	− 8 ± 3	< 0.001
RV FW GLS, %	− 24 ± 7	− 21 ± 6*	− 21 ± 8	0.309
LA GLS, %	28 ± 5	30 ± 8	24 ± 6	< 0.0001
RA GLS, %	33 ± 7	25 ± 6‡	24 ± 6	0.519
CMR—mapping				
Native T1, ms	1034 ± 32	987 ± 27‡	990 ± 22	0.486
Native T2, ms	53 ± 3	53 ± 2	53 ± 3	0.458
ECV, %	25.6 ± 4.1	25.7 ± 2.0	-	-

Numbers are mean ± SD for continuous and n (%) for categorical data

*$p < 0.05$; †$p < 0.01$; or ‡$p < 0.0001$ for all triathletes vs. controls

Baseline and post-race data were partly reported in previous publications as indicated in the "Methods and materials" section

Abbreviations: *BP*, blood pressure; *EF*, ejection fraction; *GCS*, global circumferential strain; *GLS*, global longitudinal strain; *GRS*, global radial strain; *LA*, left atrial; *LAEDVi*, left atrial end-diastolic volume index; *LAESVi*, left atrial end-systolic volume index; *LV*, left ventricular; *LVEDVi*, left ventricular end-diastolic volume index; *LVESVi*, left ventricular end-systolic volume index; *RA*, right atrial; *RAEDVi*, right atrial end-diastolic volume index; *RAESVi*, right atrial end-systolic volume index; *RV*, right ventricular; *RVEDVi*, right ventricular end-diastolic volume index; *RVESVi*, right ventricular end-systolic volume index; *RV FW*, right ventricular free wall

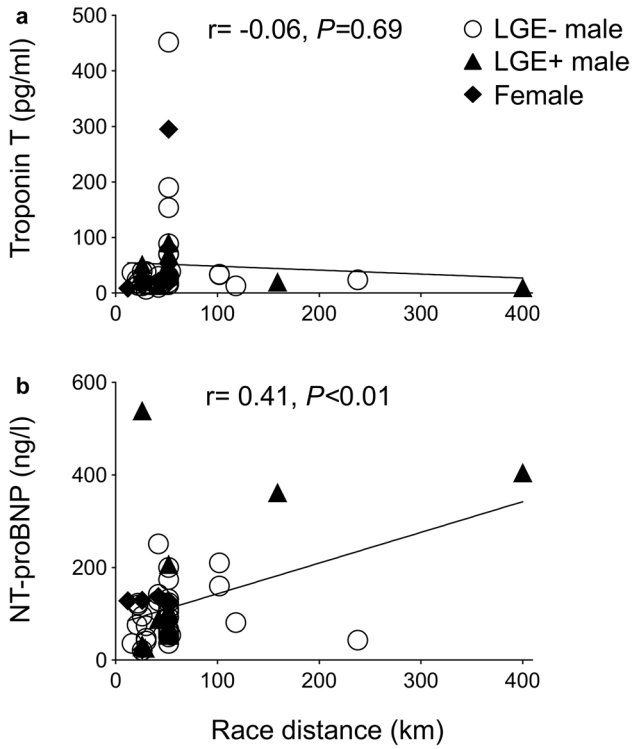

Fig. 2 Correlation between troponin T (**a**) and NT-proBNP (**b**) and the race cumulative distance

(28 ± 7 vs. 23 ± 5%, $p < 0.001$) decreased. Post-race RA GLS remained unchanged ($p = 0.266$; Table 2).

Post-race changes of myocardial strain in female triathletes

Post-race LV ($p = 0.864$) and RV EF ($p = 0.909$) were constant. Post-race LV GLS ($p = 0.891$), GCS ($p = 0.861$), and GRS ($p = 0.147$) as well as RV GLS ($p = 0.790$), GCS ($p = 0.651$), FW GLS ($p = 0.744$), and RA GLS ($p = 0.505$) remained unchanged (Table 3). Post-race LA GLS (37 ± 7 vs. 31 ± 5%, $p < 0.05$) decreased (Table 3).

Post-race changes of myocardial strain in LGE + male triathletes

Baseline CMR revealed non-ischemic myocardial fibrosis in 11 (28%) male triathletes. The LGE pattern was previously reported in detail [14, 15]. Briefly, predominantly anterolateral, inferolateral, and inferior segments of the basal LV wall were LGE+, a distribution typical for myocarditis.

Post-race LV ($p = 0.999$) and RV ejection fractions ($p = 0.999$) were unchanged in LGE + male triathletes. Post-race LV GLS (− 17 ± 2 vs. − 17 ± 2%, $p = 0.669$), GCS (− 16 ± 4 vs. − 18 ± 4%, $p = 0.219$), and GRS (38 ± 13 vs. 42 ± 9%, $p = 0.267$) as well as RV GLS (− 20 ± 4 vs. − 18 ± 7%, $p = 0.227$), GCS (− 8 ± 3 vs. − 7 ± 4%, $p = 0.616$), FW GLS (− 20 ± 7 vs. − 23 ± 7%, $p = 0.356$), and RA GLS (23 ± 6 vs. 22 ± 5%, $p = 0.585$) all remained unchanged (Table 4). LA GLS (25 ± 6 vs. 23 ± 4%, $p = 0.276$) was constant after the endurance race (Table 4). Strain values of LGE − male triathletes are detailed in Supplemental Table 1.

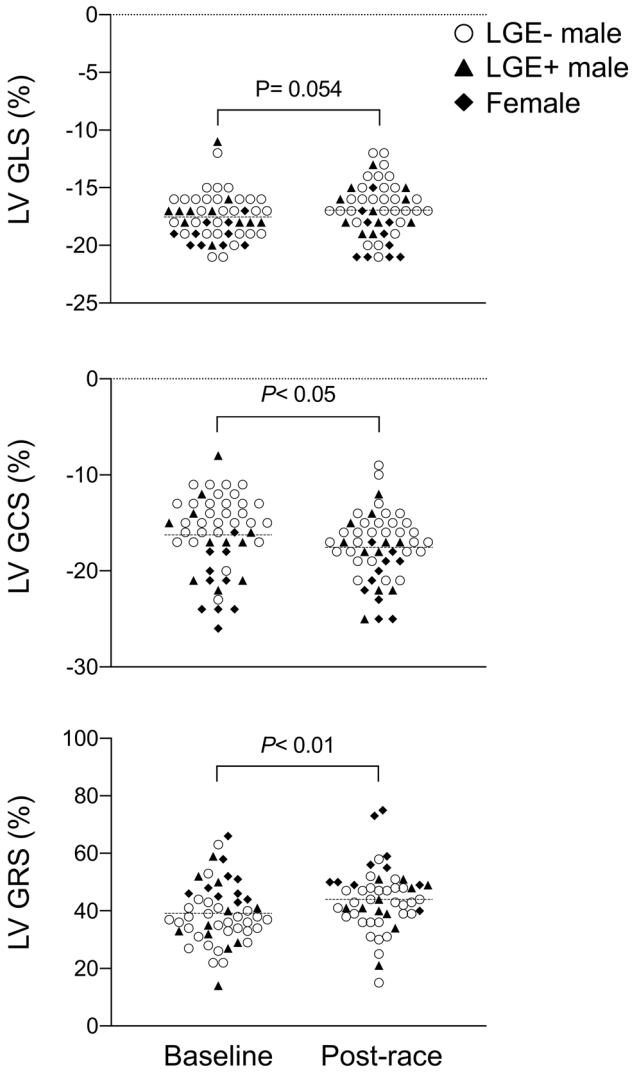

Fig. 3 Changes of LV GLS, GCS, and GRS following an acute bout of endurance exercise in male and female triathletes as assessed by feature-tracking CMR

Discussion

This prospective study analyzed biventricular and biatrial myocardial strain changes in male and female triathletes following an acute bout of endurance exercise. Further, strain analysis in a subgroup of male triathletes with focal

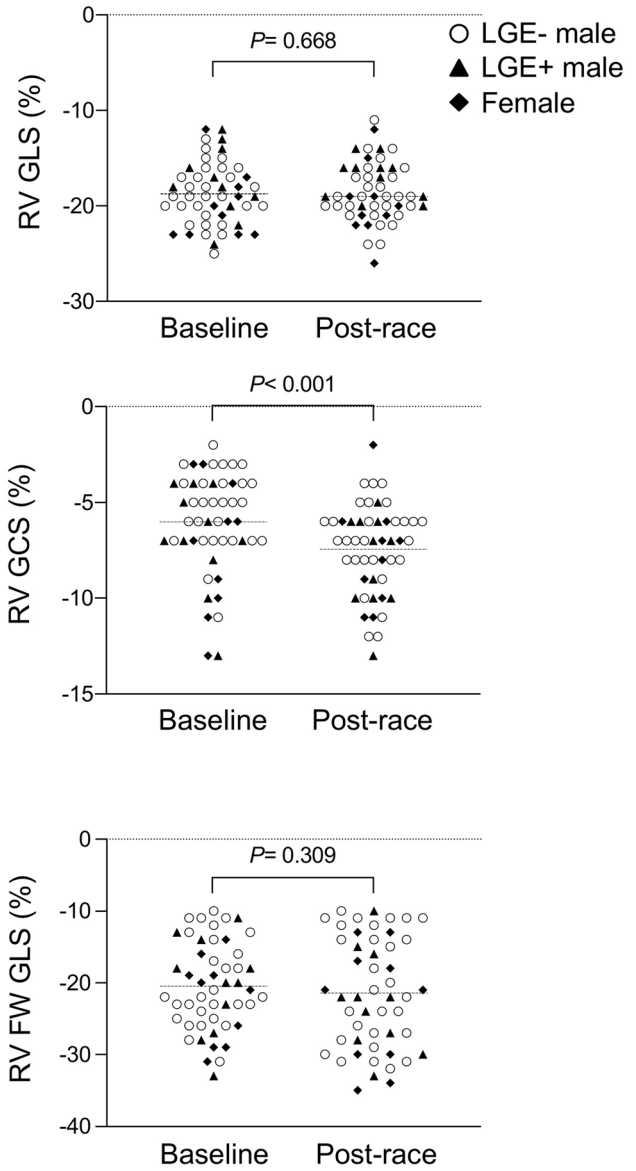

Fig. 4 Changes of RV GLS and GCS and RV free wall GLS following an acute bout of endurance exercise in male and female triathletes as assessed by feature-tracking CMR

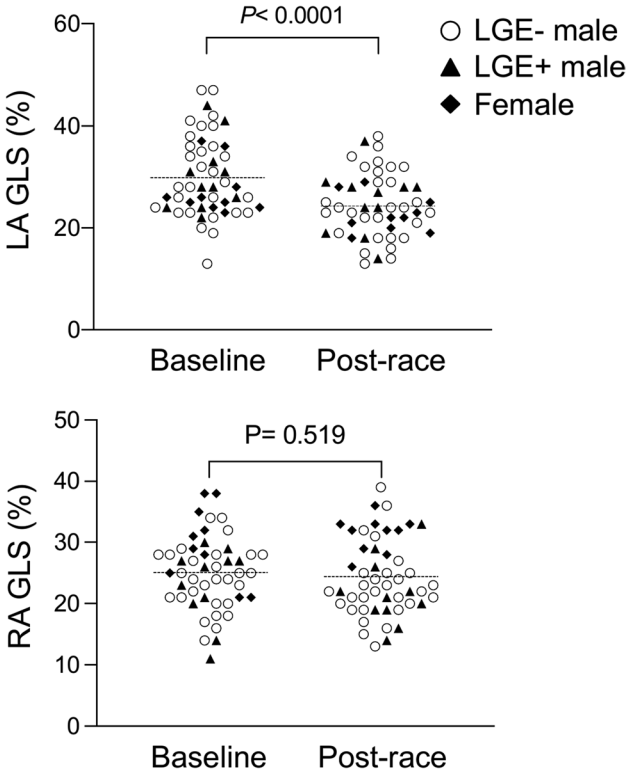

Fig. 5 Changes of LA and RA GLS following an acute bout of endurance exercise in male and female triathletes as assessed by feature-tracking CMR

myocardial fibrosis (LGE +) was performed. The major findings are as follows: (1) Left ventricular GLS was slightly reduced, whereas GCS and GRS increased following an endurance race; (2) Right ventricular GLS and free wall longitudinal strain remained constant, whereas GCS increased post-race; (3) Left atrial longitudinal strain was decreased post-race, and right atrial longitudinal strain remained constant; and (4) Male triathletes with focal myocardial fibrosis (LGE +) had constant baseline and post-race biventricular and biatrial strain parameters.

Alterations in left ventricular strain after an endurance race

Stewart et al observed in a recent study that LV GLS decreased in 10 recreationally active men after a 90-min high-intensity cycling exercise, but not after a 120-min moderate-intensity cycling [8]. Vitiello et al reported that LV GLS and GCS decreased in a cohort of 16 young men following a 180-min strenuous cycling exercise, but not GRS [19]. Further, Aengevaeren et al used CMR to investigate the influence of a marathon run on myocardial injury and cardiomyocyte integrity in highly trained males, and reported that LV GCS was attenuated post-marathon and did not recover within 2 weeks [20]. In concordance with another recent study by Cavigli et al [21], we also observed a post-race tendency of LV GLS reduction in triathletes and constant LVEF. Conversely, LV GCS and GRS were increased. There might be several explanations for this discrepancy. First, the acquisition time point of post-race CMR in our study was 2.3 h (range 1–5) and thus later than in the aforementioned echocardiographic studies, which might have provided a longer recovery period. Second, the duration and components of exercise were different. Stewart et al and Vitiello et al used a cycle ergometer in a strictly controlled in-door

Table 2 Demographics and CMR parameters of male triathletes at baseline compared to sedentary controls and post-race alterations in triathletes

	Controls ($n=22$)	Baseline Men ($n=40$)	Post-race Men ($n=40$)	p value
Clinical parameters				
Age, years	40 ± 12	44 ± 9	-	-
Body surface area, m^2	2.00 ± 0.14	2.01 ± 0.14	2.00 ± 0.14	< 0.01
Troponin T, pg/ml	5 ± 3	6 ± 4	50 ± 75	< 0.001
NT-proBNP, pg/ml	39 ± 25	45 ± 79	121 ± 108	< 0.0001
CK, U/l	210 ± 191	206 ± 156	503 ± 289	< 0.0001
CK-MB, U/l	5 ± 8	11 ± 15	33 ± 18	< 0.0001
Systolic BP at rest, mmHg	121 ± 15	126 ± 12	-	-
Diastolic BP at rest, mmHg	84 ± 11	84 ± 9	-	-
Age, years	40 ± 12	44 ± 9	-	-
CMR—left heart				
Heart rate, bpm	66 ± 12	54 ± 8^{II}	68 ± 10	< 0.0001
LV cardiac index, l/min/m^2	3.31 ± 0.89	3.29 ± 0.64	3.93 ± 0.58	< 0.0001
LVEF, %	62 ± 9	61 ± 6	62 ± 7	0.476
LV mass index, g/m^2	68 ± 8	80 ± 10^{II}	81 ± 11	0.486
LVEDVi, ml/m^2	82 ± 12	102 ± 16^{II}	96 ± 15	< 0.001
LVESVi, ml/m^2	32 ± 10	39 ± 9†	37 ± 10	0.066
LVSVi, ml/m^2	50 ± 8	62 ± 11^{II}	59 ± 10	0.113
LAEDVi, ml/m^2	13 ± 4	20 ± 9‡	17 ± 6	< 0.01
LAESVi, ml/m^2	32 ± 8	48 ± 13^{II}	37 ± 10	< 0.0001
CMR—right heart				
RVEF, %	59 ± 7	58 ± 9	59 ± 8	0.499
RVEDVi, ml/m^2	84 ± 13	105 ± 19^{II}	100 ± 19	0.051
RVESVi, ml/m^2	34 ± 10	45 ± 14†	42 ± 14	< 0.05
RVSVi, ml/m^2	49 ± 6	60 ± 11‡	58 ± 10	0.300
RAEDVi, ml/m^2	20 ± 5	30 ± 10†	29 ± 11	0.633
RAESVi, ml/ m^2	38 ± 7	52 ± 14†	47 ± 12	< 0.01
CMR—strain				
LV GLS, %	− 18 ± 2	− 17 ± 2	− 16 ± 2	< 0.05
LV GCS, %	− 18 ± 4	− 15 ± 3†	− 17 ± 3	< 0.01
LV GRS, %	44 ± 11	36 ± 10†	41 ± 9	< 0.05
RV GLS, %	− 22 ± 3	− 18 ± 3‡	− 18 ± 3	0.724
RV GCS, %	− 10 ± 3	− 6 ± 3^{II}	− 7 ± 2	< 0.001
RV FW GLS, %	− 23 ± 7	− 20 ± 6	− 21 ± 8	0.331
LA GLS, %	28 ± 5	28 ± 7	23 ± 5	< 0.001
RA GLS, %	32 ± 7	24 ± 5^{II}	23 ± 6	0.266
CMR—mapping				
Native T1, ms	1024 ± 30	983 ± 28^{II}	987 ± 20	0.512
Native T2, ms	52 ± 4	53 ± 3	53 ± 3	0.854
ECV, %	24.9 ± 3	24.9 ± 1.5	-	-

Numbers are mean ± SD for continuous and n (%) for categorical data

$^{*}p < 0.05$; $^{\dagger}p < 0.01$; $^{\ddagger}p < 0.001$; or $^{II}p < 0.0001$ for male triathletes vs. controls

Baseline and post-race data were partly reported in previous publications as indicated in the "Methods and materials" section

Abbreviations: *BP*, blood pressure; *EF*, ejection fraction; *GCS*, global circumferential strain; *GLS*, global longitudinal strain; *GRS*, global radial strain; *LA*, left atrial; *LAEDVi*, left atrial end-diastolic volume index; *LAESVi*, left atrial end-systolic volume index; *LV*, left ventricular; *LVEDVi*, left ventricular end-diastolic volume index; *LVESVi*, left ventricular end-systolic volume index; *RA*, right atrial; *RAEDVi*, right atrial end-diastolic volume index; *RAESVi*, right atrial end-systolic volume index; *RV*, right ventricular; *RVEDVi*, right ventricular end-diastolic volume index; *RVESVi*, right ventricular end-systolic volume index; *RV FW*, right ventricular free wall

Table 3 Demographics and CMR parameters of female triathletes at baseline compared to sedentary controls and post-race alterations in triathletes

	Controls ($n=6$)	Baseline Women ($n=10$)	Post-race Women ($n=10$)	p value
Clinical parameters				
Age, years	47 ± 6	46 ± 11	-	-
Body surface area, m^2	1.71 ± 0.17	1.68 ± 0.11	1.66 ± 0.08	0.273
Troponin T, pg/ml	3 ± 1	4 ± 2	56 ± 87	0.089
NT-proBNP, pg/ml	51 ± 7	45 ± 40	97 ± 41	< 0.01
CK, U/l	69 ± 20	117 ± 50	376 ± 411	0.085
CK-MB, U/l	3 ± 2	3 ± 7	27 ± 21	< 0.01
Systolic BP at rest, mmHg	123 ± 17	128 ± 23	-	-
Diastolic BP at rest, mmHg	84 ± 12	85 ± 9	-	-
Age, years	47 ± 6	46 ± 11	-	-
CMR—left heart				
LVEF, %	67 ± 6	67 ± 4	67 ± 8	0.864
Heart rate, bpm	65 ± 8	56 ± 8*	70 ± 9	< 0.01
LV cardiac index, l/min/m^2	2.89 ± 0.51	3.16 ± 0.80	3.80 ± 0.71	0.097
LV mass index, g/m^2	53 ± 8	67 ± 9†	67 ± 9	0.909
LVEDVi, ml/m^2	68 ± 8	83 ± 9†	81 ± 9	0.340
LVESVi, ml/m^2	22 ± 5	27 ± 4*	27 ± 7	0.928
LVSVi, ml/m^2	45 ± 8	56 ± 8*	54 ± 9	0.647
LAEDVi, ml/m^2	11 ± 1	18 ± 6*	16 ± 5	0.205
LAESVi, ml/m^2	35 ± 5	42 ± 10	39 ± 8	0.212
CMR—right heart				
RVEF, %	63 ± 4	65 ± 7	66 ± 7	0.909
RVEDVi, ml/m^2	68 ± 7	87 ± 12†	85 ± 9	0.523
RVESVi, ml/m^2	25 ± 4	30 ± 7	30 ± 9	0.796
RVSVi, ml/m^2	43 ± 6	57 ± 11*	55 ± 5	0.784
RAEDVi, ml/m^2	16 ± 3	25 ± 7*	23 ± 7	0.415
RAESVi, ml/ m^2	31 ± 4	50 ± 11	47 ± 9	0.225
CMR—strain				
LV GLS, %	− 21 ± 1	− 19 ± 1†	− 19 ± 2	0.891
LV GCS, %	− 23 ± 2	− 21 ± 3	− 21 ± 3	0.861
LV GRS, %	52 ± 9	50 ± 7	56 ± 11	0.147
RV GLS, %	− 23 ± 2	− 20 ± 4	− 20 ± 4	0.790
RV GCS, %	− 10 ± 1	− 7 ± 3	− 8 ± 3	0.651
RV FW GLS, %	− 27 ± 7	− 22 ± 6	− 23 ± 8	0.744
LA GLS, %	30 ± 5	37 ± 7*	31 ± 5	< 0.05
RA GLS, %	38 ± 7	30 ± 6*	31 ± 3	0.505
LV GLS, %	− 21 ± 1	− 19 ± 1†	− 19 ± 2	0.891
CMR—mapping				
Native T1, ms	1065 ± 15	999 ± 20‡	1001 ± 25	0.823
Native T2, ms	55 ± 1	53 ± 2	52 ± 2	0.218
ECV, %	30.2 ± 3.9	27.4 ± 1.5	-	-

Numbers are mean ± SD for continuous and n (%) for categorical data

*$p < 0.05$; †$p < 0.01$; or ‡$p < 0.0001$ for female triathletes vs. controls

Baseline and post-race data were partly reported in previous publications as indicated in the "Methods and materials" section

Abbreviations: *BP*, blood pressure; *EF*, ejection fraction; *GCS*, global circumferential strain; *GLS*, global longitudinal strain; *GRS*, global radial strain; *LA*, left atrial; *LAEDVi*, left atrial end-diastolic volume index; *LAESVi*, left atrial end-systolic volume index; *LV*, left ventricular; *LVEDVi*, left ventricular end-diastolic volume index; *LVESVi*, left ventricular end-systolic volume index; *RA*, right atrial; *RAEDVi*, right atrial end-diastolic volume index; *RAESVi*, right atrial end-systolic volume index; *RV*, right ventricular; *RVEDVi*, right ventricular end-diastolic volume index; *RVESVi*, right ventricular end-systolic volume index; *RV FW*, right ventricular free wall

Table 4 Demographics and CMR parameters of LGE + triathletes at baseline and post-race

	Baseline LGE + ($n = 11$)	Post-race LGE + ($n = 11$)	p value
Clinical parameters			
Body surface area, m^2	1.97 ± 0.16	1.95 ± 0.15	< 0.05
Troponin T, pg/ml	7 ± 6	39 ± 25	< 0.01
NT-proBNP, pg/ml	83 ± 144	174 ± 179	< 0.05
CK, U/l	126 ± 48	388 ± 210	< 0.01
CK-MB, U/l	4 ± 8	30 ± 21	< 0.01
Systolic BP at rest, mmHg	128 ± 16	-	-
Diastolic BP at rest, mmHg	83 ± 9	-	-
CMR—left heart			
Heart rate, bpm	55 ± 10	65 ± 9	< 0.001
LV cardiac index, l/min/m^2	3.39 ± 0.76	3.92 ± 0.52	< 0.05
LVEF, %	63 ± 8	63 ± 7	0.999
LV mass index, g/m^2	87 ± 7	87 ± 8	0.638
LVEDVi, ml/m^2	101 ± 15	97 ± 17	0.187
LVESVi, ml/m^2	37 ± 9	37 ± 11	0.999
LVSVi, ml/m^2	62 ± 12	61 ± 12	0.710
LAEDVi, ml/m^2	23 ± 8	21 ± 5	0.324
LAESVi, ml/m^2	53 ± 14	44 ± 10	< 0.05
CMR—right heart			
RVEF, %	61 ± 10	61 ± 8	0.999
RVEDVi, ml/m^2	106 ± 21	98 ± 20	0.083
RVESVi, ml/m^2	42 ± 14	38 ± 12	0.327
RVSVi, ml/m^2	65 ± 14	60 ± 11	0.194
RAEDVi, ml/m^2	32 ± 13	31 ± 11	0.393
RAESVi, ml/ m^2	54 ± 17	52 ± 15	0.377
CMR—strain			
LV GLS, %	− 17 ± 2	− 17 ± 2	0.669
LV GCS, %	− 16 ± 4	− 18 ± 4	0.219
LV GRS, %	38 ± 13	42 ± 9	0.267
RV GLS, %	− 20 ± 4	− 18 ± 7	0.227
RV GCS, %	− 8 ± 3	− 7 ± 4	0.616
RV FW GLS, %	− 20 ± 7	− 23 ± 7	0.356
LA GLS, %	25 ± 6	23 ± 4	0.276
RA GLS, %	23 ± 6	22 ± 5	0.585
CMR—mapping			
Native T1, ms	997 ± 37	993 ± 22	0.585
Native T2, ms	53 ± 3	53 ± 2	0.815
ECV, %	26.3 ± 2.2	-	-

Numbers are mean ± SD for continuous and n (%) for categorical data

Baseline and post-race data were partly reported in previous publications as indicated in the "Methods and materials" section

Abbreviations: *BP*, blood pressure; *EF*, ejection fraction; *GCS*, global circumferential strain; *GLS*, global longitudinal strain; *GRS*, global radial strain; *LA*, left atrial; *LAEDVi*, left atrial end-diastolic volume index; *LAESVi*, left atrial entad-systolic volume index; *LV*, left ventricular; *LVEDVi*, left ventricular end-diastolic volume index; *LVESVi*, left ventricular end-systolic volume index; *RA*, right atrial; *RAEDVi*, right atrial end-diastolic volume index; *RAESVi*, right atrial end-systolic volume index; *RV*, right ventricular; *RVEDVi*, right ventricular end-diastolic volume index; *RVESVi*, right ventricular end-systolic volume index; *RV FW*, right ventricular free wall

environment [8, 19]. Further, a marathon is an utterly strenuous and extended duration continuous exercise, while our triathletes participated in open-air races with varied distances and presumably less cardiac load. Third, strain parameters are not only a measure of intrinsic myocardial contractility, but are also influenced by cardiac load (i.e., end-systolic and diastolic blood pressure, LV volume) and structure [22]. It is worth noting that a recent study aimed to compare the accuracy and reproducibility of FT-CMR and speckle tracking echocardiography (STE).

in endurance athletes [23]. The authors concluded that biventricular longitudinal strain values were lower when assessed by FT-CMR compared to STE and both methods were statistically comparable and concordant when measuring LV strain, but not RV strain [23]. Thus, while comparing strain studies, the potential influence of different imaging techniques needs to be considered. The increase in LV GCS and GRS in the current study might be a compensatory mechanism for the loss of longitudinal mechanical function, as observed in early stages of progressive myocardial disease [4].

Alterations in right ventricular strain after an endurance race

A transient deterioration of RVEF and RV GLS in athletes after an endurance race has been previously demonstrated [3, 24]. However, a more recent study by Cavigli et al investigated the acute impact of an ultra-marathon on the RV and could not identify any alterations in RV GLS [21]. Similar to Cavigli et al, we observed that RV GLS and RV FW GLS did not change between baseline and post-race [21]. Our study adds to the current scientific knowledge demonstrating that RV GCS increases after an endurance race, again as a possible intrinsic compensatory mechanism [4]. The RV end-diastolic volume decreased post-race, possibly followed by an adaptation of myocardial deformation to maintain normal RVEF according to the Frank-Starling mechanism [25]. There may also be alterations in RV strain during different phases of post-race recovery, and the recovery time may depend on the duration and intensity of the endurance exercise.

Reduced left atrial and constant right atrial strain after an endurance race

The left atrium (LA) plays a crucial role in regulating LV filling by functioning as a reservoir for pulmonary venous return during ventricular systole and a booster pump for strengthening ventricular filling during late diastole [26]. D'Ascenzi et al reported in an echocardiographic study that while the LA volume in elite soccer players is increased compared to controls, LA GLS was similar [27].

The current study confirms these findings and extends the knowledge on LA adaptation following an endurance race demonstrating a volume decrease and attenuation in GLS. Our findings are consistent with previous echocardiographic data showing a decrease in LA volume and a reduction in peak atrial longitudinal strain post-exercise [28]. Consistently, Oxborough et al found that the indices of LA deformation and volume were reduced immediately post-race [29]. Even though immediate post-exercise echocardiography data is mostly reported, cardiac recovery might actually exceed 24 h [30]. The acquisition time point of post-race CMR in the current study was within 5 h, and exercise-induced cardiac alterations might have not fully subsided.

Further, we observed lower baseline RA strain in triathletes compared to controls. This finding is consistent with a prior echocardiographic study by D'Ascenzi et al, which implies that the reduction of RA GLS in athletes represents a physiological adaptation rather than an abnormality [31]. Athlete's atria are at lower strain and larger volumes facilitating a larger atrial stroke volume reserve [32]. Post-race RA GLS did not change in this study, which is partially in line with the study by Sanz-de et al, who investigated the exercise-dose-dependent impairment in atrial function [33]. An exercise load of 14 km showed no changes of post-race RA strain, but higher exercise loads induced impairment in atrial contractile function [33].

Ventricular and atrial strain in LGE + male triathletes at baseline and after an endurance race

It has been suggested that repetitive and sustained exposure to high-intensity exercise might induce cardiac microdamage associated with development of myocardial fibrosis [34]. A notion that is supported by the high prevalence of focal myocardial fibrosis in athletes detected by CMR LGE imaging [3, 35]. A subgroup analysis of male triathletes with focal myocardial fibrosis (LGE +) showed no differences at baseline and post-race regarding biventricular and biatrial strain parameters. Similarly, we previously reported that three CMR-derived variables reflecting diastolic function—early peak filling rate, atrial peak filling rate (APFR), and peak filling rate ratio (PFRR)—remained stable post-race in LGE + triathletes, whereas higher APFR and reduced PFRR were observed in LGE − triathletes [16]. Further, we previously reported on increased extracellular volume in the subgroup of LGE + triathletes, which might be indicative of increased myocardial stiffness [14, 16]. Thus, a possible explanation for the missing alterations between baseline and post-race biventricular and LA strain in LGE + male triathletes might be an increased myocardial stiffness.

Study limitations

Our study has several limitations. First, this study had a relatively small sample size, which might increase the potential of type I and II errors. Second, the subjects enrolled in the present study were predominantly male triathletes. Currently, most of our knowledge on race-induced myocardial injury is also based on male athletes, due to the paucity of data on female subjects. Further studies are needed to close this gap of knowledge. Third, the study ruled out triathletes with pre-existing cardiovascular and systemic diseases, limiting its generalizability. Finally, compressed sensing might alternate strain values; subsequent studies should clarify whether strain values would be dependent on sense factors.

Clinical implications

In this study, an endurance race led to acute alterations of biventricular and LA strain, which might be one of the mechanisms leading to an athletic cardiac remodeling. Also, it can be assumed that chronic athletic activity might be associated with an increased incidence of LGE, a potential substrate for cardiac arrhythmia. Subsequent studies should longitudinally monitor the persistence of post-race strain alterations and correlate with possible major adverse cardiac events.

Conclusions

This prospective study analyzed the post-race changes in biventricular and biatrial myocardial strain in competitive male and female triathletes. Although there were no differences between baseline and post-race LVEF and RVEF, the alterations of biventricular and left atrial strain parameters might be a possible intrinsic compensatory mechanism following an acute bout of endurance exercise rather than myocardial dysfunction. Furthermore, there were no alterations between baseline and post-race biventricular and biatrial strain parameters in male triathletes with focal myocardial fibrosis (LGE +), which might be due to increased myocardial stiffness. The combined use of strain parameters may allow a better characterization of ventricular and atrial function at rest and post-exercise as well as the cardiac adaptation mechanisms in endurance athletes.

Supplementary Information The online version contains supplementary material available at https://doi.org/10.1007/s00330-021-08401-y.

Funding Open Access funding enabled and organized by Projekt DEAL.

Declarations

Guarantor The scientific guarantor of this publication is Enver Tahir, MD.

Conflict of interest The authors of this manuscript declare no relationships with any companies whose products or services may be related to the subject matter of the article.

Statistics and biometry No complex statistical methods were necessary for this paper.

Informed consent All participants gave their written informed consent before being included in this study.

Ethical approval The ethics committee of the general medical council approved the study (PV4764).

Study subjects or cohorts overlap CMR findings including baseline exercise test parameters, ventricular volumes, T1 relaxation times, and distribution of focal myocardial fibrosis visualized by late gadolinium enhancement (LGE) imaging of male and female triathletes as well as LV strain values of male triathletes were reported in two previous publications. A third follow-up publication on 30 male triathletes described post-race ventricular and atrial volumes, diastolic LV filling patterns, and T1/T2 relaxation times.

The current study expands the number of triathletes by $N=20$. Apart from $N=10$ additional male triathletes (one with focal myocardial fibrosis), the current study also includes $N=10$ female triathletes.
The current study focuses on the alterations of left ventricular, right ventricular, and left atrial strain in male and female triathletes as well as in athletes with focal myocardial fibrosis (LGE+) following an endurance race.

Methodology
- prospective
- observational
- performed at one institution

References

1. Scharf M, Brem MH, Wilhelm M, Schoepf UJ, Uder M, Lell MM (2010) Atrial and ventricular functional and structural adaptations of the heart in elite triathletes assessed with cardiac MR imaging. Radiology 257:71–79
2. Scharf M, Brem MH, Wilhelm M, Schoepf UJ, Uder M, Lell MM (2010) Cardiac magnetic resonance assessment of left and right ventricular morphologic and functional adaptations in professional soccer players. Am Heart J 159:911–918
3. La Gerche A, Burns AT, Mooney DJ et al (2012) Exercise-induced right ventricular dysfunction and structural remodelling in endurance athletes. Eur Heart J 33:998–1006
4. Claus P, Omar AMS, Pedrizzetti G, Sengupta PP, Nagel E (2015) Tissue tracking technology for assessing cardiac mechanics: principles, normal values, and clinical applications. JACC Cardiovasc Imaging 8:1444–1460
5. Taylor RJ, Moody WE, Umar F et al (2015) Myocardial strain measurement with feature-tracking cardiovascular magnetic resonance: normal values. Eur Heart J Cardiovasc Imaging 16:871–881
6. Caselli S, Montesanti D, Autore C et al (2015) Patterns of left ventricular longitudinal strain and strain rate in olympic athletes. J Am Soc Echocardiogr 28:245–253
7. Lo Iudice F, Petitto M, Ferrone M et al (2017) Determinants of myocardial mechanics in top-level endurance athletes: three-dimensional speckle tracking evaluation. Eur Heart J Cardiovasc Imaging 18:549–555
8. Stewart GM, Chan J, Yamada A et al (2017) Impact of high-intensity endurance exercise on regional left and right ventricular myocardial mechanics. Eur Heart J Cardiovasc Imaging 18:688–696
9. Starekova J, Thottakara T, Lund GK et al (2020) Increased myocardial mass and attenuation of myocardial strain in professional male soccer players and competitive male triathletes. Int J Cardiovasc Imaging 36:2187–2197
10. Swoboda PP, Erhayiem B, McDiarmid AK et al (2016) Relationship between cardiac deformation parameters measured by cardiovascular magnetic resonance and aerobic fitness in endurance athletes. J Cardiovasc Magn Reson 18:48
11. Chan-Dewar F, Oxborough D, Shave R, Gregson W, Whyte G, George K (2010) Left ventricular myocardial strain and strain rates in sub-endocardial and sub-epicardial layers before and after a marathon. Eur J Appl Physiol 109:1191–1196
12. Balmain BN, Sabapathy S, Yamada A et al (2021) Cardiac perturbations after high-intensity exercise are attenuated in middle-aged compared with young endurance athletes: diminished stress or depleted stimuli? Am J Physiol Heart Circ Physiol 320:H159–H168
13. Christou GA, Pagourelias ED, Anifanti MA et al (2020) Exploring the determinants of the cardiac changes after ultra-long duration exercise: the echocardiographic Spartathlon study. Eur J Prev Cardiol 27:1467–1477
14. Tahir E, Starekova J, Muellerleile K et al (2018) Myocardial fibrosis in competitive triathletes detected by contrast-enhanced CMR correlates with exercise-induced hypertension and competition history. JACC Cardiovasc Imaging 11:1260–1270
15. Tahir E, Starekova J, Muellerleile K et al (2019) Impact of myocardial fibrosis on left ventricular function evaluated by feature-tracking myocardial strain cardiac magnetic resonance in competitive male triathletes with normal ejection fraction. Circ J 83:1553–1562
16. Tahir E, Scherz B, Starekova J et al (2020) Acute impact of an endurance race on cardiac function and biomarkers of myocardial injury in triathletes with and without myocardial fibrosis. Eur J Prev Cardiol 27:94–104
17. Lam HV, Groth M, Mir T et al (2020) Impact of chest wall deformity on cardiac function by CMR and feature-tracking strain analysis in paediatric patients with Marfan syndrome. Eur Radiol. https://doi.org/10.1007/s00330-020-07616-9
18. Leng S, Tan RS, Zhao X, Allen JC, Koh AS, Zhong L (2018) Validation of a rapid semi-automated method to assess left atrial

longitudinal phasic strains on cine cardiovascular magnetic resonance imaging. J Cardiovasc Magn Reson 20:71
19. Vitiello D, Cassirame J, Menetrier A et al (2013) Depressed systolic function after a prolonged and strenuous exercise. Med Sci Sports Exerc 45:2072–2079
20. Aengevaeren VL, Froeling M, Hooijmans MT et al (2020) Myocardial injury and compromised cardiomyocyte integrity following a marathon run. JACC Cardiovasc Imaging 13:1445–1447
21. Cavigli L, Zorzi A, Spadotto V et al (2021) The acute effects of an ultramarathon on biventricular function and ventricular arrhythmias in master athletes. Eur Heart J Cardiovasc Imaging. https://doi.org/10.1093/ehjci/jeab017
22. Ferferieva V, Van den Bergh A, Claus P et al (2012) The relative value of strain and strain rate for defining intrinsic myocardial function. Am J Physiol Heart Circ Physiol 302:H188-195
23. Domenech-Ximenos B, Sanz-de la Garza M, Sepulveda-Martinez A et al (2021) Assessment of myocardial deformation with CMR: a comparison with ultrasound speckle tracking. Eur Radiol. https://doi.org/10.1007/s00330-021-07857-2
24. Neilan TG, Januzzi JL, Lee-Lewandrowski E et al (2006) Myocardial injury and ventricular dysfunction related to training levels among nonelite participants in the Boston marathon. Circulation 114:2325–2333
25. La Gerche A, Jurcut R, Voigt JU (2010) Right ventricular function by strain echocardiography. Curr Opin Cardiol 25:430–436
26. Hoit BD (2014) Left atrial size and function: role in prognosis. J Am Coll Cardiol 63:493–505
27. D'Ascenzi F, Cameli M, Zaca V et al (2011) Supernormal diastolic function and role of left atrial myocardial deformation analysis by 2D speckle tracking echocardiography in elite soccer players. Echocardiography 28:320–326
28. Santoro A, Alvino F, Antonelli G, Molle R, Mondillo S (2016) Left atrial strain after maximal exercise in competitive waterpolo players. Int J Cardiovasc Imaging 32:399–405
29. Oxborough D, Whyte G, Wilson M et al (2010) A depression in left ventricular diastolic filling following prolonged strenuous exercise is associated with changes in left atrial mechanics. J Am Soc Echocardiogr 23:968–976
30. Stewart GM, Yamada A, Haseler LJ et al (2016) Influence of exercise intensity and duration on functional and biochemical perturbations in the human heart. J Physiol 594:3031–3044
31. D'Ascenzi F, Cameli M, Padeletti M et al (2013) Characterization of right atrial function and dimension in top-level athletes: a speckle tracking study. Int J Cardiovasc Imaging 29:87–94
32. Gabrielli L, Bijnens BH, Butakoff C et al (2014) Atrial functional and geometrical remodeling in highly trained male athletes: for better or worse? Eur J Appl Physiol 114:1143–1152
33. Sanz-de la Garza M, Grazioli G, Bijnens BH et al (2016) Acute, exercise dose-dependent impairment in atrial performance during an endurance race: 2D ultrasound speckle-tracking strain analysis. JACC Cardiovasc Imaging 9:1380–1388
34. van de Schoor FR, Aengevaeren VL, Hopman MT et al (2016) Myocardial fibrosis in athletes. Mayo Clin Proc 91:1617–1631
35. Breuckmann F, Möhlenkamp S, Nassenstein K et al (2009) Myocardial late gadolinium enhancement: prevalence, pattern, and prognostic relevance in marathon runners. Radiology 251:50–57

Supplemental Table 1: Demographics and CMR parameters of LGE- triathletes at baseline and post-race.

	Baseline LGE- (n= 29)	**Post-race** LGE- (n= 29)	***p* value**
Clinical parameters			
Body surface area, m²	2.03 ±0.13	2.01 ±0.13	<0.05
Troponin T, pg/ml	6 ±3	54 ±87	<0.01
NT-proBNP, pg/ml	30 ±21	100 ±58	<0.0001
CK, U/l	237 ±172	547 ±305	<0.0001
CK-MB, U/l	14 ±16	34 ±17	<0.0001
Systolic BP at rest, mmHg	125 ±11	-	-
Diastolic BP at rest, mmHg	85 ±9	-	-
CMR – left heart			
Heart rate, bpm	53 ±8	69 ±10	<0.0001
LV cardiac index, l/min/m^2	3.26 ±0.59	3.94 ±0.61	<0.0001
LVEF, %	60 ±5	61 ±7	0.434
LV mass index, g/m²	77 ±10	78 ±11	0.228
LVEDVi, ml/m²	102 ±16	95 ±15	<0.01
LVESVi, ml/m²	41 ±9	37 ±11	<0.05
LVSVi, ml/m²	61 ±10	58 ±9	0.113
LAEDVi, ml/m²	19 ±9	15 ±6	<0.01
LAESVi, ml/m²	46 ±12	34 ±9	<0.0001
CMR – right heart			
RVEF, %	57 ±8	58 ±8	0.317
RVEDVi, ml/m²	104 ±18	101 ±19	0.302
RVESVi, ml/m²	46 ±14	44 ±14	0.072
RVSVi, ml/m²	58 ±9	57 ±9	0.864
RAEDVi, ml/m²	28 ±9	28 ±11	0.879
RAESVi, ml/ m²	51 ±13	46 ±11	<0.01
CMR – Strain			
LV GLS, %	-17 ±2	-16 ±2	<0.05
LV GCS, %	-15 ±3	-16 ±3	<0.01
LV GRS, %	36 ±8	41 ±9	<0.05
RV GLS, %	-19 ±3	-20 ±5	0.562
RV GCS, %	-7 ±2	-7 ±3	0.068
RV FW, %	-20 ±6	-20 ±8	0.644
LA GLS, %	29 ±7	23 ±6	<0.001
RA GLS, %	24 ±5	23 ±6	0.344
CMR – Mapping			
Native T1, ms	978 ±21	985 ±19	0.229
Native T2, ms	53 ±2	52 ±4	0.394
ECV, %	24.9 ±1.5	-	-

Numbers are mean ±SD for continuous and n (%) for categorical data.

Baseline and post-race data were partly reported in previous publications as indicated in the materials and methods section.

Abbreviations: as in Table 1.

Supplementary Material

Previously reported data

The initial publication reported on 54 male and 29 female triathletes and included baseline exercise test parameters, ventricular volumes, T1 relaxation times, and incidence and distribution of focal LV myocardial fibrosis visualized by late gadolinium enhancement (LGE) imaging [1]. Nine of the male triathletes (17%) had focal myocardial fibrosis (LGE+) [1]. A follow-up publication reported on an expanded cohort of 78 male triathletes (19% LGE+), and the impact of focal myocardial fibrosis on global and segmental left ventricular strain [2]. A third publication focused on post-race changes in CMR parameters including ventricular and atrial volumes, diastolic LV filling patterns and T1/T2 relaxation times in thirty male triathletes only (ten LGE+) [3]. The current publication expands the post-race cohort by nine male and eleven female triathletes, including eleven LGE+ male triathletes, and focuses on post-race changes of biventricular and biatrial myocardial strain generated with the novel feature-tracking CMR technique.

Methods and Materials

Endurance race details

23 triathletes completed an Olympic distance triathlon (1.5 km swimming, 40 km cycling and 10 km running) for a cumulative time of 2.5±0.3 hours. 8 triathletes completed a marathon (42.195 km) for a cumulative time of 3.7±0.8 hours. 7 triathletes completed a sprint distance triathlon (0.5 km swimming, 20 km cycling and 5 km running) for a cumulative time of 1.3±0.2 hours. 4 triathletes completed a running competition (20.1±7.8 km) for a cumulative time of 1.7±0.8 hours. 3 triathletes completed a cycling competition (252±142 km) for a cumulative time of 9.3 ±5.5 hours. 2 triathletes completed a middle triathlon distance (2 km swimming, 80 km cycling and 20 km running) for a cumulative time of 4.7±0.1 hours. 2 triathletes completed a half marathon (21.098 km) for a cumulative time of 1.98±0.04 hours. 1 triathlete completed a duathlon (145 km cycling and 14 km running) for a cumulative time of 4.7±0.1 hours. There were no differences between the subgroups of LGE-, LGE+ and female triathletes regarding cumulative race distance (P=0.201), swimming distance (P=0.276), cycling distance (P=0.292), running distance (P=0.406) and race completion times (P=0.246).

CMR protocol

CMR was performed using a 1.5 T MR scanner equipped with a phased array surface receive coil (Achieva, Philips Healthcare).

Cine CMR – steady-state free-precession sequence

The CMR protocol included standard steady-state free-precession cine CMR in short axis for LV and right ventricle (RV) volumetry and LV mass with the following typical imaging parameters: acquired voxel size (AVS) 1.98 x 1.80 x 6 mm^3, reconstructed voxel size (RVS) 1.36 x 1.36 x 6 mm^3, gap 4 mm, 9-10 slices for full LV coverage, echo time = 1.67 ms, time to repetition = 3.34 ms, flip angle = 60°, sense factor, 2.0; 25 phases per RR interval.

T1 Mapping – MOLLI sequence

T1 mapping was performed using a Modified Look Locker Inversion Recovery (MOLLI) sequence with a 5s(3s)3s scheme on three short-axes slices (apical, mid and basal) before and 15 minutes after contrast-media administration as described before [1]. Typical imaging parameters were as follows: 1.97 x 2.00 x 10 mm^3, RVS 1.17 x 1.17 x 10 mm^3, 3 slices, echo time = 1.59 ms, time to repetition = 3.17 ms, flip angle = 35°, SENSE factor = 2, linear phase encoding, ten start-up cycles to approach steady-state prior to imaging, effective inversion times between 188 and 3382 ms.

T2-mapping – GraSE sequence

T2-mapping was performed before administration of contrast-media on identical three end-diastolic LV short-axes, corresponding to the MOLLI slices using a gradient- (echo planar imaging) and spin-echo multi-echo sequence (GraSE) in three short-axis sections [4]. Typical imaging parameters of the GraSE sequence were: Voxel size 1.05 x 1.05 x 10 mm^3, 3 slices, nine echoes with effective echo times between 12.5 and 62.4 ms, time to repetition = 800 ms (1 RR interval), one breath-hold per slice.

LGE imaging – phase-sensitive inversion recovery – PSIR sequence

Ten minutes after bolus injection of 0.2 mmol/kg gadoter acid (Dotarem®, Guerbet, Sulzbach, Germany) at a rate of 2.5 ml/s end-diastolic LGE images were acquired using end-diastolic phase-sensitive inversion recovery (PSIR) sequences: AVS 1.59 x 1.71 x 8 mm^3, RVS 0.97 x 0.98 x 8 mm^3, gap 2 mm, 9-10 slices, echo time = 2.40 ms,

time to repetition = 5.50 ms, flip angle = 15°. The optimal inversion delay was obtained from a Look-Locker experiment. LGE images were acquired in short-axis orientation covering the entire heart and in two-, three- and four-chamber views.

CMR data analysis

Two investigators (H.C. and M.W. with 3 and 4 years of experience in CMR, respectively) independently and blindly analyzed each CMR using a commercially available software (CVi42, Circle Cardiovascular Imaging Inc.). CMR parameters were indexed to the calculated body surface area (BSA) and are given as the mean of the two observers. Evaluation of LV and RV volumes and LV mass was performed in standard fashion on the short-axis cine stack [5]. The epicardial and endocardial borders of the myocardium were manually traced on end-diastolic and end-systolic images at each anatomic level encompassing the entire heart from apex to base. Trabeculae and papillary muscles were included in the ventricular volumes and excluded from the myocardial mass for reproducibility [6]. LV mass was calculated by multiplying the myocardial volume by the specific weight of cardiac muscle (1.05 mg/mL) [5]. Left (LA) and right atrial (RA) volumes and were quantified using the biplane area-length method, excluding pulmonary veins and atrial appendage [7]. Presence of LGE was analyzed visually [5]. Native T1, post-contrast T1 and ECV maps were generated using a dedicated plug-in written for the OsiriX™ software [8]. Native T1, post contrast T1 and ECV were obtained by averaging measures from basal and midventricular short-axis slices to yield final measurements [9]. Meticulous care was taken not to include the blood volume into the measurements to avoid partial volume effects [9]. Areas of focal LGE were excluded from T1 and ECV measurements to evaluate these parameters unbiased from presence of LGE. ECV was calculated using the previously established equation [10-13].

$$ECV = [1\text{-hematocrit}] * [\Delta R1]_{myocardium} / [\Delta R1]_{blood\ pool}$$

In this equation, R1 is defined as 1/T1 and Δ as the difference between pre- and late post-contrast R1 values [10-13]. Hematocrit was measured from a venous blood sample taken on the same day of CMR scan.

Data Supplement References

1 Tahir E, Starekova J, Muellerleile K et al (2018) Myocardial Fibrosis in Competitive Triathletes Detected by Contrast-Enhanced CMR Correlates With Exercise-Induced Hypertension and Competition History. JACC Cardiovasc Imaging 11:1260-1270

2 Tahir E, Starekova J, Muellerleile K et al (2019) Impact of Myocardial Fibrosis on Left Ventricular Function Evaluated by Feature-Tracking Myocardial Strain Cardiac Magnetic Resonance in Competitive Male Triathletes With Normal Ejection Fraction. Circ J 83:1553-1562

3 Tahir E, Scherz B, Starekova J et al (2020) Acute impact of an endurance race on cardiac function and biomarkers of myocardial injury in triathletes with and without myocardial fibrosis. Eur J Prev Cardiol 27:94-104

4 Baessler B, Schaarschmidt F, Stehning C, Schnackenburg B, Maintz D, Bunck AC (2015) Cardiac T2-mapping using a fast gradient echo spin echo sequence - first in vitro and in vivo experience. J Cardiovasc Magn Reson 17:67

5 Schulz-Menger J, Bluemke DA, Bremerich J et al (2020) Standardized image interpretation and post-processing in cardiovascular magnetic resonance - 2020 update : Society for Cardiovascular Magnetic Resonance (SCMR): Board of Trustees Task Force on Standardized Post-Processing. J Cardiovasc Magn Reson 22:19

6 Papavassiliu T, Kuhl HP, Schroder M et al (2005) Effect of endocardial trabeculae on left ventricular measurements and measurement reproducibility at cardiovascular MR imaging. Radiology 236:57-64

7 Le TT, Tan RS, De Deyn M et al (2016) Cardiovascular magnetic resonance reference ranges for the heart and aorta in Chinese at 3T. J Cardiovasc Magn Reson 18:21

8 Radunski UK, Lund GK, Stehning C et al (2014) CMR in patients with severe myocarditis: diagnostic value of quantitative tissue markers including extracellular volume imaging. JACC Cardiovasc Imaging 7:667-675

9 Schelbert EB, Piehler KM, Zareba KM et al (2015) Myocardial Fibrosis Quantified by Extracellular Volume Is Associated With Subsequent Hospitalization for Heart Failure, Death, or Both Across the Spectrum of Ejection Fraction and Heart Failure Stage. J Am Heart Assoc 4

10 Ugander M, Oki AJ, Hsu LY et al (2012) Extracellular volume imaging by magnetic resonance imaging provides insights into overt and sub-clinical myocardial pathology. Eur Heart J 33:1268-1278

11 Arheden H, Saeed M, Higgins CB et al (1999) Measurement of the distribution volume of gadopentetate dimeglumine at echo-planar MR imaging to quantify myocardial infarction: comparison with 99mTc-DTPA autoradiography in rats. Radiology 211:698-708

12 Schelbert EB, Testa SM, Meier CG et al (2011) Myocardial extravascular extracellular volume fraction measurement by gadolinium cardiovascular magnetic resonance in humans: slow infusion versus bolus. J Cardiovasc Magn Reson 13:16

13 Kellman P, Wilson JR, Xue H et al (2012) Extracellular volume fraction mapping in the myocardium, part 2: initial clinical experience. J Cardiovasc Magn Reson 14:64

3 Chapter 3: Publication in *European Journal of Radiology*, November 2022

Left ventricular diastolic filling patterns in competitive triathletes with and without myocardial fibrosis by cardiac magnetic resonance time-volume analysis

Hang Chen, Johanna Jungesblut, Dennis Saering, Kai Muellerleile, Antonia Beitzen-Heineke, Phillip Harms, Jennifer Erley, Bjoern Schoennagel, Jan N. Schneider, Ersin Cavus, Roland Fischer, Gunnar K. Lund, Gerhard Adam, Enver Tahir

Personal contribution:

The following research article has been published in ***European journal of Radiology***. I am the first author of the paper. I contributed the conceptualization of the study together with other co-authors and corresponding author. I post-processed and analyzed the image data. I contributed to the manuscript draft and revisions, figures, and tables preparation.

European Journal of Radiology 158 (2023) 110615

Contents lists available at ScienceDirect

European Journal of Radiology

journal homepage: www.elsevier.com/locate/ejrad

Left ventricular diastolic filling patterns in competitive triathletes with and without myocardial fibrosis by cardiac magnetic resonance time-volume analysis

Hang Chen [a], Johanna Jungesblut [a], Dennis Saering [b], Kai Muellerleile [c], Antonia Beitzen-Heineke [d], Phillip Harms [a], Jennifer Erley [a], Bjoern Schoennagel [a], Jan N. Schneider [c], Ersin Cavus [c], Roland Fischer [e,f], Gunnar K. Lund [a], Gerhard Adam [a], Enver Tahir [a,*]

[a] Department of Diagnostic and Interventional Radiology and Nuclear Medicine, University Hospital Hamburg Eppendorf, Hamburg, Germany
[b] Information Technology and Image Processing, University of Applied Sciences, Wedel, Germany
[c] Department of General and Interventional Cardiology, University Heart Center, Hamburg, Germany
[d] Department of Oncology, Hematology, BMT with Department of Pneumology, University Medical Center Hamburg, Hamburg, Germany
[e] Department of Pediatric Hematology and Oncology, University Hospital Hamburg-Eppendorf, Germany
[f] UCSF, Benioff Children's Hospital Oakland, USA

ARTICLE INFO

Keywords:
Cardiac magnetic resonance
Athletes
Cine
Diastolic function

ABSTRACT

Purpose: To investigate the influence of myocardial fibrosis on left ventricular (LV) diastolic filling patterns in triathletes compared to sedentary controls by cardiac magnetic resonance (CMR) imaging.
Method: 101 male triathletes (43 ± 11 years) and 28 controls (41 ± 10 years) were recruited and underwent 1.5 T CMR including cine SSFP series, late gadolinium enhancement (LGE) imaging and T1 mapping. Functional and morphological parameters were obtained, and CMR-based LV diastolic filling parameters such as the early peak-filling rate (EPFR), atrial peak-filling rate (APFR) and peak-filling rate ratio (PFRR = EPFR/APFR) were determined by time-volume analysis of the cine series.
Results: Non-ischemic LGE was detected in 20 triathletes (20 %) and in none of the controls. Compared to controls LGE-negative (LGE-) triathletes showed similar EPFR (216 ± 58 ml/s/m^2 vs 224 ± 69 ml/s/m^2, P = 0.52) but lower APFR (120 ± 46 ml/s/m^2 vs 147 ± 55 ml/s/m^2, $P < 0.05$), resulting in higher PFRR (2.1 ± 1 vs 1.6 ± 0.5, $P < 0.01$). LGE-positive (LGE +) triathletes had similar EPFR (212 ± 73 ml/s/m^2, $P = 0.798$), but higher APFR (149 ± 50 ml/s/m^2, $P < 0.05$) and decreased PFRR (1.6 ± 0.7, $P < 0.05$) compared to LGE- triathletes. LGE + triathletes had increased LV mass index (88 ± 10 g/m^2 vs 80 ± 12 g/m^2, $P < 0.01$) and extracellular volume (ECV) fraction (26.2 ± 2.7 % vs 24.4 ± 1.7 %, $P < 0.001$) compared to LGE- triathletes.
Conclusions: Athletic activity leads to "supernormal" LV diastolic filling pattern in LGE- triathletes, which may be attributable to increased LV myocardial flexibility and elasticity. However, LGE + triathletes demonstrate a pseudo-normalization characterized by compensatory increase of atrial contraction. Possibly, due to reduced passive elasticity associated myocardial fibrosis.

1. Introduction

Cardiac adaptation in athletes induced by endurance exercise is a well-known physiologic phenomenon [1–3]. However, there is a high incidence of myocardial fibrosis in endurance athletes compared to the sedentary general population [2,4,5]. Cardiac magnetic resonance

* Corresponding author at: Department of Diagnostic and Interventional Radiology and Nuclear Medicine University Hospital Hamburg Eppendorf Martinistr. 52 20246 Hamburg, Germany.
E-mail addresses: hang.chen@stud.uke.uni-hamburg.de (H. Chen), johanna.jungesblut@web.de (J. Jungesblut), dennis.saering@fh-wedel.de (D. Saering), kaiml@web.de (K. Muellerleile), a.beitzen-heineke@uke.de (A. Beitzen-Heineke), ph.harms@uke.de (P. Harms), j.erley@uke.de (J. Erley), b.schoennagel@uke.de (B. Schoennagel), j.schneider@uke.de (J.N. Schneider), e.cavus@uke.de (E. Cavus), fischer@uke.de (R. Fischer), g.lund@uke.de (G.K. Lund), g.adam@uke.de (G. Adam), e.tahir@uke.de (E. Tahir).

https://doi.org/10.1016/j.ejrad.2022.110615
Received 12 September 2022; Received in revised form 25 October 2022; Accepted 15 November 2022
Available online 19 November 2022

(CMR) can facilitate the evaluation of focal myocardial fibrosis by late gadolinium enhancement (LGE) imaging [6–8], diffuse myocardial fibrosis by T1 mapping and calculation of myocardial extracellular volume (ECV) fraction [9], and diastolic LV filling patterns [10]. However, there is lack of data on the influence of myocardial fibrosis in endurance athletes on the LV diastolic filling pattern by CMR.

The effect of endurance exercise on LV diastolic function among athletes of diverse ages has been evaluated in several studies to date primarily using Doppler echocardiography [3,11,12]. The ratio of LV early diastolic peak filling velocity to peak velocity during atrial contraction (E/A ratio) has been assessed and increase is well documented in endurance athletes, whereas no increase was seen in power athletes and controls [12,13]. The equivalent of the echocardiographic E/A ratio can also be determined by CMR imaging [10].

The aim of the current study was to evaluate LV diastolic functional parameters using CMR in a large cohort of triathletes compared to sedentary controls and to investigate the effect of myocardial fibrosis on LV diastolic filling patterns.

2. Material and methods

2.1. Study population

The local ethics committee (chamber of medical practitioners, PV4764) approved the study, and a written informed consent was provided by all subjects. The declaration of consent to participate in the study was signed by all subjects. A total of 101 male triathletes (43 ± 11 years, range 18–66 years) and 28 controls (41 ± 10 years, range 20–61 years) were recruited from 2014 to 2019. All triathletes were contacted through advertisement in local triathlon clubs. Inclusion criteria were endurance training for a minimum of 10 h per week and participation in competitions in the last 3 years. Control subjects were eligible, if they engaged in<3 h of exercise per week [14]. Study exclusion criteria were contraindications for CMR, systemic diseases or cardiovascular diseases. Participants were instructed to refrain from any exercise and alcohol consumption in the preceding 72 h. Any food and caffeine intake were restricted in the preceding 3 h before CMR scan [14].

The study population partly consisted of individuals who have been evaluated in previously published studies, which focused on incidence of LGE in triathletes in correlation to exercise-induced hypertension and competition history [14], impact of myocardial fibrosis on left ventricular strain [15], post-race changes in cardiac volumes, diastolic LV filling patterns and T1/T2 relaxation times [16] and the acute impact of an endurance race on myocardial strain of triathletes [17]. The current publication expands the initial cohort by 47 triathletes and focuses on diastolic LV filling patterns at rest derived by CMR. Performance test was conducted on an ergometer (Ergoselect 100, Ergoline GmbH, Bitz, Germany) using a ramp protocol to determine maximal oxygen uptake (VO_{2max}) and ventilatory thresholds. Blood samples were drawn immediately before each CMR from an antecubital vein in supine position for 5 min to obtain hematocrit, high-sensitive troponin T, and *N*-terminal pro-brain natriuretic peptide (NT-proBNP) as our previously reported [14].

2.2. CMR protocol

CMR was performed on a 1.5 T scanner equipped with a 5-channel cardiac phased array receiver coil (Achieva, Phillips Healthcare, Best, the Netherlands). The CMR protocol included standard ECG-triggered steady-state free-precession (SSFP) cine sequence (25 phases of the cardiac cycle) in short axis for volumetry of the LV and RV, and myocardial mass measurement with the following typical imaging parameters: acquired voxel size 1.98x1.80x6 mm^3, reconstructed voxel size 1.36x1.36x6 mm^3, gap 4 mm, 9–10 slices for full LV coverage, echo time = 1.67 ms, time to repetition = 3.34 ms, flip angle = 60°, parallel acquisition technique = SENSE (factor 2). 10 min after a bolus injection of 0.2 mmol/kg gadoteric acid (Dotarem®, Guerbet, Sulzbach, Germany) at a rate of 2.5 ml/s end-diastolic LGE images were acquired using an end-diastolic phase-sensitive inversion recovery (PSIR) sequences in short-axis orientation covering the entire heart and in 2-, 3- and 4-chamber views. Native and contrast T1 mapping were performed applying a modified look locker inversion recovery (MOLLI) sequence with a 5 s(3 s)3s scheme on three short-axis slices before and 15 min after administration of contrast medium [14].

2.3. CMR data analysis

Two radiologists (H.C. and E.T. with 3 and 9 years of CMR experience) blindly and independently postprocessed CMR images utilizing CVi42 software (Circle Cardiovascular Imaging Inc., Calgary, Alberta, Canada). CMR parameters are given as the average of the 2 investigators and are indexed to body surface area (BSA). Evaluation of LV and RV volumes and LV mass was performed on short-axis cine images according to the 2020 SCMR recommendations [18]. Left (LA) and right atrial (RA) volumes and EF were based on the biplane area-length method [19], measurements excluded pulmonary veins and atrial appendage.

Focal myocardial fibrosis (LGE +) was quantified on short-axis LGE images using a thresholding method with a signal intensity (SI) > 5 standard deviations (SDs) above the mean value of remote normal myocardium [18]. Areas of positive LGE were excluded from myocardial T1 values and ECV measurements. ECV fraction was calculated using the previously established equation [9,18]. LV filling patterns were analyzed with a dedicated software (CMRtools®, Cardiovascular Imaging Solutions ltd, Cambs, UK) [10,16]. In brief, LV 3D volumetry was performed by delineation of the LV endocardial borders in end-diastolic, end-systolic, and mid-diastolic short-axis views (Fig. 1). Trabeculae and papillary muscles were excluded from the LV cavity for precise and standardized analysis of time-volume curve derived LV diastolic function [20]. Thus, the construction of time-volume curves of selected or all-time frames of the cardiac cycle is possible. The temporal LV volume/time (V/t) curve is acquired plotting the cavity volumes over time (Fig. 2). The differential temporal volume/time (dV/dt) curve is characterized by two diastolic peaks including the early peak-filling rate (EPFR) and the atrial peak-filling rate (APFR) (Fig. 2), which demonstrate a strong correlation with the echocardiographic *trans*-mitral early (E) and atrial (A) peak filling velocities respectively [21]. Additionally, the peak filling rate ratio (PFRR = EPFR/APFR) was determined, which is the equivalent of the echocardiographic E/A ratio [21]. EPFR and APFR reflect the maximum speed of early active LV filling and the maximum speed of late passive LV filling secondary to atrial contraction [22].

2.4. Statistical analysis

Statistical analyses were performed with SPSS (IBM SPSS Statistics, version 28.0, Armonk, NY, USA) and GraphPad software (GraphPad Prism, version 8, San Diego, CA, USA). All continuous data were checked for normality using the D'Agostino-Pearson omnibus normality test. Normally distributed variables are presented as the mean ± SD. Continuous data were compared using the independent samples *t*-test or Wilcoxon signed rank-test as appropriate. Categorical data are presented as absolute numbers and percentage and were compared using Chi2 test or Fischer's exact test as appropriate. Statistical significance was defined as $P < 0.05$.

3. Results

3.1. Demographics and CMR characteristics of triathletes and controls

There were no differences between triathletes and controls regarding age ($P = 0.343$), BSA ($P = 0.917$), Troponin T ($P = 0.201$), and NT-

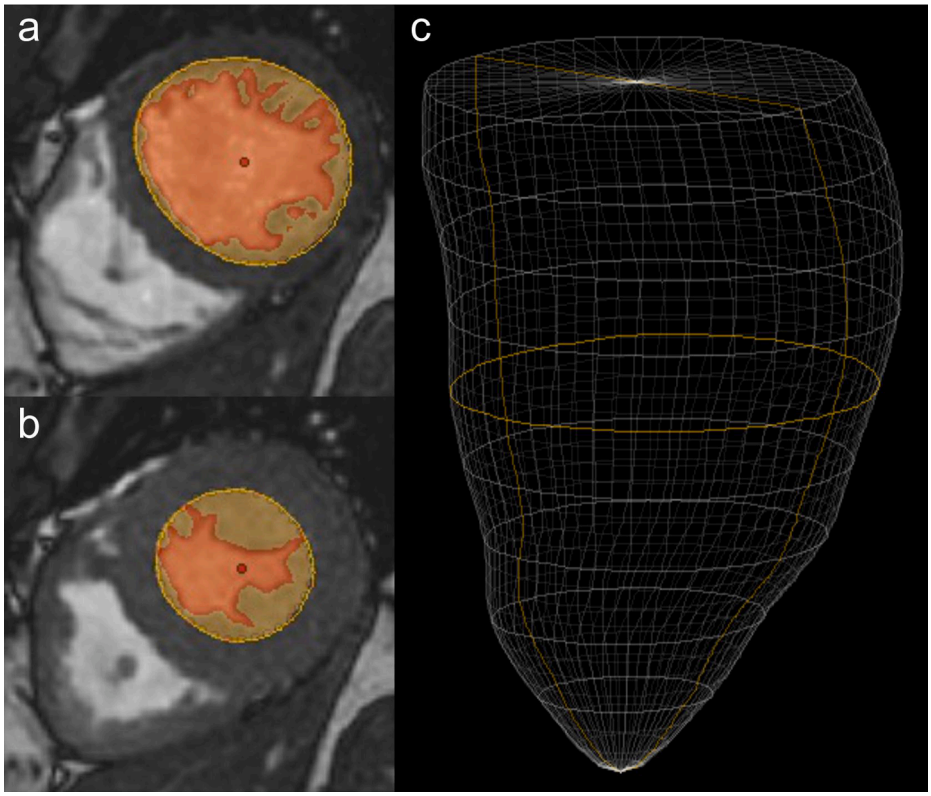

Fig. 1. 3D volumetry of the left ventricle illustrating the endocardial borders (orange line) during diastole (a) and systole (b). Endocardial borders were assessed for all slices and all cardiac phases in end-systolic, end-diastolic, and mid-diastolic short-axis views and a 3D wire model of the left ventricle was developed by dedicated software (c).

proBNP (P = 0.866) (Table 1). Exercise testing demonstrated higher peak systolic blood pressure (BP) (201 ± 29 mmHg vs 176 ± 25 mmHg, P < 0.001), VO_{2max} (53 ± 11 ml/kg/min vs 39 ± 7 ml/kg/min, P < 0.0001) and maximal power (405 ± 105 W vs 233 ± 46 W, P < 0.0001) in triathletes. Resting heart rate (HR) was lower in triathletes compared to controls (52 ± 9 bpm vs 66 ± 11 bpm, P < 0.0001). No differences were observed in systolic (P = 0.172) and diastolic BP at rest (P = 0.690), peak diastolic BP (P = 0.099) and peak HR (P = 0.989). LV CMR parameters revealed no significant differences in cardiac index (P = 0.293) and LVEF (P = 0.360) between triathletes and controls. LV mass index was higher (82 ± 12 g/m^2 vs 65 ± 9 g/m^2, P < 0.0001) and biventricular volumes were increased in triathletes compared to controls (Table 1). Triathletes had elevated atrial volumes, but LAEF (P = 0.179) and RAEF (P = 0.233) were similar (Table 1). Tissue characteristics showed that myocardial native T1 (983 ± 27 ms vs 1021 ± 31 ms, P < 0.0001) was decreased in triathletes compared to controls, but ECV fraction was similar (24.8 ± 2.1 % vs 23.9 ± 2.7 %, P = 0.109).

CMR-based LV diastolic filling analysis showed that early peak-filling rate was similar between triathletes and controls (215 ± 61 ml/s/m^2 vs 224 ± 69 ml/s/m^2, P = 0.484). Triathletes had a lower atrial peak-filling rate compared to controls (125 ± 48 ml/s/m^2 vs 147 ± 55 ml/s/m^2, P < 0.05), whereas peak-filling rate ratio was higher (1.97 ± 0.99 vs 1.63 ± 0.49, P < 0.05) (Table 1).

3.2. Prevalence and pattern of LGE in triathletes

Non-ischemic LGE was detected in 20 of the 101 triathletes (20 %), but in none of the controls. The LGE pattern was previously reported in detail [14,15]. LGE + areas were predominantly located in antero-lateral, inferolateral, and inferior segments of the basal left ventricular wall, in accordance with a distribution typical for myocarditis and LGE volume was 3.6 ± 2.4 % of the LV.

3.3. CMR characteristics of LGE- and LGE + triathletes

LGE + triathletes were older compared to LGE- triathletes (49 ± 8 years vs 42 ± 11 years, P < 0.01). BSA (P = 0.958), hsTnT (P = 0.661) and NT-proBNP (P = 0.057) were similar between both groups (Table 2). On exercise testing peak systolic BP was higher in LGE + triathletes compared to LGE- triathletes (218 ± 24 mmHg vs 196 ± 29 mmHg, P < 0.01). No differences were found in VO_{2max} (54 ± 11 ml/kg/min vs 51 ± 9 ml/kg/min, P = 0.338) and maximal power (414 ± 108 W vs 367 ± 82 W, P = 0.08; Table 2) between groups. LGE + triathletes had a higher LV mass index (88 ± 10 g/m^2 vs 80 ± 12 g/m^2, P < 0.01). No significant differences were found between LGE + and LGE- triathletes regarding ventricular and atrial functional and volume analyses. However, a significant decline in LAEF in LGE + triathletes was not evident in LGE- triathletes compared to controls, LA volume in LGE + triathletes was markedly increased compared to controls as well. Further, LGE + triathletes had increased myocardial native T1 (997 ± 40 ms vs 979 ± 21 ms, P < 0.01) and ECV fraction (26.2 ± 2.7 % vs 24.4 ± 1.7 %, P < 0.001) compared to LGE- triathletes (Table 2).

CMR-based LV diastolic filling analysis showed that LGE + and LGE- triathletes had a similar early peak-filling rate (212 ± 73 ml/s/m^2 vs 216 ± 58 ml/s/m^2, P = 0.798). However, atrial peak-filling rate (149 ± 50 ml/s/m^2 vs 120 ± 46 ml/s/m^2, P < 0.05) was higher and resulting peak-filling rate ratio (1.56 ± 0.67 vs 2.07 ± 1.03, P < 0.05) was lower in LGE + triathletes. LGE- triathletes had similar early peak-filling rate (P = 0.520) as controls, whereas atrial peak-filling rate (120 ± 46 ml/s/m^2 vs 147 ± 55 ml/s/m^2, P < 0.05) was lower and peak-filling rate ratio (2.07 ± 1.03 vs 1.63 ± 0.49, P < 0.01) higher. LGE + triathletes had similar early peak-filling rate (P = 0.547), atrial peak-filling rate (P = 0.914) and peak-filling rate ratio (P = 0.703) compared to controls (Table 2). The comparisons for CMR-based diastolic filling parameters are presented in Fig. 3.

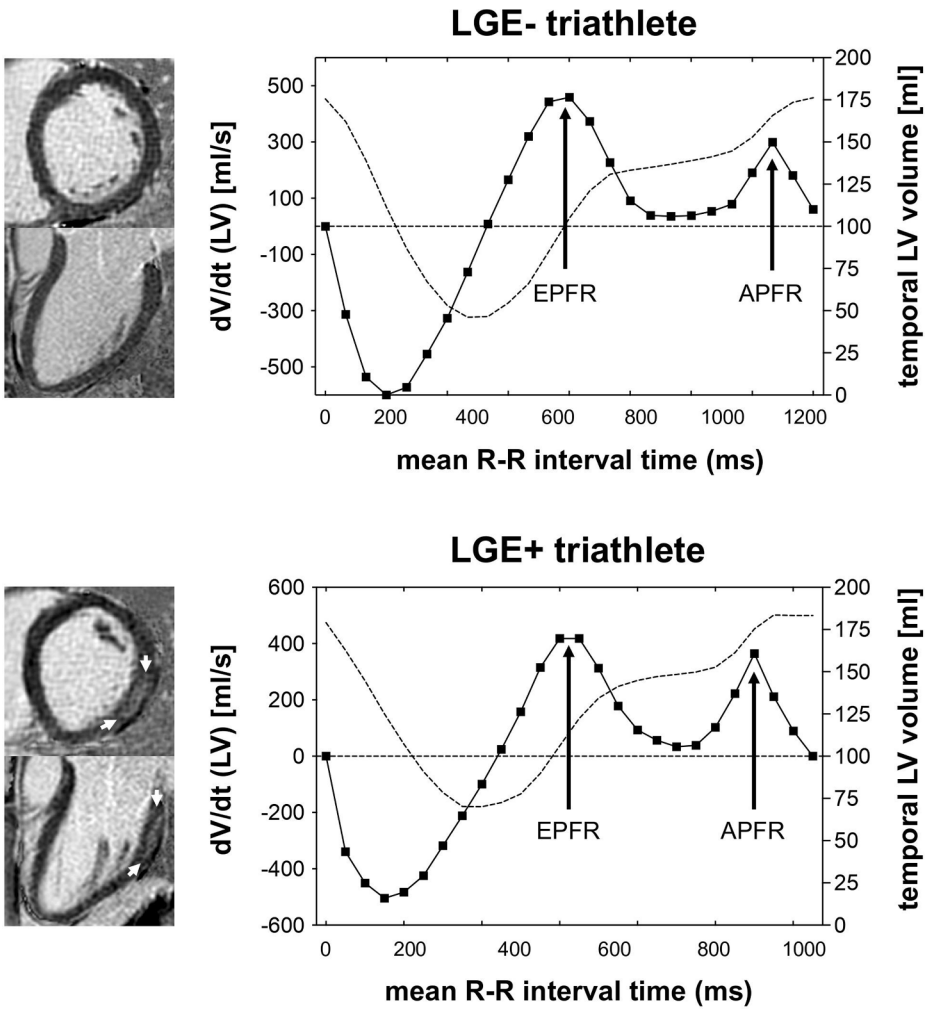

Fig. 2. The temporal volume/time (V/t) curve (dashed line) and differential temporal volume/time (dV/dt) curve (solid line) of left ventricle analyzed in LGE- triathletes (upper row) and LGE + triathletes (lower row) using cine images. From the left ventricular V/t curve, the temporal LV volume is measured as shown. The differential dV/dt curve is characterized by 2 diastolic peaks including the early peak-filling rate (EPFR) and the atrial peak-filling rate (APFR). The LGE- triathlete had normal EPFR and lower APFR, whereas the LGE + triathlete had increased APFR.

4. Discussion

This prospective, observational study investigated the CMR-based LV diastolic filling patterns in male triathletes, and the influence of focal and diffuse myocardial fibrosis assessed by LGE and T1 mapping. The principal findings are as follows: (1) 20 % of male triathletes had focal myocardial fibrosis (LGE +), and demonstrated significantly increased LV mass and ECV fraction compared to LGE- triathletes; (2) LV diastolic filling pattern in LGE- triathletes was characterized by decreased atrial peak-filling rate and resulting increased peak-filling rate ratio compared to sedentary controls; (3) LGE + triathletes however demonstrated a LV diastolic filling pattern different to LGE- triathletes and similar to sedentary controls, which was characterized by increased atrial contraction rates and consequently decreased peak-filling rate ratio. Thus, we presume that focal and diffuse myocardial fibrosis in endurance athletes have influences on LV diastolic function and may lead to a "pseudo-normalization" possibly associated with reduced passive elasticity of the hypertrophied left ventricle.

4.1. LGE in triathletes

Increased prevalence of myocardial fibrosis detected by CMR-LGE in highly trained endurance athletes has been reported in several studies [6,8,23]. Focal myocardial fibrosis (LGE +) was observed in 20 % of triathletes and none of controls in the current study, the incidence of LGE + is in concordance with the previous literature reporting 0 % to 50 % of asymptomatic athletes [6–8,23,24]. Domenech-Ximenos et al. investigated 93 highly trained triathletes and demonstrated that 35 triathletes (37.6 %) had LGE, and LGE was more prevalent in athletes than in controls [6]. A study by Bohm et al. revealed that LGE was only detected in one of 33 athletes (3 %), the authors claimed that long-term intensive endurance training seems not to be associated with myocardial fibrosis [8]. Wilson et al. reported LGE in 6 (50 %) of a small cohort of veteran endurance athletes [23], while LGE was not identified in 13 female professional handball players in another study by Kramer et al. [24]. Overall, there is a wide discrepancy regarding the prevalence of LGE in endurance athletes. Different age and gender populations, training load and duration might explain the heterogeneity of cohorts and LGE incidence.

Regarding the pattern of LGE, in our study the areas of positive LGE were predominantly located in anterolateral, inferolateral, and inferior segments of the basal LV wall, which correspond to typical non-ischemic LGE pattern. In addition, the LGE pattern in the present study was similar to the findings reported by Wilson et al., the areas of focal myocardial fibrosis exhibited a non-coronary pattern [23], while Domenech-Ximenos et al. observed LGE areas confined to the inferior interventricular septum [6].

4.2. Adaptations in LV diastolic function in LGE- triathletes ("supernormal" LV diastolic filling pattern)

Earlier publications provide evidence of a "supernormal" LV diastolic function in endurance athletes compared to sedentary subjects from the general population [25–27]. A "supernormal" LV diastolic

Table 1
Demographic and CMR parameters of triathletes and controls.

	Controls (n = 28)	Male triathletes (n = 101)	*P value*
Clinical parameters			
Age, years	41 ± 10	43 ± 11	0.343
BSA, m^2	1.99 ± 0.15	1.99 ± 0.13	0.917
Troponin T, pg/ml	4 ± 3	6 ± 7	0.201
NT-proBNP, pg/ml	36 ± 24	38 ± 54	0.866
Exercise testing			
Systolic BP at rest, mmHg	122 ± 16	128 ± 17	0.172
Diastolic BP at rest, mmHg	84 ± 12	83 ± 10	0.690
Peak systolic BP, mmHg	176 ± 25	201 ± 29	<0.001
Peak diastolic BP, mmHg	85 ± 23	94 ± 21	0.099
HR at rest, bpm	66 ± 11	52 ± 9	<0.0001
Peak HR, bpm	170 ± 15	170 ± 13	0.989
VO_{2max}, ml/kg/min	39 ± 7	53 ± 11	<0.0001
Maximal power, W	233 ± 46	405 ± 105	<0.0001
CMR – left heart			
Cardiac index, l/min/m^2	3.40 ± 0.84	3.23 ± 0.68	0.293
LVEF, %	62 ± 7	61 ± 6	0.360
LVEDVi, ml/m^2	82 ± 13	100 ± 13	<0.0001
LVESVi, ml/m^2	31 ± 9	39 ± 9	<0.0001
LVSVi, ml/m^2	50 ± 8	60 ± 9	<0.0001
LV mass index, g/m^2	65 ± 9	82 ± 12	<0.0001
LAEF, %	62 ± 8	59 ± 9	0.179
LAEDVi, ml/m^2	14 ± 4	19 ± 8	<0.01
LAESVi, ml/m^2	36 ± 9	46 ± 12	<0.001
Native T1, ms	1021 ± 31	983 ± 27	<0.0001
ECV, %	23.9 ± 2.7	24.8 ± 2.1	0.109
CMR – right heart			
RVEF, %	60 ± 6	57 ± 7	<0.05
RVEDVi, ml/m^2	84 ± 14	105 ± 17	<0.0001
RVESVi, ml/m^2	34 ± 9	45 ± 11	<0.0001
RVSVi, ml/m^2	50 ± 8	60 ± 11	<0.0001
RAEF, %	47 ± 10	45 ± 11	0.233
RAEDVi, ml/m^2	22 ± 6	31 ± 11	<0.001
RAESVi, ml/ m^2	44 ± 11	56 ± 14	<0.0001
LV diastolic filling parameters			
Early peak-filling rate, ml/s/m^2	224 ± 69	215 ± 61	0.484
Atrial peak-filling rate, ml/s/m^2	147 ± 55	125 ± 48	<0.05
Peak-filling rate ratio	1.63 ± 0.49	1.97 ± 0.99	<0.05

Numbers are presented as mean ± SD for continuous data and n (%) for categorical data.
Some of the data was partly reported in previous publications as indicated in the materials and methods section.
Abbreviations: BP, blood pressure; BSA, body surface area; CMR, cardiovascular magnetic resonance; ECV, extracellular volume; EF, ejection fraction; HR, heart rate; LA, left atrial; LAEDVi, left atrial end-diastolic volume index; LAESVi, left atrial end-systolic volume index; LGE, Late gadolinium enhancement; LV, left ventricular; LVEDVi, left ventricular end-diastolic volume index; LVESVi, left ventricular end-systolic volume index; LVSVi, ventricular stroke volume index; NT-proBNP, *N*-terminal pro-brain natriuretic peptide; RA, right atrial; RAEDVi, right atrial end-diastolic volume index; RAESVi, right atrial end-systolic volume index; RV, right ventricular; RVEDVi, right ventricular end-diastolic volume index; RVESVi, right ventricular end-systolic volume index; VO_{2max}, maximal oxygen uptake.

Table 2
Demographic and CMR parameters in LGE + and LGE- triathletes.

	Controls (n = 28)	LGE- triathletes (n = 81)	LGE + triathletes (n = 20)	*P value LGE- vs LGE+*
Clinical parameters				
Age, years	41 ± 10	42 ± 11	49 ± 8¶	<0.01
BSA, m^2	1.99 ± 0.15	1.99 ± 0.13	1.99 ± 0.13	0.958
Troponin T, pg/ml	4 ± 3	6 ± 8	7 ± 5^{II}	0.661
NT-proBNP, pg/ml	36 ± 24	33 ± 26	58 ± 108	0.057
Exercise testing				
Systolic BP at rest, mmHg	122 ± 16	127 ± 18	133 ± 16^{II}	0.169
Diastolic BP at rest, mmHg	84 ± 12	83 ± 10	84 ± 9	0.542
Peak systolic BP, mmHg	176 ± 25	196 ± 29†	218 ± 24**	<0.01
Peak diastolic BP, mmHg	85 ± 23	95 ± 22	89 ± 12	0.264
HR at rest, bpm	67 ± 12	53 ± 10§	55 ± 9$^{\#}$	0.477
Peak HR, bpm	170 ± 15	171 ± 13	165 ± 12	0.071
VO_{2max}, ml/kg/min	39 ± 7	54 ± 11§	51 ± 9**	0.338
Maximal power, W	233 ± 46	414 ± 108§	367 ± 82**	0.080
CMR – left heart				
Cardiac index, l/min/m^2	3.40 ± 0.84	3.22 ± 0.69	3.29 ± 0.69	0.653
LVEF, %	62 ± 7	61 ± 5	61 ± 8	0.778
LVEDVi, ml/m^2	82 ± 13	100 ± 14§	98 ± 12**	0.529
LVESVi, ml/m^2	31 ± 9	40 ± 9 §	38 ± 9^{II}	0.480
LVSVi, ml/m^2	50 ± 8	61 ± 9§	60 ± 10$^{\#}$	0.809
LV mass index, g/m^2	65 ± 9	80 ± 12§	88 ± 10**	<0.01
LAEF, %	62 ± 8	60 ± 9	56 ± 9^{II}	0.091
LAEDVi, ml/m^2	14 ± 4	18 ± 8†	21 ± 7**	0.101
LAESVi, ml/m^2	36 ± 9	45 ± 11‡	49 ± 12$^{\#}$	0.171
LGE size, %LV	–	–	3.6 ± 2.4	–
Native T1, ms	1021 ± 31	979 ± 21§	997 ± 40^{II}	<0.01
ECV, %	23.9 ± 2.7	24.4 ± 1.7	26.2 ± 2.7^{II}	<0.001
CMR – right heart				
RVEF, %	60 ± 6	57 ± 6*	60 ± 8	0.097
RVEDVi, ml/m^2	84 ± 14	105 ± 16§	103 ± 21$^{\#}$	0.564
RVESVi, ml/m^2	34 ± 9	46 ± 11§	42 ± 12^{II}	0.117
RVSVi, ml/m^2	50 ± 8	59 ± 10§	61 ± 14$^{\#}$	0.465
RAEF, %	47 ± 10	45 ± 11	43 ± 10	0.546
RAEDVi, ml/m^2	22 ± 6	31 ± 11‡	31 ± 10¶	0.844
RAESVi, ml/ m^2	44 ± 11	56 ± 14§	54 ± 14¶	0.501
LV diastolic filling parameters				
Early peak-filling rate, ml/s/m^2	224 ± 69	216 ± 58	212 ± 73	0.798
Atrial peak-filling rate, ml/s/m^2	147 ± 55	120 ± 46*	149 ± 50	<0.05
Peak-filling rate ratio	1.63 ± 0.49	2.07 ± 1.03†	1.56 ± 0.67	<0.05

Numbers are presented as mean ± SD for continuous data and n (%) for categorical data.
*P < 0.05, †P < 0.01 or ‡P < 0.001 or §P < 0.0001 for LGE- versus controls.
^{II}P < 0.05, ¶P < 0.01, $^{\#}$P < 0.001 or **P < 0.0001 for LGE + versus controls.
Some of the data was partly reported in previous publications as indicated in the materials and methods section.
Abbreviations: as in Table 1.

function in triathletes training for the Hawaii Ironman Triathlon was described by Douglas in 1989 as an increased ratio of echocardiographic rapid to atrial LV filling velocities [28]. D'Ascenzi et al. reported an increased peak E and lower peak A velocity in soccer players resulting in higher E/A ratio, which can be interpreted as an improvement in myocardial passive diastolic properties [25]. Claessens et al. also studied triathletes and observed a "supernormal" diastolic ventricular filling with a significantly increased E/A ratio [26]. Similarly, an echocardiographic study by Szabo et al. detected a high E/A ratio in adolescent athletes compared to non-athletes caused by significantly lower A values, whereas E values were not increased in athletes [27]. The findings of the current CMR study are in line with the previous echocardiographic literature, LGE- triathletes had a comparable "supernormal" diastolic filling pattern characterized by increased peak-filling rate ratio, which was attributable to the lower atrial peak-filling rate.

LV diastolic filling consists of two phases the early active and late passive filling. In the current study early active filling was similar between LGE- triathletes and controls as described by early peak-filling rate, whereas late passive filling described by atrial peak-filling rate

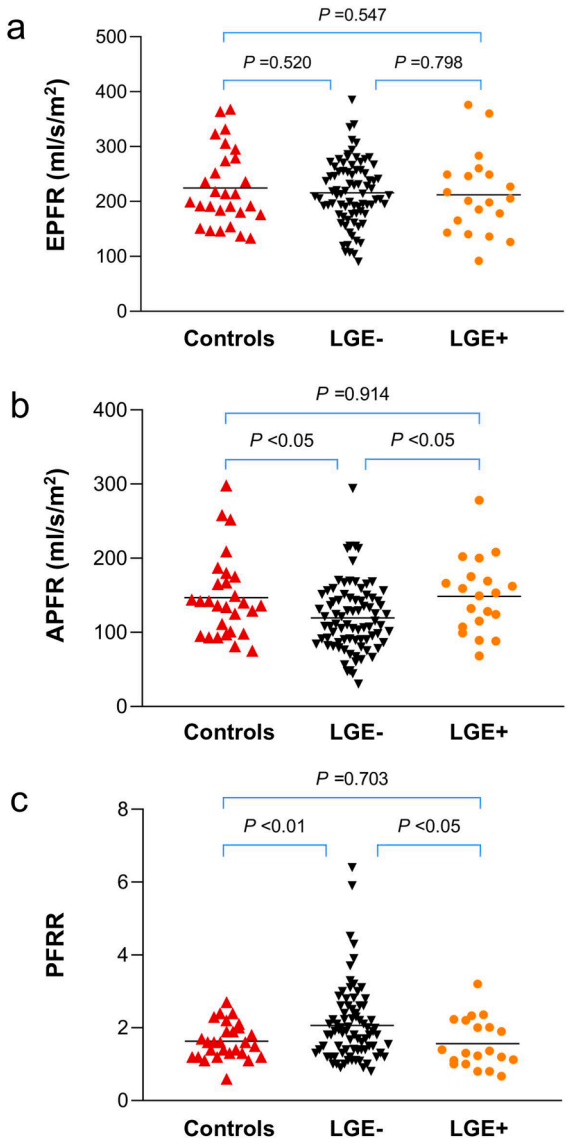

Fig. 3. CMR-based diastolic filling parameters between LGE-triathletes, LGE + triathletes and controls. (a-c) EPFR, APFR and PFRR values between LGE-triathletes, LGE + triathletes and controls. EPFR, early peak-filling rate; APFR, atrial peak-filling rate; PFRR, peak-filling rate ratio.

showed differences. Bhella et al. reported that competitive athletes have a more compliant and distensible LV than the sedentary population [29]. In a rat model of chronic exercise Burgess et al. also demonstrated that the collagen composition of LV is shifted towards a greater ratio of type III to I and postulated a favorable influence on diastolic function [30]. Another study by King et al. used Doppler tissue index to show a reduced myocardial stiffness in elite endurance athletes compared to controls [31]. Thus, the main cause for the "supernormal" LV filling seems to be the increased flexibility and elasticity of the myocardium.

4.3. "Pseudo-normalization" LV diastolic filling pattern in LGE + triathletes

LGE + triathletes in the current study demonstrated a LV diastolic filling pattern different to LGE- triathletes but similar to sedentary controls, which was characterized by increased atrial peak-filling rate and consequently decreased peak-filling rate ratio. Thus, we hypothesize that focal and diffuse myocardial fibrosis influence the LV diastolic filling pattern and LGE + triathletes might have a "pseudo-normalization" of diastolic filling. Apart from benefits in regard to LV compliance and distensibility long-term rigorous exercise might also be associated with non-physiological LV hypertrophy and myocardial fibrosis, increasing LV myocardial stiffness and decreasing LV compliance, leading to both systolic and diastolic dysfunction [32]. We detected increased myocardial native T1 and ECV fraction in normal appearing myocardium and markedly increased LV mass index in LGE + compared to LGE- triathletes. Increased ECV fraction of myocardium might be indicative of diffuse myocardial fibrosis. Recently, a study by Lee et al. reported that the degree of ECV fraction is associated with a deterioration of LV relaxation and compliance in patients with aortic stenosis [33]. Therefore, the LV diastolic filling patterns in LGE + triathletes may be influenced by diffuse myocardial fibrosis as well as increased LV mass. The thin-walled left atrium is afterload sensitive, with a decrease in LV compliance, the increased load imposed on the atrium eventually might lead to further LA dilatation and remodeling, acting as a marker of chronic diastolic burden [34].

"Pseudo-normalization" in LGE + triathletes might be thought of as the loss of adaptative benefits compared to LGE- triathletes. In the current study LGE + triathletes show a compensatory increase of atrial peak-filling rate compared to LGE- triathletes to maintain the "pseudo-normal" LV diastolic filling.

4.4. Study limitations

Differentiation of athlete's heart from other cardiomyopathies is still challenging due to the overlap features [35], and triathletes with underlying early-stage cardiomyopathies might potentially have been included. Echocardiographic data was not available and no comparison to CMR in assessing LV diastolic function was performed. Tissue-Doppler can evaluate early active diastolic function using annular tissue velocities (e') and the relationship between E and e'. However, CMR imaging has advantages in spatial resolution and tissue characterization. Currently, the results of this study can be considered only as generating a hypothesis and further studies are needed to detect the exact pathophysiological mechanism underlying the exercise-associated myocardial fibrosis and its effect on the LV diastolic filling. Further, due to the lack of a longitudinal follow-up, future studies are required to investigate how the adaptations develop and influence the individual.

5. Conclusions

This CMR study noninvasively investigated parameters of LV diastolic filling patterns in a large population of triathletes and the effect of myocardial fibrosis in comparison to sedentary controls. This study revealed that adaptations in "supernormal" LV diastolic filling pattern in LGE- triathletes may be attributed to increased flexibility and elasticity of ventricular myocardium. LGE + triathletes demonstrated a similar LV diastolic filling pattern compared to control subjects, which might be attributable to pseudo-normalization. The characteristic compensatory increase of atrial peak-filling rate in LGE + triathletes may be associated with reduced passive elasticity of the hypertrophied left ventricle due to myocardial fibrosis.

Study design:

- Prospective.
- Observational.
- Performed at one institution.

Funding statement

This research did not receive any specific grant from funding agencies in the public, commercial, or not-for-profit sectors.

Declaration of Competing Interest

The authors declare that they have no known competing financial

interests or personal relationships that could have appeared to influence the work reported in this paper.

Acknowledgements

None.

References

[1] G.M. Stewart, J. Chan, A. Yamada, J.J. Kavanagh, L.J. Haseler, K. Shiino, S. Sabapathy, Impact of high-intensity endurance exercise on regional left and right ventricular myocardial mechanics, Eur Heart J Cardiovasc Imaging 18 (6) (2017) 688–696.
[2] A. La Gerche, A.T. Burns, D.J. Mooney, W.J. Inder, A.J. Taylor, J. Bogaert, A. I. Macisaac, H. Heidbuchel, D.L. Prior, Exercise-induced right ventricular dysfunction and structural remodelling in endurance athletes, Eur Heart J 33 (8) (2012) 998–1006.
[3] L. Rundqvist, J. Engvall, M. Faresjo, E. Carlsson, P. Blomstrand, Regular endurance training in adolescents impacts atrial and ventricular size and function, Eur Heart J Cardiovasc Imaging 18 (6) (2017) 681–687.
[4] F.R. van de Schoor, V.L. Aengevaeren, M.T. Hopman, D.L. Oxborough, K.P. George, P.D. Thompson, T.M. Eijsvogels, Myocardial Fibrosis in Athletes, Mayo Clin Proc 91 (11) (2016) 1617–1631.
[5] S.M. Abdullah, K.W. Barkley, P.S. Bhella, J.L. Hastings, S. Matulevicius, N. Fujimoto, S. Shibata, G. Carrick-Ranson, M.D. Palmer, N. Gandhi, L.F. DeFina, B. D. Levine, Lifelong Physical Activity Regardless of Dose Is Not Associated With Myocardial Fibrosis, Circ Cardiovasc Imaging 9 (11) (2016).
[6] B. Domenech-Ximenos, M. Sanz-de la Garza, S. Prat-Gonzalez, A. Sepulveda-Martinez, F. Crispi, K. Duran-Fernandez, R.J. Perea, B. Bijnens, M. Sitges, Prevalence and pattern of cardiovascular magnetic resonance late gadolinium enhancement in highly trained endurance athletes, J Cardiovasc Magn Reson 22 (1) (2020) 62.
[7] F. Breuckmann, S. Möhlenkamp, K. Nassenstein, N. Lehmann, S. Ladd, A. Schmermund, B. Sievers, T. Schlosser, K.H. Jöckel, G. Heusch, R. Erbel, J. Barkhausen, Myocardial late gadolinium enhancement: prevalence, pattern, and prognostic relevance in marathon runners, Radiology 251 (1) (2009) 50–57.
[8] P. Bohm, G. Schneider, L. Linneweber, A. Rentzsch, N. Kramer, H. Abdul-Khaliq, W. Kindermann, T. Meyer, J. Scharhag, Right and Left Ventricular Function and Mass in Male Elite Master Athletes: A Controlled Contrast-Enhanced Cardiovascular Magnetic Resonance Study, Circulation 133 (20) (2016) 1927–1935.
[9] M. Ugander, A.J. Oki, L.Y. Hsu, P. Kellman, A. Greiser, A.H. Aletras, C.T. Sibley, M. Y. Chen, W.P. Bandettini, A.E. Arai, Extracellular volume imaging by magnetic resonance imaging provides insights into overt and sub-clinical myocardial pathology, Eur Heart J 33 (10) (2012) 1268–1278.
[10] B.P. Schoennagel, R. Fischer, R. Grosse, C. Berliner, M. Wehbe, G. Kurio, G. Lund, Z.J. Wang, J. Graessner, G. Adam, J. Yamamura, Peak Filling Rates Assessed by CMR Imaging Indicate Diastolic Dysfunction From Myocardial Iron Toxicity, JACC Cardiovasc Imaging 9 (11) (2016) 1353–1354.
[11] A.J. Teske, N.H. Prakken, B.W. De Boeck, B.K. Velthuis, P.A. Doevendans, M. J. Cramer, Effect of long term and intensive endurance training in athletes on the age related decline in left and right ventricular diastolic function as assessed by Doppler echocardiography, Am J Cardiol 104 (8) (2009) 1145–1151.
[12] F. Hoffmann, S. Moestl, S.V. Wooten, S. Stray-Gundersen, C.R. Tomczak, J. Tank, H. Tanaka, J. Rittweger, P.D. Chilibeck, Left Ventricular Dimensions and Diastolic Function Are Different in Throwers, Endurance Athletes, and Sprinters From the World Masters Athletics Championships, Front Physiol 12 (2021), 643764.
[13] G. Pavlik, Z. Olexó, P. Osváth, Z. Sidó, R. Frenkl, Echocardiographic characteristics of male athletes of different age, Br J Sports Med 35 (2) (2001) 95–99.
[14] E. Tahir, J. Starekova, K. Muellerleile, A. von Stritzky, J. Munch, M. Avanesov, J. M. Weinrich, C. Stehning, S. Bohnen, U.K. Radunski, E. Freiwald, S. Blankenberg, G. Adam, A. Pressler, M. Patten, G.K. Lund, Myocardial Fibrosis in Competitive Triathletes Detected by Contrast-Enhanced CMR Correlates With Exercise-Induced Hypertension and Competition History, JACC Cardiovasc Imaging 11 (9) (2018) 1260–1270.
[15] E. Tahir, J. Starekova, K. Muellerleile, E. Freiwald, A. von Stritzky, J. Munch, M. Avanesov, J.M. Weinrich, C. Stehning, E. Cavus, S. Bohnen, U.K. Radunski, S. Blankenberg, G. Adam, P. Simon, A. Pressler, M. Patten, G.K. Lund, Impact of Myocardial Fibrosis on Left Ventricular Function Evaluated by Feature-Tracking Myocardial Strain Cardiac Magnetic Resonance in Competitive Male Triathletes With Normal Ejection Fraction, Circ J 83 (7) (2019) 1553–1562.
[16] E. Tahir, B. Scherz, J. Starekova, K. Muellerleile, R. Fischer, B. Schoennagel, M. Warncke, C. Stehning, E. Cavus, S. Bohnen, U.K. Radunski, S. Blankenberg, P. Simon, A. Pressler, G. Adam, M. Patten, G.K. Lund, Acute impact of an endurance race on cardiac function and biomarkers of myocardial injury in triathletes with and without myocardial fibrosis, Eur J Prev Cardiol 27 (1) (2020) 94–104.
[17] H. Chen, M.L. Warncke, K. Muellerleile, D. Saering, A. Beitzen-Heineke, A. Kisters, M. Swiderska, E. Cavus, C.M. Jahnke, G. Adam, G.K. Lund, E. Tahir, Acute impact of an endurance race on biventricular and biatrial myocardial strain in competitive male and female triathletes evaluated by feature-tracking CMR, Eur Radiol (2021).
[18] J. Schulz-Menger, D.A. Bluemke, J. Bremerich, S.D. Flamm, M.A. Fogel, M. G. Friedrich, R.J. Kim, F. von Knobelsdorff-Brenkenhoff, C.M. Kramer, D.J. Pennell, S. Plein, E. Nagel, Standardized image interpretation and post-processing in cardiovascular magnetic resonance - 2020 update : Society for Cardiovascular Magnetic Resonance (SCMR): Board of Trustees Task Force on Standardized Post-Processing, J Cardiovasc Magn Reson 22 (1) (2020) 19.
[19] T.T. Le, R.S. Tan, M. De Deyn, E.P. Goh, Y. Han, B.R. Leong, S.A. Cook, C.W. Chin, Cardiovascular magnetic resonance reference ranges for the heart and aorta in Chinese at 3T, J Cardiovasc Magn Reson 18 (2016) 21.
[20] B.P. Schoennagel, K. Mullerleile, E. Tahir, J. Starekova, R. Grosse, J. Yamamura, P. Bannas, G. Adam, R. Fischer, Insights into diastolic function analyses using cardiac magnetic resonance imaging: impact of trabeculae and papillary muscles, Insights Imaging 12 (1) (2021) 159.
[21] M.S. Nacif, A.L.C. Almeida, A.A. Young, B.R. Cowan, A.C. Armstrong, E. Yang, C. T. Sibley, W.G. Hundley, S. Liu, J.A. Lima, D.A. Bluemke, Three-Dimensional Volumetric Assessment of Diastolic Function by Cardiac Magnetic Resonance Imaging: The Multi-Ethnic Study of Atherosclerosis (MESA), Arq Bras Cardiol 108 (6) (2017) 552–563.
[22] G.D. Aquaro, F. Pizzino, A. Terrizzi, S. Carerj, B.K. Khandheria, G. Di Bella, Diastolic dysfunction evaluated by cardiac magnetic resonance: the value of the combined assessment of atrial and ventricular function, European radiology 29 (3) (2019) 1555–1564.
[23] M. Wilson, R. O'Hanlon, S. Prasad, A. Deighan, P. Macmillan, D. Oxborough, R. Godfrey, G. Smith, A. Maceira, S. Sharma, K. George, G. Whyte, Diverse patterns of myocardial fibrosis in lifelong, veteran endurance athletes, J Appl Physiol (1985) 110 (6) (2011) 1622–1626.
[24] U. Kramer, S. Mangold, P. Krumm, A. Seeger, E. Franzen, A.M. Niess, C. D. Claussen, C. Burgstahler, Determination of Morphological and Functional Adaptations in Top Level Female Handball Players Using Cardiac MR Imaging, Deutsche Zeitschrift für Sportmedizin 2013 (11) (2013).
[25] F. D'Ascenzi, M. Cameli, V. Zaca, M. Lisi, A. Santoro, A. Causarano, S. Mondillo, Supernormal diastolic function and role of left atrial myocardial deformation analysis by 2D speckle tracking echocardiography in elite soccer players, Echocardiography 28 (3) (2011) 320–326.
[26] P.J. Claessens, C.W. Claessens, M.M. Claessens, M.C. Claessens, J.E. Claessens, Supernormal left ventricular diastolic function in triathletes, Tex Heart Inst J 28 (2) (2001) 102–110.
[27] D. Szabo, D. Nagy, C. Melczer, P. Acs, L. Ratgeber, I. Szokodi, M. Toth, A. Cziraki, K. Eklics, Z. Sarszegi, Influencing Factors of Cardiac Adaptation in Adolescent Athletes, Int J Sports Med 42 (13) (2021) 1209–1221.
[28] P.S. Douglas, Cardiac considerations in the triathlete, Med Sci Sports Exerc 21 (5 Suppl) (1989) S214–S218.
[29] P.S. Bhella, J.L. Hastings, N. Fujimoto, S. Shibata, G. Carrick-Ranson, M.D. Palmer, K.N. Boyd, B. Adams-Huet, B.D. Levine, Impact of lifelong exercise "dose" on left ventricular compliance and distensibility, J Am Coll Cardiol 64 (12) (2014) 1257–1266.
[30] M.L. Burgess, J. Buggy, R.L. Price, F.L. Abel, L. Terracio, A.M. Samarel, T.K. Borg, Exercise- and hypertension-induced collagen changes are related to left ventricular function in rat hearts, Am J Physiol 270 (1 Pt 2) (1996) H151–H159.
[31] G.J. King, R.T. Murphy, I. Almuntaser, K. Bennett, E. Ho, A.S. Brown, Alterations in myocardial stiffness in elite athletes assessed by a new Doppler index, Heart 94 (10) (2008) 1323–1325.
[32] D.F. Waterhouse, T.F. Ismail, S.K. Prasad, M.G. Wilson, R. O'Hanlon, Imaging focal and interstitial fibrosis with cardiovascular magnetic resonance in athletes with left ventricular hypertrophy: implications for sporting participation, Br J Sports Med 46 (Suppl 1) (2012) i69–i77.
[33] H.J. Lee, H. Lee, S.M. Kim, J.B. Park, E.K. Kim, S.A. Chang, E. Park, H.K. Kim, W. Lee, Y.J. Kim, S.C. Lee, S.W. Park, D.W. Sohn, J.K. Oh, S.J. Park, S.P. Lee, Diffuse Myocardial Fibrosis and Diastolic Function in Aortic Stenosis, JACC Cardiovasc Imaging 13 (12) (2020) 2561–2572.
[34] V. Sachdev, Y. Shizukuda, C.L. Brenneman, C.W. Birdsall, M.A. Waclawiw, A. E. Arai, S.A. Mohiddin, D. Tripodi, L. Fananapazir, J.F. Plehn, Left atrial volumetric remodeling is predictive of functional capacity in nonobstructive hypertrophic cardiomyopathy, Am Heart J 149 (4) (2005) 730–736.
[35] J. Kubler, C. Burgstahler, J.M. Brendel, S. Gassenmaier, F. Hagen, K. Klingel, S. C. Olthof, K. Blume, B. Wolfarth, K.A.L. Mueller, S. Greulich, P. Krumm, Cardiac MRI findings to differentiate athlete's heart from hypertrophic (HCM), arrhythmogenic right ventricular (ARVC) and dilated (DCM) cardiomyopathy, Int J Cardiovasc Imaging 37 (8) (2021) 2501–2515.

4 Chapter 4: Publication in *European Radiology*, April 2023

Left ventricular myocardial strain responding to chronic pressure overload in patients with resistant hypertension evaluated by feature-tracking CMR

Hang Chen, Fabian J. Brunner, Cansu Özden, Ulrich O. Wenzel, Johannes T. Neumann, Jennifer Erley, Dennis Saering, Kai Muellerleile, Kai-Jonathan Maas, Bjoern P. Schoennagel, Ersin Cavus, Jan N. Schneider, Stefan Blankenberg, Andreas Koops, Gerhard Adam, Enver Tahir

Personal contribution:

The following research article has been published in ***European Radiology***. I am the first author of the paper. I contributed the conceptualization of the study together with corresponding author and other co-authors. I analyzed the image data and plotted the figures. I contributed to writing the original manuscript and editing during the revisions.

European Radiology
https://doi.org/10.1007/s00330-023-09595-z

European Radiology
ESR EUROPEAN SOCIETY OF RADIOLOGY

CARDIAC

Left ventricular myocardial strain responding to chronic pressure overload in patients with resistant hypertension evaluated by feature-tracking CMR

Hang Chen[1] · Fabian J. Brunner[2,3] · Cansu Özden[1] · Ulrich O. Wenzel[4] · Johannes T. Neumann[2,3] · Jennifer Erley[1] · Dennis Saering[5] · Kai Muellerleile[2,3] · Kai-Jonathan Maas[1] · Bjoern P. Schoennagel[1] · Ersin Cavus[2,3] · Jan N. Schneider[2,3] · Stefan Blankenberg[2,3] · Andreas Koops[6] · Gerhard Adam[1] · Enver Tahir[1]

Received: 9 October 2022 / Revised: 10 January 2023 / Accepted: 3 March 2023

Abstract

Objectives The study aimed to investigate the alterations of myocardial deformation responding to long-standing pressure overload and the effects of focal myocardial fibrosis using feature-tracking cardiac magnetic resonance (FT-CMR) in patients with resistant hypertension (RH).

Methods Consecutive RH patients were prospectively recruited and underwent CMR at a single institution. FT-CMR analyses based on cine images were applied to measure left ventricular (LV) peak systolic global longitudinal (GLS), radial (GRS), and circumferential strain (GCS). Functional and morphological CMR variables, and late gadolinium enhancement (LGE) imaging were also obtained.

Results A total of 50 RH patients (63 ± 12 years, 32 men) and 18 normotensive controls (57 ± 8 years, 12 men) were studied. RH patients had a higher average systolic blood pressure than controls (166 ± 21 mmHg vs. 116 ± 8 mmHg, $p < 0.001$) with the intake of 5 ± 1 antihypertensive drugs. RH patients showed increased LV mass index (78 ± 15 g/m^2 vs. 61 ± 9 g/m^2, $p < 0.001$), decreased GLS ($-16 \pm 3\%$ vs. $-19 \pm 2\%$, $p = 0.001$) and GRS ($41 \pm 12\%$ vs. $48 \pm 8\%$, $p = 0.037$), and GCS was reduced by trend ($-17 \pm 4\%$ vs. $-19 \pm 4\%$, $p = 0.078$). Twenty-one (42%) RH patients demonstrated a LV focal myocardial fibrosis (LGE+). LGE+RH patients had higher LV mass index (85 ± 14 g/m^2 vs. 73 ± 15 g/m^2, $p = 0.007$) and attenuated GRS ($37 \pm 12\%$ vs. $44 \pm 12\%$, $p = 0.048$) compared to LGE−RH patients, whereas GLS ($p = 0.146$) and GCS ($p = 0.961$) were similar.

Conclusion Attenuation of LV GLS and GRS, and GCS decline by tendency, might be adaptative changes responding to chronic pressure overload. There is a high incidence of focal myocardial fibrosis in RH patients, which is associated with reduced LV GRS.

Clinical relevance statement Feature-tracking CMR-derived myocardial strain offers insights into the influence of long-standing pressure overload and of a myocardial fibrotic process on cardiac deformation in patients with resistant hypertension.

✉ Enver Tahir
e.tahir@uke.de

1 Department of Diagnostic and Interventional Radiology and Nuclear Medicine, University Medical Center Hamburg-Eppendorf, Hamburg, Germany

2 Department of Cardiology, University Heart & Vascular Center Hamburg, University Medical Center Hamburg-Eppendorf, Martinistr. 52, 20246 Hamburg, Germany

3 German Center for Cardiovascular Research (DZHK), Partner Site Hamburg/Kiel/Lübeck, Hamburg, Germany

4 Department of Internal Medicine, Nephrology, University Medical Center Hamburg-Eppendorf, Hamburg, Germany

5 Information Technology and Image Processing, University of Applied Sciences, Wedel, Germany

6 Institute of Radiology and Interventional Therapy, Vivantes Auguste-Viktoria-Klinikum, Berlin, Germany

Published online: 10 April 2023

Key Points

- *Variations of left ventricular strain are attributable to the degree of myocardial impairment in resistant hypertensive patients.*
- *Focal myocardial fibrosis of the left ventricle is associated with attenuated global radial strain.*
- *Feature-tracking CMR provides additional information on the attenuation of myocardial deformation responding to long-standing high blood pressure.*

Keywords Magnetic resonance imaging · Hypertension · Cardiac imaging techniques · Hypertrophy, left ventricular

Abbreviations

ABPM	Ambulant blood pressure monitoring
BMI	Body mass index
BSA	Body surface area
CMR	Cardiac magnetic resonance
DBP	Diastolic blood pressure
EDVi	End-diastolic volume index
EF	Ejection fraction
ESVi	End-systolic volume index
FT-CMR	Feature-tracking cardiac magnetic resonance
GCS	Global circumferential strain
GLS	Global longitudinal strain
GRS	Global radial strain
LA	Left atrial
LGE	Late gadolinium enhancement
LV	Left ventricular
LVH	Left ventricular hypertrophy
RA	Right atrial
RH	Resistant hypertension
RV	Right ventricular
SBP	Systolic blood pressure
SSFP	Steady-state free-precession
STE	Speckle-tracking echocardiography
SVi	Stroke volume index

Introduction

Among other cardiovascular risk factors hypertension remains a major cause of cardiovascular mortality worldwide [1]. Resistant hypertension (RH) is defined as above-goal elevated blood pressure despite the concurrent use of three or more different antihypertensive medications including a diuretic [2]. RH is associated with a higher risk of adverse cardiovascular events compared to controlled hypertension, and might be accompanied by extensive target organ damage, including left ventricular hypertrophy (LVH) [3, 4]. Myocardial fibrosis is a major determinant of hypertrophied myocardium and potentially associated with cardiovascular events, including heart failure and sudden death [5].

A recent work offers an overview of speckle-tracking echocardiography (STE) in assessing LV dysfunction in hypertension [6]. The explanation that attenuated longitudinal function and preserved circumferential and radial function are due to compensatory mechanisms has received reasonable attention, whereas longitudinal function is not always the earliest indicator in all circumstances, all three directions of function may decline in response to disease progress [6]. Although STE is the most available technique to quantify myocardial deformation, several weaknesses do exist. Reproducibility of acquisition planes is limited, which can influence particularly the evaluation of circumferential and radial strain [7]. The novel technique of feature-tracking cardiac magnetic resonance (FT-CMR), despite suffering from through-plane motion effects and having a lower spatial and temporal resolution than STE, has a better performance in measuring longitudinal, radial, and circumferential strain [7, 8]. Furthermore, the majority of the patient populations included in the previous echocardiographic literature had controlled mild to moderate hypertension [6].

Therefore, the main purpose of this study was to investigate the alterations of myocardial deformation responding to long-standing pressure overload and to elucidate the degree of myocardial impairment using FT-CMR. The secondary objective was to identify the potential effects of focal myocardial fibrosis in RH patients.

Materials and methods

Study population

The prospective study was approved by the local research ethics committee and complied with the Declaration of Helsinki. All participants gave written informed consent. This study recruited consecutive RH patients at a single institution and included 16 patients who were recruited in a previously publication [9]. The initial publication reported the effects of a renal denervation procedure on LV mass, myocardial strain, and diastolic function in RH patients [9].

The enrollment of criteria and diagnostic definitions have been detailed previously [9]. Briefly, RH patients were diagnosed according to the current guideline: blood pressure ≥ 140/90 mmHg despite the intake of at least 3 antihypertensive drugs in full dosages including a diuretic [2, 10].

The demographic and anthropometric characteristics were collected accordingly. Main exclusion criteria were as follows: (1) severe renal failure (estimated glomerular filtration rate [eGFR] < 30 mL/min/1.73 m^2), (2) significant stenosis and prior stenting or dilatation of renal arteries, (3) myocardial infarction < 6 months before planned renal denervation, (4) diabetes mellitus type I, and (5) persisting atrial fibrillation [9]. All patients underwent an office and 24-h ambulant blood pressure monitoring (ABPM). In addition, 18 healthy individuals, who underwent CMR scans for this particular research purpose, were enrolled to serve as a control group and had no known cardiovascular or systematic diseases.

CMR acquisition

CMR was performed on a 1.5-T scanner equipped with a 5-channel cardiac-phased array receiver coil (Achieva, Philips Medical Systems). Standard retrospectively gated, ECG-triggered steady-state free-precession cine images (25 phases per cardiac cycle) were acquired in short- and long-axis (2-, 3-, and 4-chamber) views using a breath-hold technique with the following typical parameters: acquired voxel size $1.98 \times 1.80 \times 6$ mm^3, reconstructed voxel size $1.36 \times 1.36 \times 6$ mm^3, gap 4 mm, 9–10 slices for full LV coverage, echo time = 1.67 ms, time to repetition = 3.34 ms, flip angle = 60°, parallel acquisition technique = SENSE [factor 2]). Ten minutes after a bolus injection of 0.2 mmol/kg gadoteric acid (Dotarem®, Guerbet) at a rate of 2.5 mL/s late gadolinium enhancement (LGE) images were acquired using an end-diastolic phase-sensitive inversion-recovery sequence in short-axis direction covering the entire heart and in 2-, 3-, and 4-chamber views.

CMR data analysis

CMR images were post-processed independently and blindly using a commercially available software (CVi42, Circle Cardiovascular Imaging Inc.). CMR parameters are given as the mean of two investigators and are indexed to body surface area (BSA). For LV volume and mass evaluation, the endo- and epicardial contours were delineated in systole and diastole in a stack of short-axis cine slices covering the whole LV with inclusion of the papillary muscles as part of the LV volume [11]. For right ventricular (RV) volume evaluation, the endocardial contours were delineated in systole and diastole in a stack of short-axis cine slices covering the whole RV [11]. Left (LA) and right atrial (RA) volumes and LV ejection fraction (EF) were calculated based on the biplane area-length method [12], measurements excluded pulmonary veins and atrial appendage. LVH was defined as LV mass index > 81 g/m^2 for men and > 61 g/m^2 for women [13]. Focal myocardial fibrosis (LGE +) was identified and assessed visually using short- and long-axis LGE images.

LV myocardial strain analysis was performed with cine images using the feature-tracking software (Segment, version 2.1.R.6108, Medviso), through computing interframe deformation fields using an endocardial tracking strategy based on non-rigid image registration [14, 15]. LV peak systolic global longitudinal (GLS), radial (GRS), and circumferential strain (GCS) were measured on the long-axis (2-, 3-, and 4-chamber) and three short-axis (apical, mid, and basal) slices by manual delineation of the endo- and epicardial contours at end-diastole. Endo- and epicardial contours were automatically propagated by the software throughout the cardiac cycle to calculate myocardial strain.

Statistical analysis

All statistical analyses were performed using SPSS (version 28.0, IBM) and GraphPad Prism (version 9.2.0). All continuous data were checked for normality using the D'Agostino-Pearson omnibus normality test. Numerical variables are presented as the mean ± SD. Differences of continuous data between the groups were performed using the independent samples *t*-test or Wilcoxon signed rank-test as appropriate. Categorical data are presented as absolute numbers (percentage) and were compared using $\chi 2$ test or Fischer's exact test as appropriate. Multivariate linear regression analyses were conducted to identify the independent associations of clinical and CMR-derived parameters with strain. $p < 0.05$ was regarded as statistically significant.

Results

Clinical characteristics

A total of 50 consecutive RH patients (63 ± 12 years, 32 men) and 18 normotensive controls (57 ± 8 years, 12 men) were eventually enrolled. A flowchart of the study is presented in Figure S1. Cardiovascular risk factors and antihypertensive medication of RH patients are detailed in Table 1. There were no statistical differences in gender distribution ($p = 0.839$) and age ($p = 0.055$) between RH patients and normotensive controls. RH patients had higher BSA ($p = 0.004$) and body mass index (BMI) ($p < 0.001$) than controls. Office systolic blood pressure (SBP) (166 ± 21 mmHg) and diastolic blood pressure (DBP) (91 ± 17 mmHg) were elevated in RH patients despite the intake of 5 ± 1 antihypertensive drugs. The mean of 24-h ABPM, SBP, and DBP of the patient group were 149 ± 18 mmHg and 84 ± 16 mmHg, respectively (Table 2).

Table 1 Clinical characteristics of RH patients

	RH patients ($n=50$)
Risk factors	
Coronary artery disease, *n* (%)	13 (26)
Ischemic stroke, *n* (%)	4 (8)
Type 2 diabetes, *n* (%)	17 (34)
Smoker, *n* (%)	15 (30)
Hypercholesterolemia, *n* (%)	21 (42)
Antihypertensive medications	
Number of antihypertensive drugs, *n*	5 ± 1
Diuretics, *n* (%)	50 (100)
ACE inhibitors/ARBs, *n* (%)	41 (82)
Beta blockers, *n* (%)	39 (78)
Moxonidine or Clonidine, *n* (%)	28 (56)
Calcium channel blockers, *n* (%)	35 (70)
Aldosterone antagonists, *n* (%)	2 (4)
Alpha-adrenoreceptor antagonist, *n* (%)	8 (16)
Renin inhibitors, *n* (%)	9 (18)
Alpha-adrenoreceptor agonists, *n* (%)	2 (4)
Vasodilators, *n* (%)	4 (8)

Values are presented as mean ± SD for continuous data and *n* (%) for categorical data

ACE angiotensin-converting enzyme, *ARBs* angiotensin II receptor blockers, *RH* resistant hypertension

CMR findings

CMR findings of the study subjects are summarized in Table 2. RH patients showed similar LVEF (62 ± 9% vs. 64 ± 7%, $p=0.276$) and LV/LA volumes, but markedly increased LV mass index (78 ± 15 g/m^2 vs. 61 ± 9 g/m^2, $p<0.001$) compared to controls. In the patient group, 28 (56%) had LVH. No differences were observed between the groups regarding RV function and volumes. Feature-tracking analyses showed attenuated LV GLS (− 16 ± 3% vs. − 19 ± 2%, $p=0.001$) and GRS (41 ± 12% vs. 48 ± 8%, $p=0.037$) in RH patients. LV GCS had a downward tendency (− 17 ± 4% vs. − 19 ± 4%, $p=0.078$) (Table 2 and Fig. 1).

Demographics, blood pressure, and CMR findings of LGE + and LGE − RH patients.

In 21 out of 50 (42%) RH patients, a focal myocardial fibrosis (LGE+) of the LV was detected. A total of 7 ischemic and 14 non-ischemic LGE patterns were visualized as shown in Fig. 2a. A schematic overview is given in Fig. 2b depicting the segmental distribution of focal myocardial fibrosis in LGE + RH patients. LGE areas were predominantly localized in the LV basal inferior and inferolateral segments, whereas midventricular anteroseptal and apical septal segments showed no focal myocardial fibrosis.

LGE − and LGE + RH patients had significantly higher BMI and office SBP than controls (all $p<0.001$), increased LV mass index was found in both LGE − ($p=0.004$) and LGE + ($p<0.001$) RH patients. The two RH subgroups and controls had similar cardiac functional and anatomical parameters. Compared to normotensive controls, LV GLS was decreased in LGE + (− 15 ± 3% vs. − 19 ± 2%, $p<0.001$) and LGE − RH patients (− 16 ± 3% vs. − 19 ± 2%, $p=0.015$), GRS was decreased in LGE + RH (37 ± 12% vs. 48 ± 8%, $p=0.002$), but not in LGE − RH patients (44 ± 12% vs. 48 ± 8%, $p=0.269$) (Table 2). There were no statistical differences in LV GCS between controls and LGE − ($p=0.101$) and LGE + ($p=0.127$) RH patients, but a trend for attenuation.

There was a greater proportion of male patients in the LGE + RH group ($p=0.007$) (Table 2). LGE + RH patients had higher BSA (2.16 ± 0.15 m^2 vs. 2.01 ± 0.23 m^2, $p=0.017$) than LGE − RH patients. Age ($p=0.727$) and BMI ($p=0.842$) were similar. Office SBP (160 ± 18 mmHg vs. 164 ± 39 mmHg, $p=0.716$) and DBP (91 ± 16 mmHg vs. 88 ± 25 mmHg, $p=0.629$), ABPM SBP (148 ± 20 mmHg vs. 150 ± 18 mmHg, $p=0.857$) and DBP (84 ± 16 mmHg vs. 84 ± 16 mmHg, $p=0.935$) were similar. CMR revealed a higher LV mass index in LGE + RH patients with 85 ± 14 g/m^2 than in LGE − RH patients with 73 ± 15 g/m^2 ($p=0.007$). Patients with LVH had a similar distribution between the LGE − and LGE + RH subgroups. No significant differences regarding cardiac function and volumes were observed (Table 2). Feature-tracking analyses showed that LGE + RH patients had attenuated LV GRS (37 ± 12% vs. 44 ± 12%, $p=0.048$) compared to LGE − RH patients, whereas there were no differences in LV GLS (− 15 ± 3% vs. − 16 ± 3%, $p=0.146$) and GCS (− 17 ± 5% vs. − 17 ± 4%, $p=0.961$) (Fig. 1).

Associations of clinical and CMR-derived parameters with strain

Univariate regression analyses showed that LV stroke volume index (LVSVi) and LV mass index in RH patients were associated with LV GLS ($R=-0.443$, $p=0.001$ and $R=0.466$, $p<0.001$, respectively), GRS ($R=0.420$, $p=0.003$ and $R=-0.392$, $p=0.005$, respectively), and GCS ($R=-0.307$, $p=0.03$ and $R=0.289$, $p=0.041$, respectively) (Fig. 3). After adjustment for age, gender, BMI, and BP, multivariate regression analyses demonstrated that LV end-systolic volume index (LVESVi), LVSVi, and LV mass index were independently associated with LV GLS ($\beta=0.301$, $p=0.002$; $\beta=-0.689$, $p<0.001$ and $\beta=0.558$, $p<0.001$, respectively; model $R^2=0.713$) and GRS ($\beta=-0.447$;

Table 2 Demographics, blood pressure, and CMR parameters in controls and RH patients as well as their subgroups stratified by the presence of LGE

	Controls ($n=18$)	RH patients ($n=50$)	p value[†]	LGE − RH patients ($n=29$)	LGE + RH patients ($n=21$)	p value[‡]
Demographics						
Age, years	57 ± 8	63 ± 12	0.055	62 ± 13	64 ± 10*	0.727
BSA, m^2	1.90 ± 0.23	2.07 ± 0.21	**0.004**	2.01 ± 0.23	2.16 ± 0.15***	**0.017**
BMI, kg/m^2	25 ± 4	31 ± 5	**< 0.001**	31 ± 6***	30 ± 4***	0.842
Male, *n* (%)	12 (67)	32 (64)	0.839	14 (48)	18 (86)	**0.007**
Blood pressure parameters						
Office SBP, mmHg	116 ± 8	166 ± 21	**< 0.001**	164 ± 39***	160 ± 18***	0.716
Office DBP, mmHg	77 ± 11	91 ± 17	**0.001**	88 ± 25	91 ± 16**	0.629
ABPM SBP, mmHg	–	149 ± 18	–	150 ± 18	148 ± 20	0.857
ABPM DBP, mmHg	–	84 ± 16	–	84 ± 16	84 ± 16	0.935
LV and LA CMR parameters						
LVEF, %	64 ± 7	62 ± 9	0.276	63 ± 8	59 ± 11	0.171
Heart rate, beats/min	67 ± 13	69 ± 11	0.499	69 ± 11	69 ± 11	0.879
LV mass index, g/m^2	61 ± 9	78 ± 15	**< 0.001**	73 ± 15**	85 ± 14***	**0.007**
LVH all, *n* (%)	–	28 (56)	–	16 (55)	12 (57)	0.890
Male (mass > 81 g/m^2), *n* (%)	–	14 (28)	–	5 (36)	9 (50)	0.419
Female (mass > 61 g/m^2), *n* (%)	–	14 (28)	–	11 (73)	3 (100)	0.311
LVEDVi, mL/m^2	75 ± 12	75 ± 16	0.856	72 ± 15	78 ± 16	0.155
LVESVi, mL/m^2	27 ± 7	29 ± 11	0.388	27 ± 10	32 ± 12	0.119
LVSVi, mL/m^2	48 ± 10	45 ± 9	0.227	45 ± 8	46 ± 11	0.578
LAEDVi, mL/m^2	20 ± 6	24 ± 14	0.059	24 ± 14	25 ± 14	0.769
LAESVi, mL/m^2	42 ± 11	43 ± 15	0.660	43 ± 13	44 ± 18	0.842
RV and RA CMR parameters						
RVEF, %	61 ± 6	63 ± 9	0.385	63 ± 8	62 ± 10	0.622
RVEDVi, mL/m^2	74 ± 13	72 ± 13	0.460	72 ± 12	72 ± 15	0.889
RVESVi, mL/m^2	29 ± 7	27 ± 8	0.313	26 ± 8	28 ± 9	0.575
RVSVi, mL/m^2	46 ± 9	45 ± 10	0.837	45 ± 9	45 ± 11	0.785
RAEDVi, mL/m^2	25 ± 10	23 ± 9	0.535	23 ± 8	23 ± 10	0.929
RAESVi, mL/m^2	43 ± 14	39 ± 11	0.248	39 ± 9	39 ± 13	0.937
LV strain parameters						
LV GLS, %	− 19 ± 2	− 16 ± 3	**0.001**	− 16 ± 3*	− 15 ± 3***	0.146
LV GRS, %	48 ± 8	41 ± 12	**0.037**	44 ± 12	37 ± 12**	**0.048**
LV GCS, %	− 19 ± 4	− 17 ± 4	0.078	− 17 ± 4	− 17 ± 5	0.961
LGE pattern						
Ischemic, *n* (%)	–	7 (14)	–	–	7 (33)	–
Non-ischemic, *n* (%)	–	14 (28)	–	–	14 (67)	–

Values are presented as mean ± SD for continuous data and *n* (%) for categorical data

Values in **bold** denote significant differences between groups

[†]Comparison between RH patients and controls

[‡]Comparison between LGE − and LGE + RH patients

*$p < 0.05$, **$p < 0.01$, ***$p < 0.001$ for LGE − or LGE + RH patients vs. controls

Abbreviations: *ABPM*, ambulatory blood pressure monitoring; *BMI*, body mass index; *BSA*, body surface area; *DBP*, diastolic blood pressure; *GCS*, global circumferential strain; *GLS*, global longitudinal strain; *GRS*, global radial strain; *LA*, left atrial; *LAEDVi*, left atrial end-diastolic volume index; *LAESVi*; left atrial end-systolic volume index; *LGE*, late gadolinium enhancement; *LV*, left ventricular; *LVEF*, left ventricular ejection fraction; *LVEDVi*, left ventricular end-diastolic volume index; *LVESVi*, left ventricular end-systolic volume index; *LVH*, left ventricular hypertrophy; *LVSVi*, left ventricular stroke volume index; *RA*, right atrial; *RAEDVi*, right atrial end-diastolic volume index; *RAESVi*; right atrial end-systolic volume index; *RH*, resistant hypertension; *RV*, right ventricular; *RVEF*, right ventricular ejection fraction; *RVEDVi*, right ventricular end-diastolic volume index; *RVESVi*, right ventricular end-systolic volume index; *RVSVi*, right ventricular stroke volume index; *SBP*, systolic blood pressure

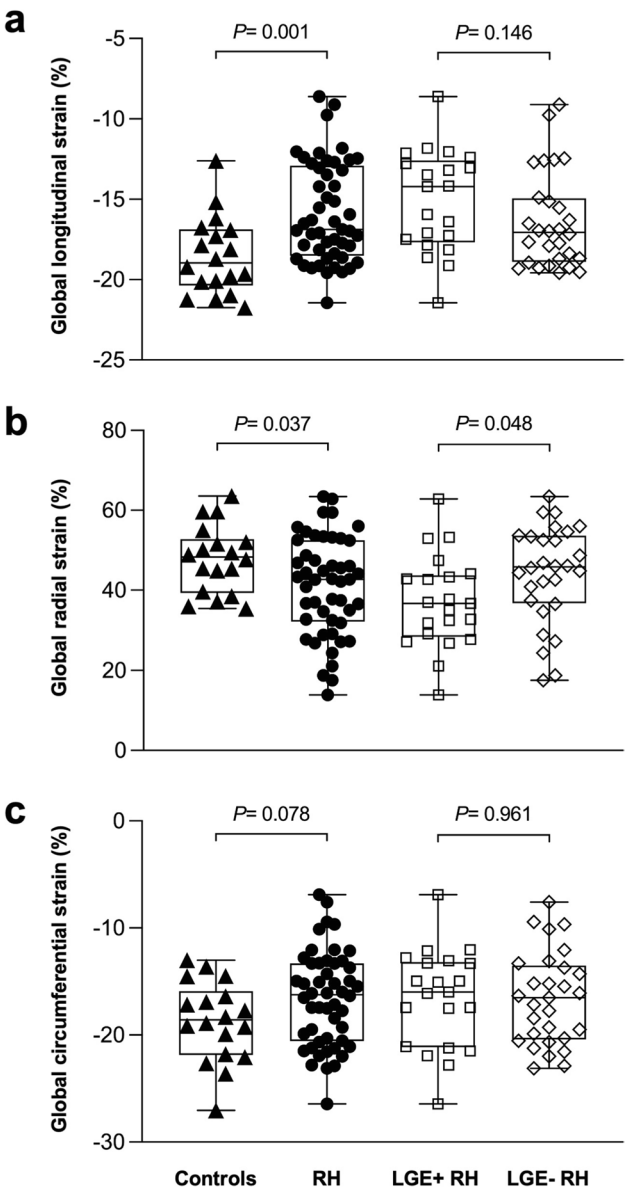

Fig. 1 The comparisons of LV global longitudinal (**a**), radial (**b**), and circumferential (**c**) strain among RH patients with and without LGE and controls. LGE, late gadolinium enhancement; LV, left ventricular; RH, resistant hypertension

$\beta = 0.616$ and $\beta = -0.379$, respectively, all $p < 0.001$; model $R^2 = 0.685$). LVESVi and LVSVi were independently associated with LV GCS ($\beta = 0.711$, $p < 0.001$; $\beta = -0.413$, $p < 0.001$, respectively; model $R^2 = 0.588$) (Table 3). Multivariate regression analyses in normotensive controls showed that considering the covariates of age, gender, BMI, and BP, LVSVi was independently associated with LV GLS ($\beta = -0.521$, $p = 0.027$, model $R^2 = 0.271$), LVESVi was independently associated with LV GRS ($\beta = -0.675$, $p = 0.002$, model $R^2 = 0.456$), and LVESVi and LVSVi were independently associated with LV GCS ($\beta = 0.722$ and $\beta = -0.615$, all $p < 0.001$; model $R^2 = 0.746$) (Table 4).

Discussion

This study analyzed cardiac morphology and function in RH patients compared to normotensive controls using CMR. The novel method of FT-CMR was used to determine LV global peak systolic strain and LGE imaging was used to investigate the influence of focal myocardial fibrosis on LV myocardial deformation. The main findings are (1) RH patients had significantly higher LV mass index and attenuated LV GLS and GRS in comparison to normotensive controls, whereas GCS was attenuated by trend; (2) 21 RH patients (42%) demonstrated a focal myocardial fibrosis (LGE+), predominantly localized in the basal inferior and inferolateral LV segments; (3) in the subgroup analysis, LGE+RH patients had a markedly reduced LV GLS compared to controls, attenuated GRS compared to LGE−RH patients and controls, and GCS was also attenuated by trend; and (4) LV mass index and stroke volume index were associated with multidirectional strain in RH patients.

Long-standing pressure overload causing strain alterations

In this study, a decrease of LV GLS and GRS was observed in RH patients compared to normotensive controls, GCS did not differ statistically, but showed a decreasing trend. LV strain is sensitive to and influenced by afterload alteration [16], and its altering patterns are determined by the fiber structure of the myocardium and its interaction with local wall stress [17]. Longitudinal strain represents the contraction of the subendocardial fibers, while circumferential shortening reflects the contraction of the subepicardial fibers, and both contribute to radial thickening [8]. LV subendocardial fibers are more vulnerable to increased wall stress, ischemia, and microvascular dysfunction, and thus longitudinal strain is prone to impairment at an early phase of hypertension even before hypertrophy has occurred [18–20] and is a sensitive marker for subclinical LV dysfunction [17, 21].

The alterations in radial and circumferential strain are more complex compared to longitudinal strain, especially with the progression of the given disease and the presence of LVH. Imbalzano et al detected reduced longitudinal strain by STE in hypertensive patients both with and without LVH, and those with LVH had reduced radial and increased circumferential strain [18]. Wang et al showed a reduction in all three strain components in patients with systolic heart failure, while patients with diastolic heart failure and preserved LVEF had reduced longitudinal and radial strain, but circumferential strain was preserved [21]. In the current

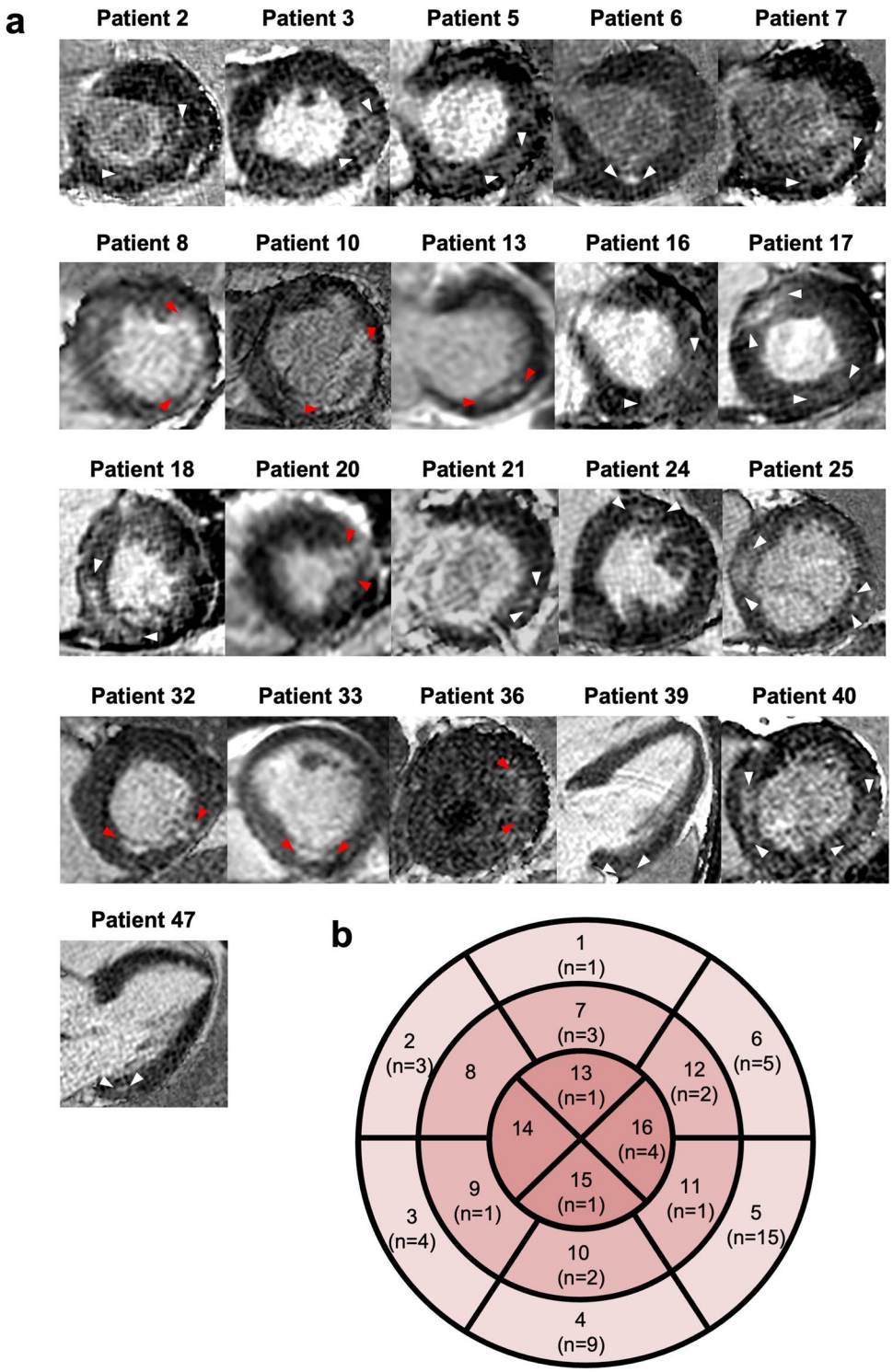

Fig. 2 **a** LGE images depicting the focal myocardial fibrosis in LGE + RH patients. Short- and long-axis LGE images depicting an ischemic (red arrowheads) and non-ischemic (white arrowheads) pattern in 21 (42%) LGE + RH patients. **b** Schematic representation of fibrosis localization in LGE + RH patients. LGE areas were predominantly localized in the LV basal inferior (segment 4) and inferolateral (segment 5) segments, whereas midventricular anteroseptal (segment 8) and apical septal (segment 14) segments showed no focal myocardial fibrosis. LGE, late gadolinium enhancement; LV, left ventricular; RH, resistant hypertension

cohort, longitudinal and radial strain was decreased and circumferential strain was preserved in analogy, and more than half (56%) of the patients had LVH due to persistent high-pressure overload. The anatomic differences of myocardial fibers may explain the potential robustness of circumferential strain in terms of clinically significant LV dysfunction [22]. Thus, different stages of hypertensive heart disease seem to be associated with different longitudinal, radial, and circumferential strain response, which may provide a possible explanation for the above discrepancy.

Of note, in the current study, there was a borderline difference of age between controls and RH patients; age-dependency may contribute to the compensation of age-related LV stiffness by radial strain [23]. However, a multivariate

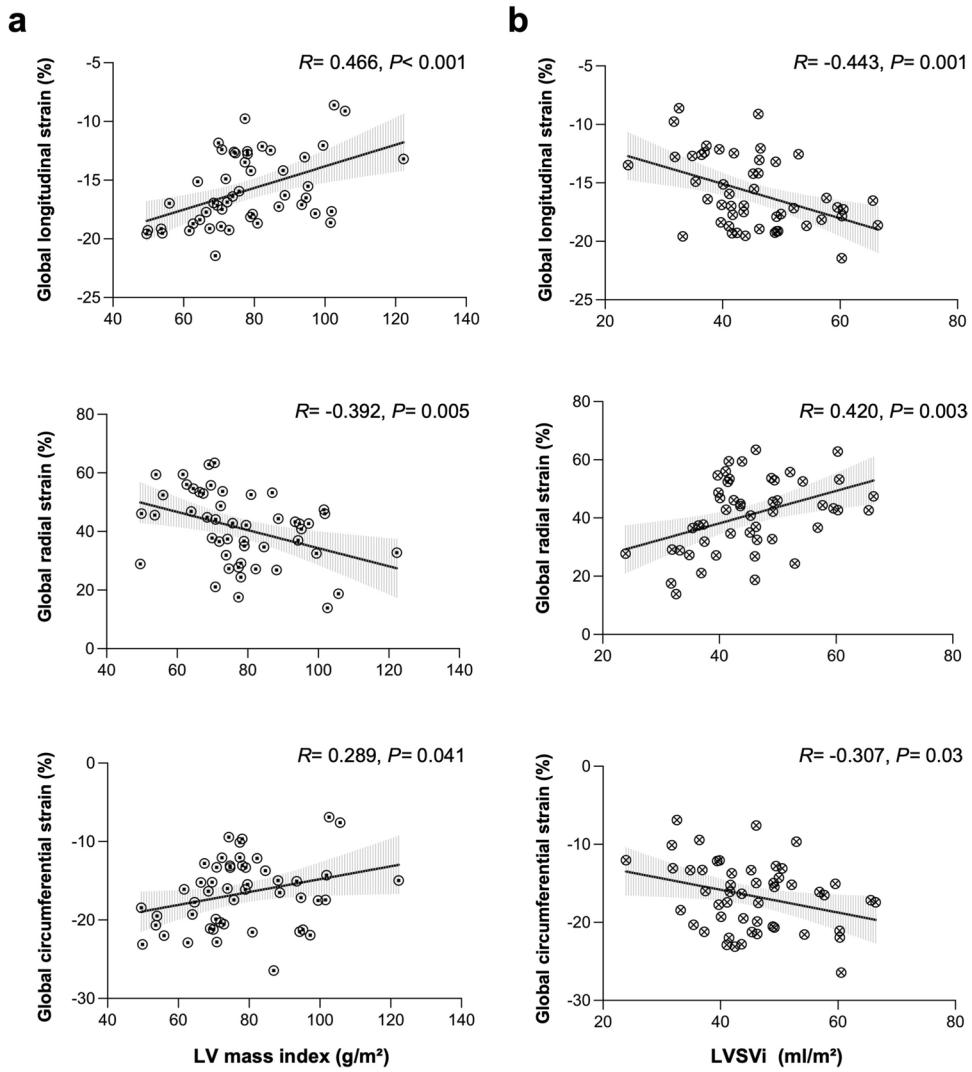

Fig. 3 The associations of LV mass index (**a**) and LVSVi (**b**) with LV global deformation parameters in RH patients. The gray shade indicates the 95% confidence interval. Increase in LV mass index and decrease in LVSVi were associated with decrease in longitudinal, radial, and circumferential strain. LV, left ventricular; LVSVi, left ventricular stroke volume index; RH, resistant hypertension

regression analysis after adjustment for age showed that RH remained independently associated with LV GLS and GRS, but not with GCS (Table S1).

Taken together, our results support the notion that the attenuation of longitudinal and radial strain in RH patients might constitute a LV adaptation as a response to a long-standing pressure overload. The tendential decrease of circumferential strain might be explained with the subepicardial layer being affected to a lesser degree in this RH patient cohort.

Prevalence of LGE in RH

Recently, an observational study reported that 145 (18%) of 786 patients with essential hypertension had non-ischemic LGE; they were more likely to be men and had greater LV mass and decreased strain [24]. Also, Wang et al detected 29.9% LGE + in their hypertension group [25]. In contrast, our cohort showed a higher prevalence of LGE (42%) with a predominantly non-ischemic pattern, suggesting that RH might be associated with a higher prevalence of LGE than controlled hypertension.

Myocardial fibrosis is a common end point of many cellular and noncellular pathological processes in hypertension; the severity and duration of hypertension might be responsible for the development of cardiac remodeling [26, 27]. In our study, LGE + RH patients had higher LV mass index; increased LV mass in remodeling is due to expanded extracellular interstitium and myocardial cell volume [28]. In the presence of an expanded interstitium, focal replacement fibrosis (non-ischemic LGE) is regarded as a result from the progression of interstitial fibrosis [24]. Increased collagen deposition in the extracellular interstitium induces stiffness and reduction of end-diastolic myofiber length, consequently inducing weakened contraction [29].

Table 3 Univariate and multivariate linear regression analysis of clinical factors and CMR parameters on LV deformation in RH patients

	LV GLS		LV GRS		LV GCS	
	Univariate	Multivariate	Univariate	Multivariate	Univariate	Multivariate
	R	*β*	*R*	*β*	*R*	*β*
Clinical factors						
Age (years)	0.116		−0.194	−0.183*	−0.128	
BSA (m^2)	0.089		−0.044		0.116	
BMI (kg/m^2)	0.121		0.008		0.130	
Male	−0.309*		0.224		−0.087	
Office SBP (mmHg)	0.251		−0.113		0.017	
Office DBP (mmHg)	0.374**		−0.380**		0.070*	
CMR parameters						
Heart rate (beats/min)	0.337*		−0.374**		0.364**	
LVEDVi (mL/m^2)	0.089		−0.141		0.286*	
LVESVi (mL/m^2)	0.489***	0.301**	−0.544***	−0.447***	0.649***	0.711***
LVSVi (mL/m^2)	−0.443**	−0.689***	0.420**	0.616***	−0.307*	−0.413***
LV mass index (g/m^2)	0.466***	0.558***	−0.392**	−0.379***	0.289*	
RVEDVi (mL/m^2)	−0.133		0.074		0.114	
RVESVi (mL/m^2)	0.278		−0.339*		0.337*	
RVSVi (mL/m^2)	−0.404**		0.375**		−0.118	
LAEDVi (mL/m^2)	0.153		−0.169		0.126	
LAESVi (mL/m^2)	−0.139		0.046		−0.005	
RAEDVi (mL/m^2)	0.264		−0.338*		0.317*	
RAESVi (mL/m^2)	−0.034		−0.106		0.138	
R^2		0.713		0.685		0.588

Variates with $p < 0.05$ in the univariate analysis as well as age, gender, BMI, SBP, and DBP were included in the multivariate analysis. β is the standardized regression coefficient of stepwise multivariate linear regression analysis

*$p < 0.05$; **$p < 0.01$; ***$p < 0.001$

Abbreviations as in Tables 1 and 2

Differences in strain between LGE + and LGE − RH patients

Our results showed that reduction in longitudinal strain was observed in both LGE − and LGE + RH patients, compatible with an early decrease of longitudinal systolic function. However, while LGE − RH patients showed similar radial strain compared to controls, a worsening radial strain emerged in LGE + RH patients.

Generally, radial strain has been shown to have large ranges between studies and the variability of segmental strain remains rather high [8]. Nevertheless, radial strain can help to distinguish cardiac sarcoidosis from dilated cardiomyopathy [30], can predict clinical outcome in hypertrophic cardiomyopathy [31], and is more predictive for scar (defined with LGE) transmurality than longitudinal strain [32]. In fact, the underlying mechanisms responsible for worsening radial strain have not been completely defined yet. Radial strain represents the global myocardial function in the radial direction, which is influenced by the deformation of all myocardial layers. Thus, it seems reasonable to assume that once focal myocardial fibrosis visualizable by LGE has occurred it might contribute to the reduction of LV radial strain.

Earlier echocardiographic studies have investigated the effects of myocardial fibrosis on LV deformation through identifying the association of plasma markers of myocardial fibrosis with strain alterations. Kang et al found increasing tissue inhibitor of matrix metalloproteinase (TIMP)-1 in hypertensive patients with normal LVEF correlated with attenuation of longitudinal strain, whereas circumferential and radial strain were not attenuated [19]. Poulsen et al showed that hypertensive patients had decreased longitudinal strain and increased amino-terminal propeptide of procollagen type III, accompanied by an inverse correlation of the two parameters [20]. Plasma markers emerge in an early stage of a myocardial fibrotic process in mild to moderate hypertensive patients and indirectly reflect myocardial fibrosis, and may lack specificity in the case of concomitant fibrotic diseases (e.g., cardiac fibrosis combined with liver or kidney fibrosis) [33]. However, the patients in the current study rather suffered a late fibrotic process due to

Table 4 Univariate and multivariate linear regression analysis of clinical factors and CMR parameters on LV deformation in the control group

	LV GLS		LV GRS		LV GCS	
	Univariate	Multivariate	Univariate	Multivariate	Univariate	Multivariate
	R	*β*	*R*	*β*	*R*	*β*
Clinical factors						
Age (years)	−0.045		0.266		−0.018	0.395*
BSA (m^2)	−0.317		0.169		0.002	
BMI (kg/m^2)	−0.047		0.204		0.053	
Male	0.136		0.074		0.182	
Office SBP (mmHg)	0.138		0.263		−0.047	
Office DBP (mmHg)	−0.172		0.114		−0.282	
CMR parameters						
Heart rate (beats/min)	0.251		−0.136		0.038	
LVEDVi (mL/m^2)	−0.236		−0.203		−0.125	
LVESVi (mL/m^2)	0.290		−0.675**	−0.675**	0.543*	0.722***
LVSVi (mL/m^2)	−0.521*	−0.521*	0.272		−0.587*	−0.615***
LV mass index (g/m^2)	−0.096		−0.045		−0.415	
RVEDVi (mL/m^2)	−0.064		−0.251		−0.287	
RVESVi (mL/m^2)	0.120		−0.336		0.187	
RVSVi (mL/m^2)	−0.175		−0.084		−0.567*	
LAEDVi (mL/m^2)	−0.007		−0.028		0.464	
LAESVi (mL/m^2)	−0.377		0.083		0.149	
RAEDVi (mL/m^2)	−0.109		0.108		0.146	
RAESVi (mL/m^2)	−0.222		0.004		0.030	
R^2		0.271		0.456		0.746

Variates with $p < 0.05$ in the univariate analysis as well as age, gender, BMI, SBP, and DBP were adjusted in the multivariate analysis. β is the standardized regression coefficient of stepwise multivariate linear regression analysis

*$p < 0.05$; **$p < 0.01$; ***$p < 0.001$

Abbreviations as in Tables 1 and 2

long-standing arterial hypertension. LGE-CMR is a visual approach to directly display focal myocardial fibrosis [34]. Identifying the strain differences in RH patients with and without focal myocardial fibrosis might provide data on the extent of myocardial layer impairment and offer insights into the influence of a long-standing pressure overload and a myocardial fibrotic process on cardiac deformation.

Limitations

The sample size in our study was small, which may have had an influence on the power to identify differences between study groups. However, all participants were recruited consecutively and prospectively according to the stringent selection criteria; future studies with larger populations are warranted to corroborate the consistency and reproducibility of our preliminary findings. Second, although some risk factors had been adjusted for multivariate regression analyses, several potential confounders, such as the dosages of antihypertensive drugs and sodium intake, may have an additional effect. Age-matching of controls and RH patients was not precise, but a multivariate analysis did not alter the results after adjustment for age. Another limitation is the lack of detailed information about the duration of hypertension. Nevertheless, all recruited patients were classified as RH according to the ESC guidelines and extensive diagnostics had been previously performed at our tertiary university medical center excluding secondary causes of hypertension. It can be assumed that hypertension has been developing over a long period of time during the aging process in the vast majority of the current elder cohort. Further, FT-CMR is performed mainly based on a block-matching algorithm, which requires a careful tuning of the search region and solving for displacements between short-distance regions [7]. Thus, radial strain being calculated over smaller regions between endo- and epicardium is less reliable than longitudinal and circumferential strain [7].

Conclusions

Our study revealed that attenuation of LV global longitudinal and radial strain as well as the tendency of circumferential strain attenuation might be consecutive adaptations responding to long-standing pressure overload in RH patients, and global circumferential strain attenuation only by tendency might be attributable to a still partially preserved subepicardial layer. Further, focal myocardial fibrosis has a high incidence in RH patients, presents primarily with a non-ischemic LGE pattern predominantly localized in the basal inferior and inferolateral LV segments, and is associated with reduced global radial strain. Therefore, FT-CMR-derived myocardial strain offers insights into the influence of long-standing pressure overload and of a myocardial fibrotic process on cardiac deformation in RH.

Supplementary Information The online version contains supplementary material available at https://doi.org/10.1007/s00330-023-09595-z.

Funding Open Access funding enabled and organized by Projekt DEAL. The authors state that this work has not received any funding.

Declarations

Guarantor The scientific guarantor of this publication is Enver Tahir, MD.

Conflict of interest The authors of this manuscript declare no relationships with any companies, whose products or services may be related to the subject matter of the article.

Statistics and biometry No complex statistical methods were necessary for this paper.

Informed consent All participants gave their written informed consent before being included in this study.

Ethical approval The ethics committee of the general medical council approved the study.

Previous reports of the study cohort The study population included 16 RH patients, who were included in a previously publication. The initial publication reported on the effects of a renal denervation procedure in RH patients. In brief, changes in LV mass, myocardial strain, and diastolic function were assessed before and on a 12-month follow-up after renal denervation.

Tahir E, Koops A, Warncke ML et al (2019) Effect of renal denervation procedure on left ventricular mass, myocardial strain and diastolic function by CMR on a 12-month follow-up. Jpn J Radiol 37:642-650.

Methodology
- prospective
- observational
- performed at one institution

References

1. Roth GA, Mensah GA, Johnson CO et al (2020) Global burden of cardiovascular diseases and risk factors, 1990–2019: Update From the GBD 2019 Study. J Am Coll Cardiol 76:2982–3021
2. Williams B, Mancia G, Spiering W et al (2018) 2018 ESC/ESH Guidelines for the management of arterial hypertension. Eur Heart J 39:3021–3104
3. Kaplan NM (2005) Resistant hypertension. J Hypertens 23:1441–1444
4. Daugherty SL, Powers JD, Magid DJ et al (2012) Incidence and prognosis of resistant hypertension in hypertensive patients. Circulation 125:1635–1642
5. Weber KT, Brilla CG, Janicki JS (1993) Myocardial fibrosis: functional significance and regulatory factors. Cardiovasc Res 27:341–348
6. Alsharari R, Oxborough D, Lip GYH, Shantsila A (2021) Myocardial strain imaging in resistant hypertension. Curr Hypertens Rep 23:24
7. Amzulescu MS, De Craene M, Langet H et al (2019) Myocardial strain imaging: review of general principles, validation, and sources of discrepancies. Eur Heart J Cardiovasc Imaging 20:605–619
8. Claus P, Omar AMS, Pedrizzetti G, Sengupta PP, Nagel E (2015) Tissue tracking technology for assessing cardiac mechanics: principles, normal values, and clinical applications. JACC Cardiovasc Imaging 8:1444–1460
9. Tahir E, Koops A, Warncke ML et al (2019) Effect of renal denervation procedure on left ventricular mass, myocardial strain and diastolic function by CMR on a 12-month follow-up. Jpn J Radiol 37:642–650
10. Mahfoud F, Urban D, Teller D et al (2014) Effect of renal denervation on left ventricular mass and function in patients with resistant hypertension: data from a multi-centre cardiovascular magnetic resonance imaging trial. Eur Heart J 35:2224–2231b
11. Schulz-Menger J, Bluemke DA, Bremerich J et al (2020) Standardized image interpretation and post-processing in cardiovascular magnetic resonance - 2020 update : Society for Cardiovascular Magnetic Resonance (SCMR): Board of Trustees Task Force on Standardized Post-Processing. J Cardiovasc Magn Reson 22:19
12. Le TT, Tan RS, De Deyn M et al (2016) Cardiovascular magnetic resonance reference ranges for the heart and aorta in Chinese at 3T. J Cardiovasc Magn Reson 18:21
13. Olivotto I, Maron MS, Autore C et al (2008) Assessment and significance of left ventricular mass by cardiovascular magnetic resonance in hypertrophic cardiomyopathy. J Am Coll Cardiol 52:559–566
14. Morais P, Marchi A, Bogaert JA et al (2017) Cardiovascular magnetic resonance myocardial feature tracking using a non-rigid, elastic image registration algorithm: assessment of variability in a real-life clinical setting. J Cardiovasc Magn Reson 19:24
15. Tahir E, Starekova J, Muellerleile K et al (2019) Impact of myocardial fibrosis on left ventricular function evaluated by

feature-tracking myocardial strain cardiac magnetic resonance in competitive male triathletes with normal ejection fraction. Circ J 83:1553–1562
16. Donal E, Bergerot C, Thibault H et al (2009) Influence of afterload on left ventricular radial and longitudinal systolic functions: a two-dimensional strain imaging study. Eur J Echocardiogr 10:914–921
17. Baltabaeva A, Marciniak M, Bijnens B et al (2008) Regional left ventricular deformation and geometry analysis provides insights in myocardial remodelling in mild to moderate hypertension. Eur J Echocardiogr 9:501–508
18. Imbalzano E, Zito C, Carerj S et al (2011) Left ventricular function in hypertension: new insight by speckle tracking echocardiography. Echocardiography 28:649–657
19. Kang SJ, Lim HS, Choi BJ et al (2008) Longitudinal strain and torsion assessed by two-dimensional speckle tracking correlate with the serum level of tissue inhibitor of matrix metalloproteinase-1, a marker of myocardial fibrosis, in patients with hypertension. J Am Soc Echocardiogr 21:907–911
20. Poulsen SH, Andersen NH, Heickendorff L, Mogensen CE (2005) Relation between plasma amino-terminal propeptide of procollagen type III and left ventricular longitudinal strain in essential hypertension. Heart 91:624–629
21. Wang J, Khoury DS, Yue Y, Torre-Amione G, Nagueh SF (2008) Preserved left ventricular twist and circumferential deformation, but depressed longitudinal and radial deformation in patients with diastolic heart failure. Eur Heart J 29:1283–1289
22. Mangion K, McComb C, Auger DA, Epstein FH, Berry C (2017) Magnetic resonance imaging of myocardial strain after acute ST-segment-elevation myocardial infarction: a systematic review. Circ Cardiovasc Imaging 10:e006498
23. Andre F, Steen H, Matheis P et al (2015) Age- and gender-related normal left ventricular deformation assessed by cardiovascular magnetic resonance feature tracking. J Cardiovasc Magn Reson 17:25
24. Iyer NR, Le TT, Kui MSL et al (2022) Markers of focal and diffuse nonischemic myocardial fibrosis are associated with adverse cardiac remodeling and prognosis in patients with hypertension: the REMODEL study. Hypertension 79:1804–1813
25. Wang S, Hu H, Lu M et al (2017) Myocardial extracellular volume fraction quantified by cardiovascular magnetic resonance is increased in hypertension and associated with left ventricular remodeling. Eur Radiol 27:4620–4630
26. Hill JA, Olson EN (2008) Cardiac plasticity. N Engl J Med 358:1370–1380
27. Kuruvilla S, Janardhanan R, Antkowiak P et al (2015) Increased extracellular volume and altered mechanics are associated with LVH in hypertensive heart disease, not hypertension alone. JACC Cardiovasc Imaging 8:172–180
28. Rodrigues JC, Amadu AM, Ghosh Dastidar A et al (2017) ECG strain pattern in hypertension is associated with myocardial cellular expansion and diffuse interstitial fibrosis: a multi-parametric cardiac magnetic resonance study. Eur Heart J Cardiovasc Imaging 18:441–450
29. Pichler G, Redon J, Martinez F et al (2020) Cardiac magnetic resonance-derived fibrosis, strain and molecular biomarkers of fibrosis in hypertensive heart disease. J Hypertens 38:2036–2042
30. Tsuji T, Tanaka H, Matsumoto K et al (2013) Capability of three-dimensional speckle tracking radial strain for identification of patients with cardiac sarcoidosis. Int J Cardiovasc Imaging 29:317–324
31. Smith BM, Dorfman AL, Yu S et al (2014) Relation of strain by feature tracking and clinical outcome in children, adolescents, and young adults with hypertrophic cardiomyopathy. Am J Cardiol 114:1275–1280
32. Maret E, Todt T, Brudin L et al (2009) Functional measurements based on feature tracking of cine magnetic resonance images identify left ventricular segments with myocardial scar. Cardiovasc Ultrasound 7:53
33. Rubis P, Dziewiecka E, Szymanska M et al (2021) Lack of relationship between fibrosis-related biomarkers and cardiac magnetic resonance-assessed replacement and interstitial fibrosis in dilated cardiomyopathy. Cells 10:1295
34. Karamitsos TD, Arvanitaki A, Karvounis H, Neubauer S, Ferreira VM (2020) Myocardial tissue characterization and fibrosis by imaging. JACC Cardiovasc Imaging 13:1221–1234

Table S1: Age-adjusted association of RH with LV deformation.

LV strain parameters	Unstandardized coefficient†	95% CI	*P* value
LV GLS, %	2.684	1.071, 4.297	**0.001**
LV GRS, %	-6.695	-12.987, -0.402	**0.037**
LV GCS, %	2.333	-0.060, 4.726	0.056

†Unstandardized coefficient of RH adjusted by age.

Values in **bold** denote statistical significance.

Abbreviations: CI, confidence interval; GCS, global circumferential strain; GLS, global longitudinal strain; GRS, global radial strain; LV, left ventricular; RH, resistant hypertension.

Figure S1: Flow chart of the study.

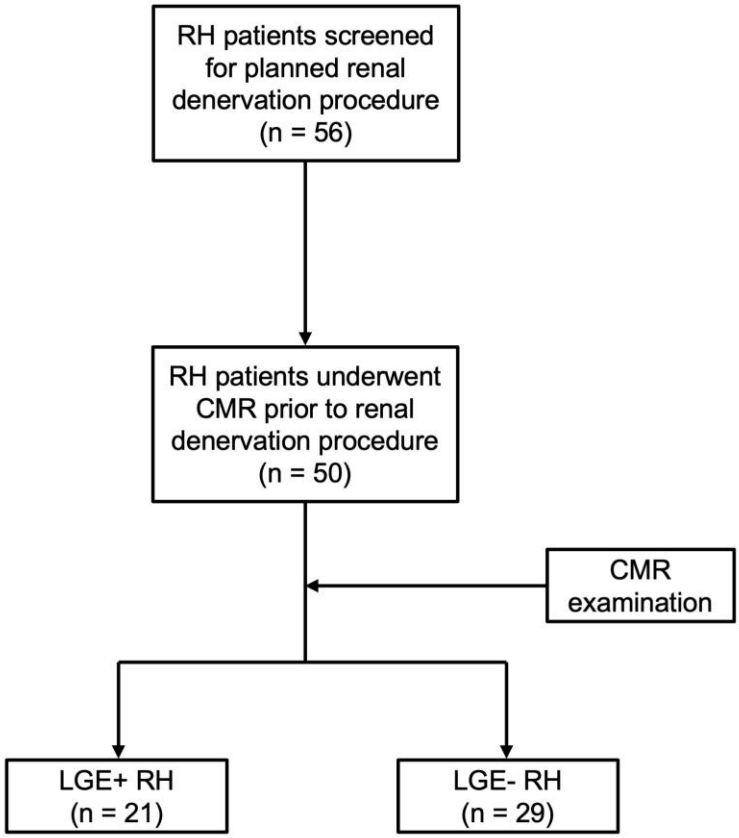

5 Chapter 5: Unpublished Manuscript, in preparation

Cardiac magnetic resonance imaging shows impaired systolic function and myocardial tissue alterations in germ cell cancer survivors after platinum-based chemotherapy

Antonia Beitzen-Heineke, Christina Rolling, Christoph Seidel, Jennifer Erley, Isabel Molwitz, Kai Muellerleile, Dennis Saering, Juliana Senftinger, Niklas Börschel, Nils Engel, Carsten Bokemeyer, Gerhard Adam, Enver Tahir* & Hang Chen*

*contributed equally

Personal contribution:

The following manuscript is currently in preparation. I am the shared last author of this research article. I participated in the study design with first author and co-last author. I post-processed and analyzed the image data with co-last author and plotted the Figure 3. I contributed the manuscript draft preparation.

Impaired systolic function and myocardial tissue alterations in long-term germ cell cancer survivors after platinum-based chemotherapy

Antonia Beitzen-Heineke, MD[1], Christina Charlotte Rolling, MD[1], Christoph Seidel, MD[1], Jennifer Erley, MD[2], Isabel Molwitz, MD[2], Kai Muellerleile, MD[3], Dennis Saering, PhD[4], Juliana Senftinger, MD[3], Niklas Börschel MD[1], Nils Wolfgang Engel, MD[1], Carsten Bokemeyer, MD[1], Gerhard Adam, MD[2], Enver Tahir, MD[2*] & Hang Chen, MD[2*]

[1]Department for Oncology, Hematology and Bone Marrow Transplantation with the Section of Pneumology, University Medical Center Hamburg Eppendorf, Hamburg, Germany

[2]Department of Diagnostic and Interventional Radiology and Nuclear Medicine, University Hospital Hamburg Eppendorf, Hamburg, Germany

[3]Department of General and Interventional Cardiology, University Heart Center, Hamburg, Germany

[4]Information Technology and Image Processing, University of Applied Sciences, Wedel, Germany

*contributed equally

Corresponding Author

Dr. med. Antonia Beitzen-Heineke
Martinistr. 52
20246 Hamburg
Germany
+49 15222827127
a.beitzen-heineke@uke.de

Abstract

Background

Germ cell cancer (GCC) survivors are at increased risk for cardiovascular disease. We aimed to investigate the long-term effects of platinum-based combination chemotherapy (PBCT) on cardiac function and myocardial tissue in GCC survivors by cardiac magnetic resonance (CMR) imaging.

Methods

44 asymptomatic GCC survivors (age 44 (22-66) years) ≥3 years after PBCT (follow-up time 10 (4-22) years) and 21 age-matched healthy controls underwent CMR assessment including left ventricular (LV) and right ventricular (RV) ejection fraction (EF), strain analysis, late gadolinium enhancement (LGE) imaging, and T1/T2 mapping.

Results

LV- and RVEF were significantly lower in GCC survivors compared to controls (LVEF 56 ±5% *vs.* 59 ±5%, *p*=.017; RVEF 50 ±7% *vs.* 55 ±7%, *p*=.008). 7% (3/44) of survivors showed reduced LVEF (<50%), and 41% (18/44) showed borderline LVEF (50-54%). Strain analysis revealed significantly reduced deformation compared to controls (LV global longitudinal strain (GLS) -13 ±2% *vs.* -15 ±1%, *p*<.001; RV GLS -15 ±4% *vs.* -19 ±4%, *p*=.005). Tissue characterization revealed focal myocardial fibrosis in 9 survivors (20%) and lower myocardial native T1 relaxation times in survivors compared to controls (1202 ±25ms *vs.* 1226 ±37ms, *p*=.016). Attenuation of systolic function was observed after only two cycles of PBCT.

Conclusion

Based on CMR evaluation combination chemotherapy with cumulative cisplatin ≥200 mg/m² is associated with attenuation of biventricular systolic function and myocardial

tissue alterations in long-term GCC survivors. Further investigations into risk factors of cardiac toxicity and long-term outcome should be integrated in GCC survivorship programs.

Keywords

germ cell cancer; testicular cancer; survivorship; cardiooncology; cardiotoxicity; chemotherapy-induced cardiotoxicity; cisplatin toxicity

Introduction

Germ-cell cancer (GCC) is the most common cancer in young men aged between 20 to 40 years. Due to an excellent sensitivity to platinum-based chemotherapy and the use of multimodal treatment approaches using chemotherapy and secondary tumor resection, cure rates of more than 90% can be achieved even in metastatic disease.[1-3] As a result, long-term toxicities after GCC treatment are of particular importance in this group of cancer survivors with a life expectancy of several decades.

Long-term sequelae of chemo- and radiotherapy for GCC include metabolic syndrome and cardiovascular disease.[4] Risk estimates for cardiovascular disease range from 1.3- to 5.7-fold after platinum-based chemotherapy compared to surgery only.[5-8] Therefore, optimization of cardiovascular risk factors is recommended in GCC survivorship care. However, knowledge about cardiac function and myocardial alterations in GCC survivors is limited and no specific recommendations for cardiological examinations in GCC survivors do exist. Previous studies investigating cardiac function of GCC survivors using echocardiography described impaired diastolic function but no impairment of systolic function.[9-13]

Echocardiography is widely used to monitor cardiac function in patients undergoing potentially cardiotoxic cancer treatment. Using strain analysis, early changes in cardiac contractility can be detected before LVEF changes are manifest.[14,15] Strain imaging assesses the myocardial deformation capacity by quantifying the shortening of a myocardial segment in percent from end-diastole to end-systole. Assessment of LVEF and global longitudinal strain (GLS) using echocardiography is recommended in patients receiving a potentially cardiotoxic treatment.[16,17] LV global circumferential strain (GCS) is also predictive of chemotherapy-related cardiotoxicity but has not been established as a screening parameter.[18] In case of insufficient imaging quality, cardiac

magnetic resonance (CMR) imaging, which represents the gold standard for quantification of cardiac function and volumes, is recommended as an alternative imaging modality in evaluating cardiotoxicity.[16,19,20] Characterization of myocardial tissue by CMR may provide further information on cardiac changes during oncological treatment.[19] T1/T2 mapping and late gadolinium enhancement (LGE) enable identification of interstitial fibrosis and edema and LGE patterns allow to distinguish ischemic from non-ischemic scar tissue.[20]

Therefore, this study aimed to gain insights on long-term cardiac effects of platinum-based combination chemotherapy (PBCT) by characterizing cardiac function and myocardial tissue in GCC survivors using CMR imaging.

Methods

Study population

The study was approved by the local ethics committee (PV7173) and carried out in accordance with the Declaration of Helsinki. All participants gave written informed consent. Forty-six asymptomatic men with a history of GCC ≥ 3 years after completion of PBCT were prospectively recruited at the University Medical Center Hamburg-Eppendorf between March 2020 and January 2022 and underwent a CMR scan. General exclusion criteria were MRI contraindications, previous radiotherapy, any history of coronary artery disease, heart failure, and arrhythmia. A historic cohort of 21 age-matched healthy men was used as controls. One participant from the survivor group was excluded from analysis because of extensive ischemic myocardial fibrosis and one patient withdrew consent due to claustrophobia (Supplemental Figure 1).

Anamnestic cardiovascular risk factors and medication were documented and a laboratory analysis was performed including NT-proBNP, Troponin I, cholesterol, low density lipoprotein (LDL), high density lipoprotein (HDL), glomerular filtration rate (GFR), creatinine, and testosterone levels.

CMR protocol

CMR was performed on a 3.0 T scanner (Ingenia, Philips Medical Systems, Best, The Netherlands) as previously described.[21] Imaging was performed using a standard retrospective ECG-triggered steady-state free-precession (SSFP) cine sequence in short- and long-axis views with 25 cardiac phases. Native and post-contrast T1 mapping were performed with a motion-corrected modified look-locker inversion (MOLLI) recovery sequence using the 5s (3s) 3s scheme. T2 mapping was performed with a free-breathing navigator-gated black-blood prepared gradient and spin-echo

(GraSE) hybrid sequence in the basal, mid, and apical slices corresponding to the MOLLI sequence. LGE imaging with a phase sensitive inversion recovery (PSIR) sequence was acquired 10 minutes after injecting 0.15 mmol/kg of gadoterate meglumine (Dotarem™, Sulzbach, Germany).

CMR data analysis

CMR images were post-processed independently and blindly in random order by two investigators (E.T. and H.C.) using CVi42 software (Circle Cardiovascular Imaging Inc, Calgary, Alberta, Canada) as previously described.[21]

Statistical analysis

Statistical analysis was performed using SPSS for Windows, version 28.0.1.1 (IBM SPSS Statistics, Armonk, NY, USA). Graphs were generated using ggplot2 via RStudio (version 2022.12.0.353, Boston, MA, USA). Demographic data are presented as median (range), continuous parameters as mean ± SD, and categorical data as absolute numbers and percentages. Normality of continuous data was assessed using Shapiro-Wilk test. Man-Whitney-U-Test was used for statistical analysis of demographic data, t-test for metric data, and Fisher's exact test for categorical variables. Pearson's correlation or Spearman's correlation were applied as appropriate. All p values are two-sided and considered significant at $p<.05$.

Results

Baseline demographics and tumor characteristics

Median age of survivors was 44 (22-66) years. There were no significant differences in age, weight, height, body mass index (BMI) and BSA between survivors and controls (Table 1). Median follow-up time after completion of PBCT was 10 (4-22) years. Thirty-six percent of survivors had seminoma and 64% had non-seminoma. Initial disease stage was I in 25%, II in 45% and III in 30% of survivors, respectively (Table 2). In total, 33 (75%) survivors had received one and 11 (25%) had received two or more lines of therapy as detailed in Table 2. A total of 10 survivors had received high dose chemotherapy followed by autologous stem cell transplantation.

Cardiac function, volumes and mass

Detailed results of CMR-derived parameters are presented in Supplemental Table 1. LVEF and RVEF were significantly lower in GCC survivors compared to controls (LVEF 56 ±5% *vs.* 59 ±5%, p=.017; RVEF 50 ±7% *vs.* 55 ±7%, p=.008; Figure 1 A and B). Three survivors (7%) showed reduced LVEF <50% and 18 (41%) survivors presented with borderline LVEF between 50-54%. RV end-systolic volume index (RVESVi), a marker of ventricle remodeling, was significantly higher (45 ±10 ml/m² *vs.* 38 ±11 ml/m², p=.01) and there was a trend towards higher LVESVi in survivors compared to controls (39 ±9 ml/m² *vs.* 35 ±10 ml/m², p=.084; Supplemental Table 1). No significant differences were found for heart rate, LV cardiac index (cardiac output per minute related to BSA), LV mass index, atrial volumes, ventricular systolic and ventricular end-diastolic volumes, respectively (Supplemental Table 1).

Myocardial strain

Strain analysis revealed significantly lower myocardial deformation of the left and right ventricle in survivors compared to controls as measured by GLS (LV GLS -13 ±2% *vs.* -15 ±1%, $p<.001$; RV GLS -15 ±4% *vs.* -19 ±4%, $p=.005$; Figure 1C and D) and LV GCS (-14 ±2% *vs.* -16 ±2%, $p<.001$; Figure 1E). No significant differences were found for RV GCS, LV radial strain, and RV free wall longitudinal strain (Figure 1F-H).

Myocardial tissue characterization

Myocardial native T1 mapping revealed lower T1 relaxation times in survivors compared to controls (1202 ±25ms *vs.* 1226 ±37ms, $p=.016$; Figure 2A). Survivors with decreased or borderline LVEF <55% had lower myocardial T1 values when compared to those with LVEF ≥55% (1191 ±22ms *vs.* 1211 ±25ms, $p=.007$; Table 3). A moderate positive correlation was found between native T1 values and LVEF ($r(41)=.346$, $p=.023$), and RVEF ($r(41)=.314$, $p=.04$), respectively. There was a moderate negative correlation between native T1 values and LV GLS ($r(41)=-0.341$, $p=.025$), and a strong negative correlation between native T1 values and RV GLS ($r(41)=-.534$, $p<.001$), respectively. T2 values and ECV did not differ between groups (Figure 2B-C). However, survivors with LVEF <55% had significantly lower percentage of ECV compared with survivors with normal LVEF (Table 3).

Eight survivors (18%) showed non-ischemic LGE indicating focal myocardial fibrosis (scar) and one survivor (2%) showed ischemic LGE (Figure 3 and Supplemental Table 1). Four survivors with non-ischemic LGE had normal LVEF (≥55%) and 4 survivors with non-ischemic LGE had borderline LVEF (50-54%) (Table 3).

Cardiac parameters in association with chemotherapy dose

A drop in LVEF was observed after merely two cycles of PBCT (Figure 4). Therefore, cardiac parameters and clinical characteristics were compared between survivors who received one cycle of chemotherapy (carboplatin AUC7 or cisplatin 100 mg/m², n=7) and those who received at least two cycles (cisplatin ≥200 mg/m² ± carboplatin, n=37).

Survivors who had received ≥2 cycles of PBCT showed significantly higher body weight and BSA (Table 4). No differences were found for anamnestic cardiovascular risk factors or medication. Laboratory analysis revealed significantly impaired renal functional parameters and lower testosterone levels, and a trend towards higher cholesterol levels in survivors after ≥2 cycles of PBCT. No significant differences were found for cardiac biomarkers Troponin T and NT-proBNP (Table 4). Two survivors who had received >2 cycles of PBCT showed elevated high-sensitive Troponin I. Both individuals presented with non-ischemic LGE not fulfilling criteria for acute myocarditis; acute myocardial infarction was ruled out in both individuals.

LVEF was significantly lower in survivors after ≥2 cycles of PBCT compared to survivors who had received one cycle of chemotherapy (54 ±5% *vs.* 62 ±5%, $p<.001$; Table 4). Strain analysis showed a significant decrease in LV and RV GCS after ≥2 cycles of PBCT (LV GCS -13 ±2% *vs.* -16 ±2%, $p<.001$; RV GCS -8 ±3% *vs.* -10 ±2%, $p=.046$; Table 4), indicating decreased myocardial deformation after higher doses of chemotherapy. No significant changes were found for RVEF, LV GLS, and RV GLS, respectively. Notably, all survivors with focal LGE had received ≥2 cycles of PBCT (Table 4). Multivariate regression analysis showed that association of chemotherapy cycles with LVEF, LV GCS and RV GCS, respectively, was independent of testosterone levels, renal function, body weight, and BSA.

Cardiac parameters did not differ between survivors who had received high-dose chemotherapy and autologous stem cell transplantation and those without high-dose chemotherapy.

Cardiac parameters in association with clinical and laboratory parameters

GCC survivors with anamnestic arterial hypertension had lower native T1 values (1179 ±19ms *vs.* 1207 ±24ms, p=.003). Anamnestic dyslipidemia or smoking status, age and time of follow-up were not associated with differences in cardiac parameters. A weak negative correlation was found for LV GLS and HDL level ($r(42)$=-.347, p=.021). Beyond that, systolic functional parameters and T1 values did not correlate with levels of cholesterol, LDL, HDL, and testosterone, respectively.

Discussion

To the best of our knowledge, this is the first study to extensively characterize cardiac alterations in long-term survivors of GCC using CMR imaging. The study has three major findings: 1. We found attenuated systolic function in GCC survivors almost 10 years after therapy completion as measured by EF and strain analysis after only two cycles of PBCT; 2. tissue characterization revealed that focal myocardial fibrosis detected by LGE was common in GCC survivors, and 3. survivors presented with decreased native T1 values compared to controls.

Previous studies investigating cardiac function of GCC survivors mainly used echocardiography. A recent study by Bjerring *et al.* performed echocardiography including strain analysis 30 years after cisplatin-based chemotherapy for GCC and found no differences in biventricular systolic function between survivors and controls.[9] In contrast, using CMR as a more sensitive technique, the current study demonstrated subclinical attenuation of systolic function after cisplatin-based chemotherapy, but not after one course of carboplatin. This functional impairment was observed after a threshold of two cycles of cisplatin-based combination chemotherapy (at ≥ 200 mg/m² cumulative dose) without further dose-dependent decline beyond that, although data on this association are clearly still limited. These findings indicate PBCT has more extensive effects on the heart than known so far. This observation is supported by a previous *in vivo* study which described cisplatin-induced development of LV dysfunction and depressed cardiomyocyte contraction in mice which was associated with mitochondrial abnormalities, endoplasmic reticulum stress response and apoptosis.[22] However, considering the results of Bjerring *et al.* with a longer follow-up of 30 years, the observed subclinical changes in systolic function might not necessarily progress to clinical manifestation of heart failure.[9] In a population-based cohort study

mortality due to non-ischemic cardiac disease was increased in GCC survivors following combined chemo- and radiotherapy, but not after chemotherapy alone.[23] Nevertheless, in the current study 4 out of 45 asymptomatic survivors had decreased LVEF, raising the question, whether specific cardiological examinations e. g. CMR should be included into the follow-up routine of GCC survivors.

The lower T1 values strongly indicated myocardial tissue changes after PBCT compared to controls. A decrease of native T1 values in patients shortly after anthracycline administration has previously been described and identified as a predictor of subsequent anthracycline-induced cardiomyopathy.[24] The two main determinants of an increase in native T1 values are myocardial edema and increased interstitial space, e.g. because of diffuse interstitial fibrosis or amyloid deposition. A decrease in native T1 is described in iron or lipid overload.[25] Interestingly, we found that worse systolic functional parameters in survivors correlated with a decrease in native T1 values, pointing towards functional consequences of these tissue alterations. It remains unclear which myocardial tissue alterations underlie the detected native T1 decrease in GCC survivors. However, decreased T1 values, no differences in ECV compared to healthy controls, and lower ECV in survivors with LVEF below 55% argue against diffuse interstitial fibrosis in the myocardium of GCC survivors. Instead, the current study revealed a high prevalence (18%) of focal myocardial fibrosis as identified by mid-wall/subepicardial LGE. Previous studies reported non-ischemic LGE in 4-9% of cancer patients and in 2.8-4% of healthy individuals.[26-28] The clinical significance of non-ischemic LGE in cancer survivors remains unclear. In general, presence of LGE has a prognostic value in patients with preexisting heart disease, whereas subjects with minor non-ischemic LGE and no further structural or functional cardiac abnormalities are considered to have a favorable outcome.[20,29]

Lower T1 values in patients with anamnestic arterial hypertension and association of lower HDL with worse LV GLS indicate that the observed functional changes and tissue alterations might be a secondary sequela. However, these associations were not robustly detected for all functional parameters. Based on this study we cannot draw a conclusion on whether the observed cardiac effects are a result of direct chemotherapy-induced cardiotoxicity or rather a secondary result of metabolic changes or arterial hypertension.

Our study has some shortcomings. A major limitation of CMR imaging is that diastolic function cannot be validly assessed. Furthermore, this study does not allow to differentiate which chemotherapy agent is the cause of the observed cardiac effects. Even though almost every chemotherapy cycle contained a platinum agent, most survivors had also received several cycles of bleomycin and etoposide. However, survivors treated with only one cycle of carboplatin single agent did not seem to be at increased risk. Longitudinal studies with baseline CMR examinations and a longer follow-up are needed in order to elucidate the clinical significance and prognostic value of the subclinical systolic impairment observed in this cohort.

In conclusion, this study revealed for the first time that subclinical attenuation of biventricular systolic function characterized by decreased EF and myocardial deformation, and changes in myocardial tissue characteristics can be detected in long-term asymptomatic GCC survivors following PBCT. This study emphasizes the need for more in depths investigations into the risk of cardiotoxicity associated with PBCT and points to the importance of long-term cardiovascular follow-up in GCC survivors as well as to education programs to avoid additional cardiac risk behavior in this survivorship population.

Acknowledgements

The authors wish to thank the survivors and healthy individuals who participated in this study.

Funding

This study was partially sponsored by the Barbara and Wilfried Mohr Stiftung Hamburg, Germany.

Declaration of Interest Statement

All authors declare that they have no conflicts of interest related to this study.

References

1. Hanna N, Einhorn LH. Testicular Cancer: A Reflection on 50 Years of Discovery. *Journal of Clinical Oncology*. 2014/10/01 2014;32(28):3085-3092. doi:10.1200/JCO.2014.56.0896
2. Beyer J, Collette L, Sauvé N, et al. Survival and New Prognosticators in Metastatic Seminoma: Results From the IGCCCG-Update Consortium. *J Clin Oncol*. May 10 2021;39(14):1553-1562. doi:10.1200/jco.20.03292
3. Gillessen S, Sauvé N, Collette L, et al. Predicting Outcomes in Men With Metastatic Nonseminomatous Germ Cell Tumors (NSGCT): Results From the IGCCCG Update Consortium. *J Clin Oncol*. May 10 2021;39(14):1563-1574. doi:10.1200/jco.20.03296
4. Chovanec M, Lauritsen J, Bandak M, et al. Late adverse effects and quality of life in survivors of testicular germ cell tumour. *Nat Rev Urol*. Apr 2021;18(4):227-245. doi:10.1038/s41585-021-00440-w
5. Belt-Dusebout AWvd, Nuver J, Wit Rd, et al. Long-Term Risk of Cardiovascular Disease in 5-Year Survivors of Testicular Cancer. *Journal of Clinical Oncology*. 2006;24(3):467-475. doi:10.1200/jco.2005.02.7193
6. Haugnes HS, Wethal T, Aass N, et al. Cardiovascular risk factors and morbidity in long-term survivors of testicular cancer: a 20-year follow-up study. *J Clin Oncol*. Oct 20 2010;28(30):4649-57. doi:10.1200/jco.2010.29.9362
7. Huddart RA, Norman A, Shahidi M, et al. Cardiovascular Disease as a Long-Term Complication of Treatment for Testicular Cancer. *Journal of Clinical Oncology*. 2003;21(8):1513-1523. doi:10.1200/jco.2003.04.173
8. Lauritsen J, Hansen MK, Bandak M, et al. Cardiovascular Risk Factors and Disease After Male Germ Cell Cancer. *J Clin Oncol*. Feb 20 2020;38(6):584-592. doi:10.1200/jco.19.01180
9. Bjerring AW, Fosså SD, Haugnes HS, et al. The cardiac impact of cisplatin-based chemotherapy in survivors of testicular cancer: a 30-year follow-up. *Eur Heart J Cardiovasc Imaging*. Mar 22 2021;22(4):443-450. doi:10.1093/ehjci/jeaa289
10. Altena R, Hummel YM, Nuver J, et al. Longitudinal changes in cardiac function after cisplatin-based chemotherapy for testicular cancer. *Ann Oncol*. Oct 2011;22(10):2286-93. doi:10.1093/annonc/mdr408
11. Nuver J, Smit AJ, Sleijfer DT, et al. Left ventricular and cardiac autonomic function in survivors of testicular cancer. *Eur J Clin Invest*. Feb 2005;35(2):99-103. doi:10.1111/j.1365-2362.2005.01460.x
12. Altena R, de Haas EC, Nuver J, et al. Evaluation of sub-acute changes in cardiac function after cisplatin-based combination chemotherapy for testicular cancer. *Br J Cancer*. Jun 16 2009;100(12):1861-6. doi:10.1038/sj.bjc.6605095
13. van Schinkel LD, Willemse PM, van der Meer RW, et al. Chemotherapy for testicular cancer induces acute alterations in diastolic heart function. *Br J Cancer*. Aug 20 2013;109(4):891-6. doi:10.1038/bjc.2013.445
14. Negishi K, Negishi T, Haluska BA, Hare JL, Plana JC, Marwick TH. Use of speckle strain to assess left ventricular responses to cardiotoxic chemotherapy and cardioprotection. *Eur Heart J Cardiovasc Imaging*. Mar 2014;15(3):324-31. doi:10.1093/ehjci/jet159
15. Thavendiranathan P, Poulin F, Lim KD, Plana JC, Woo A, Marwick TH. Use of myocardial strain imaging by echocardiography for the early detection of cardiotoxicity in patients during and after cancer chemotherapy: a systematic review. *J Am Coll Cardiol*. Jul 1 2014;63(25 Pt A):2751-68. doi:10.1016/j.jacc.2014.01.073
16. Lyon AR, López-Fernández T, Couch LS, et al. 2022 ESC Guidelines on cardio-oncology developed in collaboration with the European Hematology Association (EHA), the European Society for Therapeutic Radiology and Oncology (ESTRO) and the International Cardio-Oncology Society (IC-OS). *Eur Heart J*. Aug 26 2022;doi:10.1093/eurheartj/ehac244
17. Liu JE, Barac A, Thavendiranathan P, Scherrer-Crosbie M. Strain Imaging in Cardio-Oncology. *JACC CardioOncol*. Dec 2020;2(5):677-689. doi:10.1016/j.jaccao.2020.10.011

18. Narayan HK, French B, Khan AM, et al. Noninvasive Measures of Ventricular-Arterial Coupling and Circumferential Strain Predict Cancer Therapeutics-Related Cardiac Dysfunction. *JACC Cardiovasc Imaging*. Oct 2016;9(10):1131-1141. doi:10.1016/j.jcmg.2015.11.024
19. Jeong D, Gladish G, Chitiboi T, Fradley MG, Gage KL, Schiebler ML. MRI in cardio-oncology: A review of cardiac complications in oncologic care. *J Magn Reson Imaging*. Nov 2019;50(5):1349-1366. doi:10.1002/jmri.26895
20. Ponikowski P, Voors AA, Anker SD, et al. 2016 ESC Guidelines for the diagnosis and treatment of acute and chronic heart failure: The Task Force for the diagnosis and treatment of acute and chronic heart failure of the European Society of Cardiology (ESC)Developed with the special contribution of the Heart Failure Association (HFA) of the ESC. *Eur Heart J*. Jul 14 2016;37(27):2129-2200. doi:10.1093/eurheartj/ehw128
21. Tahir E, Azar M, Shihada S, et al. Myocardial injury detected by T1 and T2 mapping on CMR predicts subsequent cancer therapy-related cardiac dysfunction in patients with breast cancer treated by epirubicin-based chemotherapy or left-sided RT. *Eur Radiol*. Mar 2022;32(3):1853-1865. doi:10.1007/s00330-021-08260-7
22. Ma H, Jones KR, Guo R, Xu P, Shen Y, Ren J. Cisplatin compromises myocardial contractile function and mitochondrial ultrastructure: role of endoplasmic reticulum stress. *Clin Exp Pharmacol Physiol*. Apr 2010;37(4):460-5. doi:10.1111/j.1440-1681.2009.05323.x
23. Hellesnes R, Myklebust TÅ, Fosså SD, et al. Testicular Cancer in the Cisplatin Era: Causes of Death and Mortality Rates in a Population-Based Cohort. *Journal of Clinical Oncology*. 2021/11/10 2021;39(32):3561-3573. doi:10.1200/JCO.21.00637
24. Muehlberg F, Funk S, Zange L, et al. Native myocardial T1 time can predict development of subsequent anthracycline-induced cardiomyopathy. *ESC Heart Fail*. Aug 2018;5(4):620-629. doi:10.1002/ehf2.12277
25. Radenkovic D, Weingärtner S, Ricketts L, Moon JC, Captur G. T1 mapping in cardiac MRI. *Heart Failure Reviews*. 2017/07/01 2017;22(4):415-430. doi:10.1007/s10741-017-9627-2
26. Modi K, Joppa S, Chen KA, et al. Myocardial damage assessed by late gadolinium enhancement on cardiovascular magnetic resonance imaging in cancer patients treated with anthracyclines and/or trastuzumab. *Eur Heart J Cardiovasc Imaging*. Mar 22 2021;22(4):427-434. doi:10.1093/ehjci/jeaa279
27. Domenech-Ximenos B, Sanz-de la Garza M, Prat-González S, et al. Prevalence and pattern of cardiovascular magnetic resonance late gadolinium enhancement in highly trained endurance athletes. *Journal of Cardiovascular Magnetic Resonance*. 2020/09/03 2020;22(1):62. doi:10.1186/s12968-020-00660-w
28. Turkbey EB, Nacif MS, Guo M, et al. Prevalence and Correlates of Myocardial Scar in a US Cohort. *Jama*. Nov 10 2015;314(18):1945-54. doi:10.1001/jama.2015.14849
29. Lota Amrit S, Tsao A, Owen R, et al. Prognostic Significance of Nonischemic Myocardial Fibrosis in Patients With Normal LV Volumes and Ejection-Fraction. *JACC: Cardiovascular Imaging*. 2021/12/01 2021;14(12):2353-2365. doi:10.1016/j.jcmg.2021.05.016

Tables

Table 1. Baseline characteristics of GCC survivors compared to controls.

Demographics, median (range)	**GCC survivors** (n = 44)	**Controls** (n = 21)	***p* value**
Age, years	44 (22-66)	44 (22-67)	0.614
Weight, kg	88 (67-125)	85 (53-120)	0.370
Height, m	1.83 (1.7-1.95)	1.83 (1.65-1.95)	0.457
Body surface area, m^2	2.1 (1.83-2.51)	2.06 (1.57-2.47)	0.313
Body mass index, kg/m^2	27 (20-36)	25 (20-35)	0.421
Abbreviations: GCC, germ cell cancer.			

Table 2. Tumor characteristics and chemotherapy regimens.

	GCC survivors (n = 44)
Diagnosis, No. (%)	
Seminoma	16 (36)
Non-Seminoma	28 (64)
Initial disease stage, No. (%)	
I A-B	11 (25)
II A-C	20 (45)
III A-C	13 (30)
Time of follow-up, years, median (range)	10 (4-22)
Number of therapy lines, No. (%)	
1	33 (75)
2	6 (14)
3	4 (9)
4	1 (2)
Number of platinum-based chemotherapy cycles, No. (%)	
1	7 (16)
2	4 (9)
3	12 (27)
4	12 (27)
≥5	9 (21)
Chemotherapy regimens, No. (%)	
1st line carboplatin AUC7 + PEB + PEI + HD PEI + GOP	7 (16) 1 (2) 1 (2)
1st line PEB* + HD CE + HD CE + TI + PEI + PEI + HD CE	28 (64) 2 (5) 2 (5) 2 (5) 1 (2)
1st line PEI** + HD PEI + TI + HD CE	5 (11) 1 (2) 1 (2)
1st line cisplatin/etoposide	2 (5)
1st line HD PEI	2 (5)
Total high dose chemotherapy, No. (%)	10 (23)

Abbreviations: AUC, area under the curve; CE, carboplatin/etoposide; GCC, germ cell cancer; GOP, gemcitabine/oxaliplatin/paclitaxel; HD, high dose; PEB cisplatin/etoposide/bleomycin; PEI, cisplatin/etoposide/ ifosfamide; TI, paclitaxel/ifosfamide.

* one patient was switched to cisplatin/etoposide and one was switched to PEI due to bleomycin-toxicity

**one patient received first cycle without ifosphamide due to intensive care stay

Table 3. Myocardial tissue characteristics in GCC survivors depending on LVEF.

	LVEF <55% (n=21)	**LVEF ≥55%** (n=23)	***p* value**
Native T1 time, ms, mean ±SD	1191 ±22	1211 ±25	**0.007**
ECV, %, mean ±SD	24.2 ±1.4	25.6 ±1.9	**0.008**
LGE presence (non-ischemic), No. (%)	4 (19)	4 (17)	-

Abbreviations: ECV, extra cellular volume; LGE, late gadolinium enhancement; LVEF, left ventricular ejection fraction.

Table 4. Clinical characteristics and cardiac parameters depending on number of platinum-based chemotherapy cycles.

	Platinum-based chemotherapy		***p* value**
	1 cycle (n=7)	**≥2 cycles** (n=37)	
Demographics, median (range)			
Age, years	44 (29-55)	44 (22-66)	0.832
Follow-up, years	10 (6-22)	10 (4-22)	0.919
Height, m	1.78 (1.7-1.87)	1.83 (1.75-1.95)	0.212
Weight, kg	77 (72-100)	90 (67-125)	**0.023**
BMI, kg/m²	24 (22-29)	27 (20-36)	0.111
BSA, m²	2.02 (1.83-2.25)	2.13 (1.87-2.51)	**0.025**
Medical history, No. (%)			
Dyslipidemia	2 (29)	6 (16)	0.593
Diabetes mellitus	-	2 (5)	
Arterial hypertension	1 (14)	7 (19)	0.624
Former or active smoker	3 (43)	17 (46)	0.606
Antihypertensive Medication	1 (14)	8 (22)	0.557
Lipid-lowering drug	1 (14)	1 (3)	0.296
Cardiac parameters, mean ±SD			
Heart rate, beats/min	66 ±15	68 ±13	0.683
Left heart			
LVEF, %	62 ±5	54 ±5	**<0.001**
LV mass index, g/m²	53 ±5	59 ±5	0.270
LVEDVi, mL/m²	85 ±13	87 ±14	0.733
LVESVi, mL/m²	32 ±6	40 ±8	**0.023**
LVSVi, mL/m²	53 ±9	47 ±8	0.072
LAEDVi, mL/m²	14 ±4	16 ±7	0.398
LAESVi, mL/m²	30 ±9	33 ±9	0.442
Right heart			
RVEF, %	53 ±7	49 ±7	0.2
RVEDVi, mL/m²	92 ±16	89 ±15	0.526
RVESVi, mL/m²	43 ±10	45 ±10	0.643
RVSVi. mL/m²	49 ±10	44 ±9	0.138
RAEDVi, mL/m²	28 ±8	25 ±8	0.379
RAESVi, mL/ m²	44 ±6	41 ±12	0.501
Strain parameters			
LV GLS, %	-14 ±2	-13 ±2	0.339
LV GCS, %	-16 ±2	-13 ±2	**<0.001**
LV GRS, %	20 ±8	20 ±6	0.865
RV GLS, %	-16 ±6	-15 ±4	0.642
RV FWLS, %	-18 ±9	-19 ±6	0.740
RV GCS, %	-10 ±2	-8 ±3	**0.046**
LGE presence, No. (%)			
Non-ischemic LGE	-	8 (22)	
Ischemic LGE	-	1 (2)	
Mapping parameters			

Native global T1, ms	1207 ±21	1201 ±26	0.531
Native global T2, ms	45 ±3	45 ±3	0.707
ECV, %	26 ±2	25 ±2	0.053
Laboratory Findings, mean ±SD			
Cholesterol (mg/dl)	181 ±31	203 38	0.082
HDL (mg/dl)	50 ±12	46 ±12	0.207
LDL (mg/dl)	104 ±28	123 ±33	0.081
Testosteron	6 ±3	4 ±2	**0.002**
Troponin (pg/ml)	3 ±2	9 ±25	0.535
NT-proBNP (ng/L)	45 ±12	49 ±33	0.727
Creatinine (mg/dl)	0.9 ±0.1	1.1 ±0.2	**0.027**
GFR (ml/Min)	100 ±16	87 ±16	**0.025**

Abbreviations: BMI, body mass index; BSA, body surface area; ECV, extracellular volume; FWLS, free wall longitudinal strain; GCC, germ cell cancer; GCS, global circumferential strain; GFR, glomerular filtration rate; GLS, global longitudinal strain; GRS, global radial strain; HDL, high density lipoprotein; LA, left atrial; LAEDVi, left atrial end-diastolic volume index; LAESVi, left atrial end-systolic volume index; LDL low density lipoprotein; LGE, late gadolinium enhancement; LV, left ventricular; LVEDVi, left ventricular end-diastolic volume index; LVEF, left ventricular ejection fraction; LVESVi, left ventricular end-systolic volume index; LVSVi, left ventricular stroke volume index; RA, right atrial; RAEDVi, right atrial end-diastolic volume index; RAESVi, right atrial end-systolic volume index; RV, right ventricular; RVEDVi, right ventricular end-diastolic volume index; RVESVi, right ventricular end-systolic volume index.

Figure Legends

Figure 1. Systolic function in germ cell cancer survivors compared to age-matched controls.

Left and right ventricular systolic functional parameters were assessed by cardiac magnetic resonance imaging in asymptomatic germ cell cancer survivors after platinum-based chemotherapy (n=44) and age-matched healthy controls (n=21): (A) Left ventricular ejection fraction (LVEF), (B) right ventricular ejection fraction (RVEF), (C) LV global longitudinal strain (GLS), (D) RV GLS, (E) LV global circular strain (GCS), (F) RV GCS, (G) LV global radial strain (LV GRS), and (H) RV free wall longitudinal strain (FWLS) are shown. Data are presented as mean ±SD. T-Test was performed.

Figure 2. Myocardial tissue alterations in germ cell cancer survivors.

Myocardial tissue was characterized by cardiac magnetic resonance imaging in germ cell cancer survivors after asymptomatic platinum-based chemotherapy (n=44) and age-matched healthy controls (n=18) by T1/T2 mapping. (A) Native T1 time, (B) native T2 time, and (C) extra cellular volume (ECV) were assessed. Data are presented as mean ±SD. T-Test was performed.

Figure 3. Non-ischemic LGE in germ cell cancer survivors.

Myocardial tissue was characterized by cardiac magnetic resonance imaging in asymptomatic germ cell cancer survivors after platinum-based chemotherapy (n=44) and age-matched healthy controls (n=21) by late gadolinium enhancement (LGE) imaging. Short-axis and long-axis images of eight germ cell cancer survivors with non-ischemic LGE are shown. Arrows indicate non-ischemic LGE lesions. LGE lesions are predominantly located at subepicardial, and mid-wall left ventricular segments. Two

patients had LGE lesions located at the posterior right ventricular insertion point (survivor 3 and 8).

Figure 4. LVEF impairment after two cycles of platinum-based chemotherapy.

Graph shows left ventricular ejection fraction (LVEF) in germ cell cancer survivors (n=44) measured by cardiac magnetic resonance imaging for subgroups depending on the number of platinum-based chemotherapy cycles received. T-test was applied.

Figure 1. Systolic function in germ cell cancer survivors compared to age-matched controls.

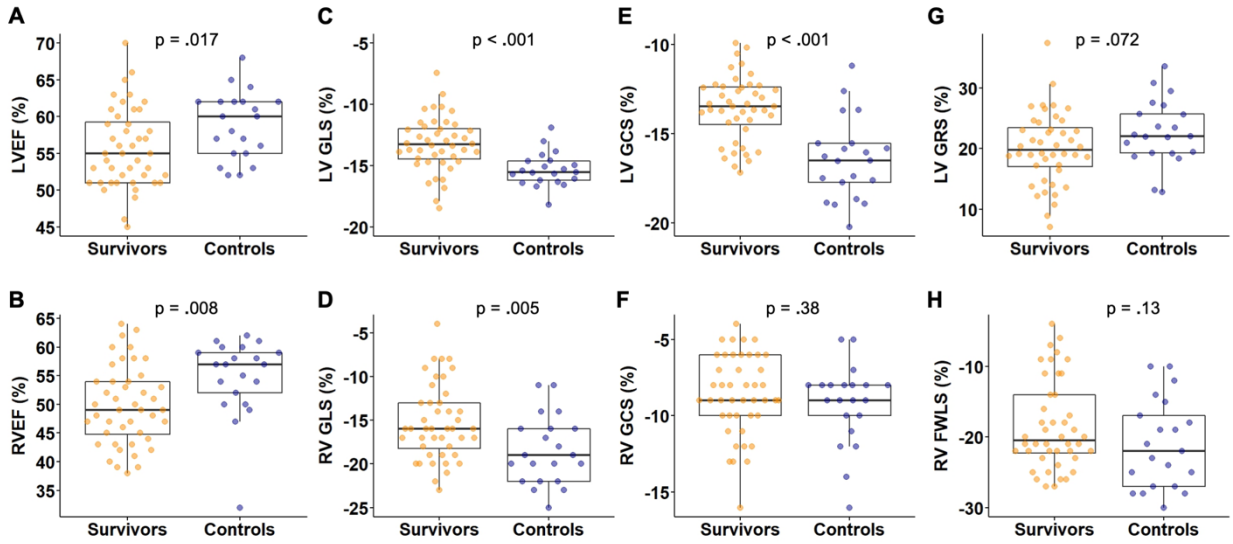

Figure 2. Myocardial tissue alterations in germ cell cancer survivors.

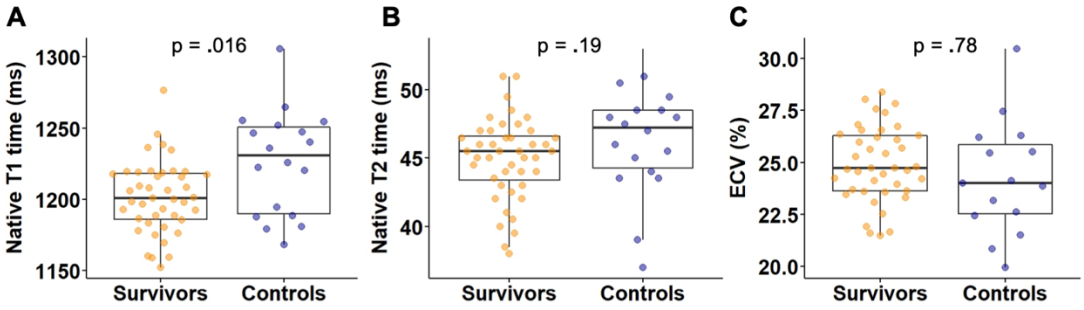

Figure 3. Non-ischemic LGE in germ cell cancer survivors.

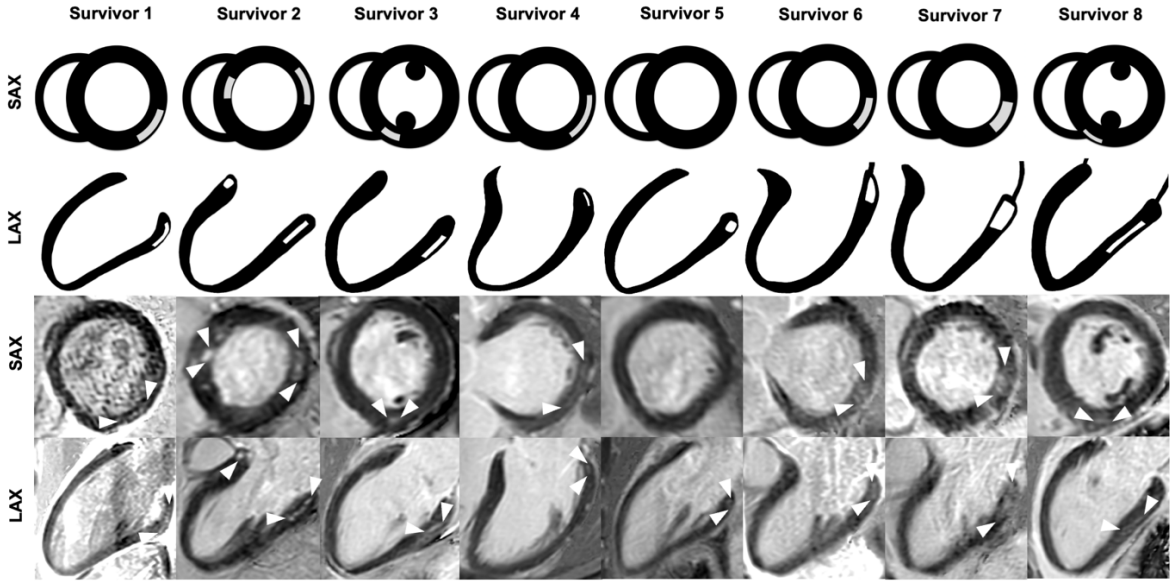

Figure 4. LVEF impairment after two cycles of platinum-based chemotherapy.

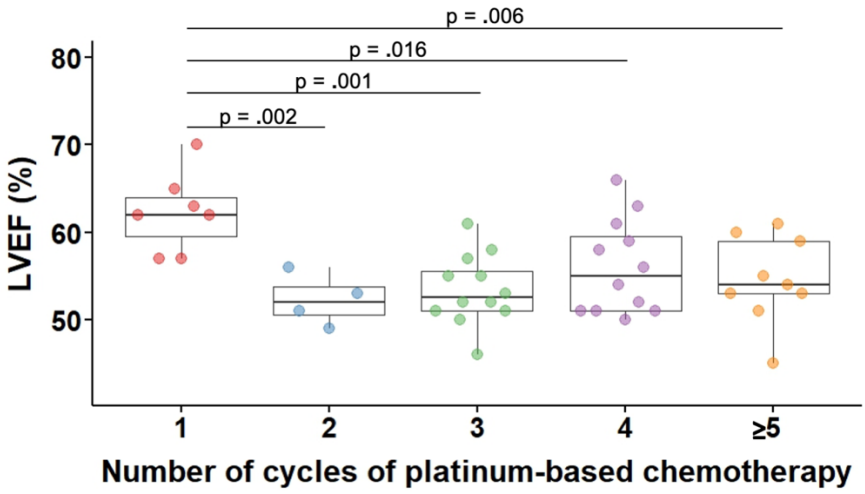

Supplementary Data

Supplementary Material and Methods

CMR data analysis

Corresponding short-axis maps were used to carefully delineate endo- and epicardial contours with 10% endo- and epicardial offsets to avoid contamination. Evaluation of LV and RV volumes and LV mass was performed in standard fashion using short-axis cine images.[1] The presence of LGE was visually analyzed. LGE areas were excluded for T1 and ECV quantification. Extracellular volume (ECV) fraction was calculated using a previously validated equation.[2] CMR parameters are presented as mean of two observers and indexed to the body surface area (BSA).

Myocardial strain values were generated based on cine CMR images using feature-tracking software Segment (version 2.1.R.6108, Medviso, Lund, Sweden).[3] GLS and global radial strain (GRS) were derived from three long-axis (2-, 3-, and 4-chamber views) cine series, whereas GCS was measured on three short-axis (apical, mid, and basal slices) cine series. Endo- and epicardial contours were manually delineated on end-diastolic images and were then automatically propagated by the software throughout the cardiac cycle generating myocardial strain.[3]

1. Schulz-Menger J, Bluemke DA, Bremerich J, et al. Standardized image interpretation and post processing in cardiovascular magnetic resonance: Society for Cardiovascular Magnetic Resonance (SCMR) board of trustees task force on standardized post processing. *J Cardiovasc Magn Reson*. May 1 2013;15(1):35. doi:10.1186/1532-429x-15-35
2. Kellman P, Wilson JR, Xue H, Ugander M, Arai AE. Extracellular volume fraction mapping in the myocardium, part 1: evaluation of an automated method. *Journal of Cardiovascular Magnetic Resonance*. 2012/09/10 2012;14(1):63. doi:10.1186/1532-429X-14-63
3. Morais P, Marchi A, Bogaert JA, et al. Cardiovascular magnetic resonance myocardial feature tracking using a non-rigid, elastic image registration algorithm: assessment of variability in a real-life clinical setting. *J Cardiovasc Magn Reson*. Feb 17 2017;19(1):24. doi:10.1186/s12968-017-0333-y

Supplementary Table 1. Cardiac parameters of GCC survivors compared to controls.

	GCC survivors (n= 44)	**Controls** (n= 21)	***p* value**
Left heart, mean ±SD			
Heart rate, beats/min	68 ±13	67 ±13	0.379
LV cardiac index, L/min/m²	3.2 ±0.69	3.2 ±0.71	0.443
LVEF, % >55%, No. (%) 50%-54%, No. (%) <50%, No. (%)	56 ±5 23 (52) 18 (41) 3 (7)	59 ±5 18 (86) 3 (14) -	0.017 - - -
LV mass index, g/m²,	58 ±11	58 ±12	0.992
LVEDVi, mL/m²	87 ±14	83 ±18	0.388
LVESVi, mL/m²	39 ±9	35 ±10	0.084
LVSVi, mL/m²	48 ±8	49 ±9	0.793
LAEDVi, mL/m²	16 ±7	13 ±4	0.133
LAESVi, mL/m²	33 ±9	30 ±8	0.2
Right heart, mean ±SD			
RVEF, %	50 ±7	55 ±7	0.008
RVEDVi, mL/m²	89 ±15	83 ±15	0.111
RVESVi, mL/m²	45 ±10	38 ±11	0.01
RVSVi, mL/m²	44 ±10	45 ±9	0.789
RAEDVi, mL/m²	25 ±8	23 ±8	0.332
RAESVi, mL/ m²	42 ±11	39 ±15	0.446
Strain parameters, mean ±SD			
LV GLS, %	-13 ±2	-15 ±1	<0.001
LV GCS, %	-14 ±2	-16 ±2	<0.001
LV GRS, %	20 ±6	23 ±5	0.072
RV GLS, %	-15 ±4	-19 ±4	0.005
RV FWLS, %	-19 ±6	-21 ±6	0.13
RV GCS, %	-9 ±3	-9 ±3	0.38
LGE presence, No. (%)			
Non-ischemic LGE	8 (18)	-	-
Ischemic LGE	1 (2)	-	-
Mapping parameters, mean ±SD	(n=44)	(n=18)	
Native global T1, ms	1202 ±25	1226 ±37	0.016
Native global T2, ms	45 ±3	46 ±4	0.19
ECV, %	25 ±2	24 ±3	0.78

Abbreviations: ECV, extracellular volume; FWLS, free wall longitudinal strain; GCC, germ cell cancer; GCS, global circumferential strain; GLS, global longitudinal strain; GRS, global radial strain; LA, left atrial; LAEDVi, left atrial end-diastolic volume index; LAESVi, left atrial end-systolic volume index; LGE, late gadolinium enhancement; LV, left ventricular; LVEDVi, left ventricular end-diastolic volume index; LVEF, left ventricular ejection fraction; LVESVi, left ventricular end-systolic volume index; LVSVi, left ventricular stroke volume index; RA, right atrial; RAEDVi, right atrial end-diastolic volume index; RAESVi, right atrial end-systolic volume index; RV, right ventricular; RVEDVi, right ventricular end-diastolic volume index; RVESVi, right ventricular end-systolic volume index.

Supplementary Figure 1. Flow chart of recruitment of study participants

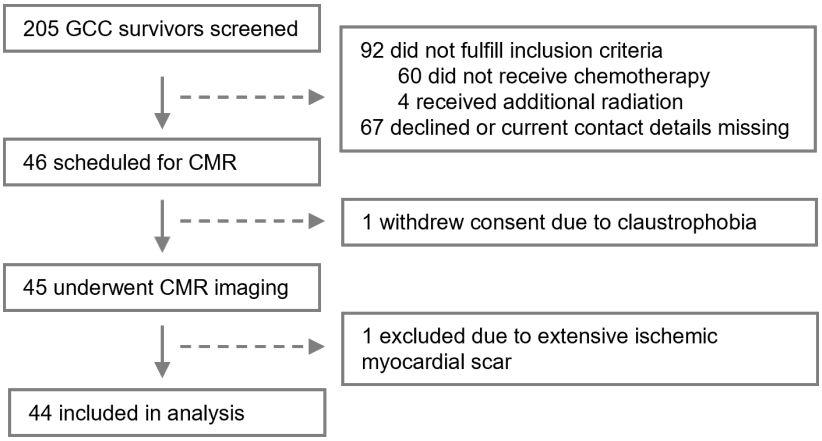

6 Discussion

6.1 Acute effect of an endurance race on myocardial deformation

Chapter 2 presents a study on the acute changes in biventricular and biatrial myocardial strain in competitive triathletes after an endurance exercise. Subgroup analysis was also conducted to investigate the influence of focal myocardial fibrosis on acute changes of myocardial strain in triathletes with focal myocardial fibrosis (LGE+).

6.1.1 Post-race alterations in biventricular strain

Our findings demonstrated that LV GLS showed a declining trend, whereas LV GCS and GRS increased after an endurance race. Recent evidence supports post-race alterations in LV myocardial strain. LV GLS was attenuated in 10 recreationally active men after 90-min high-intensity cycling, but not after 120-min moderate-intensity cycling (Stewart *et al*., 2017). LV GLS and GCS decreased following a 180-min strenuous cycling exercise (Vitiello *et al*., 2013). A tendency of a reduction in LV GLS was observed in master athletes after running an ultra-marathon, while their LVEF remained constant (Cavigli *et al.*, 2022). There may be some underlying reasons for these discrepancies. First, the average CMR acquisition time pre- and post-race in our study was 2.3 hours and thus later than in the aforementioned studies, which might have provided a longer recovery period. Second, the duration and components of exercise were different. Third, strain parameters are not only a measure of intrinsic myocardial contractility, but are also influenced by cardiac load (*i.e.*, blood pressure, LV volume) and structure (Ferferieva *et al.*, 2012). It is also worth noting that there is potential influence of different imaging techniques (CMR-FT *vs.* speckle tracking echocardiography). Further, the increase in LV GCS and GRS might be a compensatory mechanism for the loss of longitudinal mechanical function, as observed in early stages of progressive myocardial disease (Claus *et al*., 2015).

RV GLS and FW longitudinal strain did not differ before and after the race, whereas GCS was elevated. Previous studies demonstrated a transient deterioration of RVEF and RV GLS in athletes after an endurance race (Neilan *et al.*, 2006, La Gerche *et al.*,

2012). In line with our findings, Cavigli *et al.* observed that RV GLS and RV FW longitudinal strain did not differ between baseline and post-race (Cavigli *et al.*, 2022). Alterations in RV strain may also occur during different phases of post-race recovery, and the recovery time may depend on the duration and intensity of the endurance exercise. The post-race RV end-diastolic volume decreased, possibly followed by an adaptation of myocardial deformation to maintain normal RVEF according to the Frank-Starling mechanism (La Gerche *et al.*, 2010). Therefore, we proposed that the increase in RV GCS observed following an endurance race, again is a potential intrinsic compensatory mechanism (Claus *et al.*, 2015).

6.1.2 Post-race reduced left atrial strain and constant right atrial strain

In this study, it was observed that LA GLS decreased after the endurance race. Our findings are in concordance with previous echocardiographic data reporting LA deformation and volume were reduced immediately after exercise (Santoro *et al.*, 2016, Oxborough *et al.*, 2010). D'Ascenzi *et al*. reported that compared to controls, LA volume increased in elite soccer players and LA GLS was similar (D'Ascenzi *et al.*, 2011). Cardiac recovery might actually exceed 24 hours (Stewart *et al.*, 2016), the acquisition window of post-race CMR in our study was within 5 hours, thus exercise-induced cardiac alterations might have not fully subsided.

In addition, post-race RA GLS remained unchanged, which is partially in line with the study by Sanz-de la Garza *et al.*, who scrutinized the exercise-dose-dependent impairment in atrial function (Sanz-de la Garza *et al.*, 2016). Post-race RA strain did not alter at an exercise load of 14 km, whereas higher exercise loads would result in atrial contractile dysfunction (Sanz-de la Garza *et al.*, 2016). Atrial contractile function can be sustained or even potentially increased until advanced stages of disease (Kurt *et al.*, 2009). Atrial strain responses to different exercise load might mimic the atrial contractile function at different stages of disease. Thus the variability in post-race atrial strain may provide additional information on the physiological upper limit of individuals.

6.1.3 Post-race strain in LGE+ triathletes

A subgroup analysis showed that male triathletes with focal myocardial fibrosis had similar baseline and post-race myocardial strain. Repetitive and sustained exposure to high-intensity exercise might induce cardiac microdamage associated with development of myocardial fibrosis (van de Schoor *et al*., 2016). A previous publication by our group reported that CMR-derived post-race diastolic functional variables, including early peak-filling rate (EPFR), atrial peak-filling rate (APFR) and peak-filling rate ratio (PFRR), remained stable in triathletes with focal myocardial fibrosis, whereas higher APFR and reduced PFRR were observed in those without focal myocardial fibrosis (Tahir *et al*., 2020). A similar influence of focal myocardial fibrosis on diastolic filling pattern was also observed in the second project of this thesis. Elevated ECV in triathletes with focal myocardial fibrosis might be indicative of increased myocardial stiffness (Tahir *et al*., 2018, Tahir *et al*., 2019). Therefore, increased myocardial stiffness might contribute to the unaltered biventricular and LA strain in triathletes with focal myocardial fibrosis before and after the race.

To summarize, an endurance race induces acute alterations of myocardial deformation, which might be one of the mechanisms leading to cardiac remodeling in athlete's heart. Post-race alterations of biventricular and left atrial strain are presumed to an intrinsic compensatory mechanism rather than substantial myocardial dysfunction. Further, the lack of post-race alterations in strain observed in male triathletes with focal myocardial fibrosis may be due to increased myocardial stiffness. The combined use of strain parameters allows a better characterization of cardiac function at rest and post-race and helps elucidate some of the mechanisms of cardiac adaptation in endurance athletes.

6.2 Diastolic filling patterns in competitive triathletes

In chapter 3 we investigated the LV diastolic filling patterns in competitive triathletes compared to sedentary controls by time-volume analyses based on CMR cine images, and further explored the influence of myocardial fibrosis on LV diastolic filling. In this project, 101 male triathletes and 28 sedentary controls were recruited. CMR-derived LV diastolic filling parameters consisted of EPFR, APFR and PFRR (PFRR=EPFR/APFR). The triathletes showed a high prevalence of focal myocardial

fibrosis, and showed two different LV diastolic filling patterns in the presence (LGE+) and absence (LGE-) of focal myocardial fibrosis.

6.2.1 LGE in triathletes

Focal myocardial fibrosis was detected by CMR-LGE in 20% of triathletes and none of the controls in this study, the incidence of focal myocardial fibrosis is consistent with previous studies reporting 0-50% of asymptomatic athletes (Breuckmann *et al.*, 2009, Bohm *et al.*, 2016, Domenech-Ximenos *et al*., 2020, Kramer *et al*., 2013, Wilson *et al.*, 2011a). Domenech-Ximenos *et al*. reported that the incidence of LGE was 37.6% in 93 highly trained triathletes, and LGE was more prevalent in athletes than in controls (Domenech-Ximenos *et al*., 2020). In a study conducted by Kramer *et al.*, LGE was not detected in 13 female professional handball players (Kramer *et al.*, 2013). However, Wilson *et al.* found LGE in 6 (50%) of a small cohort of veteran endurance athletes (Wilson *et al.*, 2011a). Bohm *et al.* demonstrated that LGE was only detected in one of 33 (3%) athletes and long-term intensive endurance training was possibly not associated with myocardial fibrosis (Bohm *et al.*, 2016). In general, there is a wide variance regarding the prevalence of LGE in endurance athletes. Age, gender, training load and duration can be identified as potential contributors to these discrepancies in the incidence of focal myocardial fibrosis.

Areas of LGE in our cohort were mainly located in LV basal anterolateral, inferolateral, and inferior segments, which corresponded to a typical non-ischemic LGE pattern. This pattern is consistent with previous literature reporting that areas of focal myocardial fibrosis showed a non-coronary pattern (Wilson *et al.*, 2011a).

6.2.2 “Supernormal” LV diastolic filling pattern

In 1989, Douglas described a “supernormal” LV diastolic function as an increased ratio of echocardiographic rapid to atrial LV filling velocities in the Hawaii Ironman Triathlon (Douglas, 1989). Previous echocardiographic literature provides more evidence for the “supernormal” LV diastolic function in endurance athletes in contrast to sedentary

subjects (Claessens *et al*., 2001, D'Ascenzi *et al*., 2011, Szabo *et al*., 2021). Claessens *et al.* reported that triathletes have a “supernormal” diastolic ventricular filling with a significantly increased E/A ratio (Claessens *et al.*, 2001). D’Ascenzi *et al.* also observed an increased peak E and lower peak A velocity resulting in higher E/A ratio in soccer players, which can be interpreted as an improvement in myocardial passive diastolic properties (D'Ascenzi *et al*., 2011). Szabo *et al*. detected a similar high E/A ratio in adolescent athletes compared to non-athletes caused by significantly lower A values, whereas E values were not increased in athletes (Szabo *et al.*, 2021). Our findings are in line with the previous data, LGE- triathletes showed a comparable “supernormal” diastolic filling pattern characterized by increased PFRR, which was attributable to the lower APFR.

LV diastolic filling includes two phases the early active and late passive filling. In the current study early active filling was similar between LGE- triathletes and controls as described by EPFR, whereas late passive filling described by APFR showed differences. Competitive athletes are reported to have a more compliant and distensible LV than the sedentary population (Bhella *et al*., 2014). Burgess *et al*. used a rat model to demonstrate that, the collagen composition of LV is shifted towards a greater ratio of type III to I, and postulated its favorable influence on diastolic function (Burgess *et al.*, 1996). King *et al*. used Doppler tissue index to show a reduced myocardial stiffness in elite endurance athletes compared to controls (King *et al*., 2008). Therefore, the “supernormal” LV filling might be attributable to benign adaptations to exercise due to increased flexibility and elasticity of the myocardium. Endurance exercise offers benefits, but excessive exercise combined with environmental factors may predispose to cardiomyopathies. Further studies are still needed to quantify exercise intensity and environmental influence required to reach the threshold.

6.2.3 “Pseudo-normalization” LV diastolic filling pattern in LGE+ triathletes

The triathletes in this study were divided into LGE+ and LGE- groups according to the presence or absence of focal myocardial fibrosis. According to our findings, LGE+ triathletes demonstrated a LV diastolic filling pattern similar to sedentary controls but distinct from LGE- triathletes, which was characterized by increased APFR and consequently decreased PFRR. While diffuse myocardial fibrosis is difficult to be

identified through macroscopic LGE, ECV could potentially detect diffuse myocardial fibrosis missed by LGE (Kellman *et al.*, 2012a). An earlier study using T1 mapping assessed myocardial injury in apparently normal myocardium of patients with myocarditis and demonstrated hidden myocardial injury with significantly higher native T1 and ECV compared to healthy volunteers (Radunski *et al.*, 2017). In the current study, increased myocardial native T1 and ECV were also detected in normal appearing myocardium in LGE+ compared to LGE- triathletes. Thus we might assume that the apparently normal myocardium of LGE+ triathletes may also suffer from a diffuse pathological fibrotic process.

Apart from benefits regarding the LV compliance and distensibility, long-term rigorous exercise might also be associated with non-physiological LV hypertrophy and myocardial fibrosis, increasing LV myocardial stiffness and decreasing LV compliance, resulting in cardiac dysfunction (Waterhouse *et al.*, 2012). Recently, Lee *et al.* reported that the degree of ECV is associated with a deterioration of LV relaxation and compliance in patients with aortic stenosis (Lee *et al.*, 2020). Hence, the LV diastolic filling patterns in LGE+ triathletes might be influenced by diffuse myocardial fibrosis as well as increased LV mass. Based on the different LV diastolic filling patterns between the two subgroups, we propose a hypothesis that focal and diffuse myocardial fibrosis may have an impact on the LV diastolic filling pattern. In particular, LGE+ triathletes show a compensatory increase in APFR compared to LGE- triathletes to maintain a “pseudo-normal” LV diastolic filling. In addition, the thin-walled left atrium is afterload sensitive, with a decrease in LV compliance, the increased load imposed on the atrium eventually might lead to further LA dilatation and remodeling, acting as a marker of chronic diastolic burden (Sachdev *et al*., 2005). When triathletes develop myocardial fibrosis, the “pseudo-normalization” of LV diastolic filling in LGE+ triathletes may indicate a loss of adaptive benefits compared to LGE- triathletes. This loss could also be considered as the effect of insufficient recovery or reduced capability for adaptation due to pathologic myocardial fibrosis.

Time-volume analysis by CMR provides a better characterization of the LV diastolic filling patterns in endurance athletes, brings more implications on understanding and differentiating a physiologic and pathologic cardiac phenotype induced by physical activity and potentially might help evaluate the need for observation or even treatment.

6.3 Alterations of myocardial deformation in resistant hypertension

In chapter 4, we analyzed the alterations of LV myocardial deformation in patients with resistant hypertension compared to normotensive controls using FT-CMR. This work demonstrates that variations of LV myocardial strain are attributable to the degree of myocardial impairment in resistant hypertensive patients. Attenuation of LV GLS and GRS, and GCS decline by tendency might be adaptive changes responding to prolonged pressure overload, whereas preserved GCS might constitute a LV compensatory mechanism. Moreover, focal myocardial fibrosis visualized by LGE has a high incidence in patients with resistant hypertension and is associated with a reduced LV GRS.

6.3.1 Strain alteration responding to long-standing pressure overload

The findings from the strain analysis indicated a reduction in both LV GLS and GRS, while GCS did not exhibit a statistically significant difference but demonstrated a decreasing trend in resistant hypertensive patients. Several possible explanations may account for these variations. LV myocardial strain is sensitively influenced by afterload (Donal *et al.*, 2009) and its alterations depend on the fiber structure and local wall stress (Baltabaeva *et al*., 2008). Longitudinal strain denotes the contraction of the subendocardial fibers, circumferential strain represents the contraction of the subepicardial fibers, and both contribute to radial strain (Claus *et al.*, 2015). LV subendocardial myocardial fibers are more vulnerable to increased wall stress, and are more easily injured in the early stage of hypertension (Kang *et al*., 2008, Imbalzano *et al*., 2011). Thus longitudinal strain can be a sensitive marker for subclinical LV dysfunction.

In contrast to longitudinal strain, the changes in circumferential and radial strain are more complicated, in particular with the progression of hypertension and the presence of LV hypertrophy. Imbalzano *et al.* utilized speckle-tracking echocardiography to measure strain in hypertensive patients with and without LV hypertrophy and found that both groups had reduced longitudinal strain. However, those with LVH had decreased radial strain and increased circumferential strain (Imbalzano *et al.*, 2011).

Similarly, Wang *et al*. observed a reduction in all three directional strain in patients with systolic heart failure, whereas patients with diastolic heart failure and preserved LVEF had reduced longitudinal and radial strain, but circumferential strain was preserved (Wang *et al.*, 2008). Our cohort revealed a decline in GLS and GRS, whereas GCS was preserved in analogy. Additionally, 56% of the enrolled patients demonstrated LV hypertrophy that could possibly be associated with sustained high blood pressure. The anatomic difference of myocardial fibers may explain the potential robustness of circumferential strain under circumstance of significant clinical LV dysfunction (Mangion *et al*., 2017). Therefore, variations of LV myocardial strain are likely associated with different stages of hypertensive heart disease.

From the above findings, we conclude that attenuation of LV GLS and GRS in patients with resistant hypertension might constitute a LV adaptation responding to a long-standing pressure overload. The tendential decrease of GCS can be explained with subepicardial layers suffering less impairment in this cohort, which might constitute a LV compensatory mechanism.

6.3.2 LGE in resistant hypertension

Previous studies reported a prevalence of LGE of 18%-29.9% in hypertensive patients (Wang *et al*., 2017, Iyer *et al*., 2022). Our work detected LGE in 42% of patients with a predominantly non-ischemic pattern. This finding indicates that resistant hypertension is likely to be associated with a higher prevalence of LGE than controlled hypertension.

The severity and duration of hypertension are responsible for the development of cardiac remodeling (Kuruvilla *et al.*, 2015). LGE+ patients in the current study had a higher LV mass index. Increased LV mass in cardiac remodeling is induced by expanded extracellular interstitium and myocardial cell volume (Rodrigues *et al.*, 2017). Importantly, in the presence of an expanded interstitium, the progression of interstitial fibrosis eventually leads to focal replacement fibrosis (Iyer *et al*., 2022). Increased collagen deposition in the extracellular interstitium induces stiffness and reduction of end-diastolic myofiber length, finally resulting in attenuated contraction (Pichler *et al.*, 2020).

While LGE- patients exhibited a comparable GRS to healthy controls, a worsening GRS was observed in LGE+ patients. Radial strain usually has large ranges, and the variability of segmental strain remains rather high (Claus *et al*., 2015). Despite this, radial strain has demonstrated the ability to predict clinical outcomes in hypertrophic cardiomyopathy (Smith *et al*., 2014) and exhibits superior predictive performance for scar transmurality compared to longitudinal strain (Maret *et al.*, 2009). However, the underlying mechanism behind attenuated radial strain remains elusive. Radial strain reflects the global myocardial function in the radial direction, which is influenced by the deformation of all myocardial layers. As such, the different GRS between patients with and without LGE suggests that focal myocardial fibrosis visualized by LGE is associated with the reduction of LV GRS.

By applying CMR-FT analysis to assess strain alterations, combined with visualization for focal myocardial fibrosis by LGE, more insights can be obtained into the extent of myocardial layer impairment resulting from long-standing pressure overload and myocardial fibrotic process on cardiac deformation in resistant hypertension.

6.4 Platinum-related impairment in cardiac function and myocardial tissue

Testicular cancer is the most common solid malignancy among young adult men and its incidence has risen over the past two decades (Cheng *et al.*, 2018). Nowadays platinum-based chemotherapy is the mainstay of the treatment for testicular cancer, which has a high cure rate due to an excellent sensitivity to platinum-based chemotherapy and in combination with a variety of other treatments (Hanna and Einhorn, 2014). The chemotherapy-induced side effects also cause concerns in regard to cardiotoxicity. Platinum-containing chemotherapy has been reported to increase the risk of cardiovascular disease in testicular cancer survivors (van den Belt-Dusebout *et al.*, 2007, Huddart *et al*., 2003), and deterioration of diastolic function also occurs (Altena *et al.*, 2011). Given the increased cardiovascular risk may offset partial survival benefit, there is a need to investigate the possible cardiac impairment induced by platinum-based chemotherapy in testicular cancer survivors in order to improve long-term outcomes.

In Chapter 5, multiparametric CMR imaging was used to investigate the long-term cardiac impairment caused by platinum-based chemotherapy in germ cell cancer survivors. This work provides several insights into the characteristics of late cardiac impairment.

6.4.1 Attenuation in biventricular systolic function

Systolic function decreased in germ cell cancer survivors during a median follow-up of 10 years characterized by decreased biventricular EF and myocardial deformation after completion of platinum-based chemotherapy. Similarly a prior echocardiographic study also reported an impaired RV function, but there was no reduction in LV systolic function in female germ cell cancer survivors after platinum-based chemotherapy (Murbraech *et al.*, 2015). Further, Bjerring *et al.* (Bjerring *et al.*, 2021) did not observe any impairment in LV systolic function in long-term testicular cancer survivors. The subgroup analysis based on the chemotherapy cycle demonstrated that the functional impairment emerged after a threshold of two-cycles of chemotherapy. The explanations for these differences are controversial, but might correlate with heterogeneities in both follow-up time and cumulative dosage of chemotherapy.

In addition, it is worth noting that a decline in biventricular GCS was observed in survivors who received two or more cycles of chemotherapy compared to those with one cycle of chemotherapy. However, other strain parameters (biventricular GLS and RV FW longitudinal strain) did not differ. The association between cumulative dosage of chemotherapy and GCS hints that GCS may serve as the most sensitive indicator for subclinical systolic dysfunction among the three strain components following treatment with platinum-based chemotherapy. Previous literature reported that contraction of the subendocardial fibers contributes to longitudinal shortening, whereas contraction of the subepicardial fibers contributes to circumferential shortening and both aspects contribute to radial thickening (Claus *et al.*, 2015). These anatomic differences of myocardial fibers may explain the potential superiority of circumferential strain in detecting clinically significant LV dysfunction (Mangion *et al.*, 2017). As such, it is possible that the preserved GCS constitutes a compensatory mechanism to maintain biventricular EF.

6.4.2 Alterations in myocardial tissue characteristics

Non-ischemic focal myocardial fibrosis occurred in 8 (18%) survivors and an ischemic pattern in one (2%) survivor. Previous data on the prevalence of LGE ranges from 0% to 19%, and its association with cancer chemotherapies is still controversial (Modi *et al*., 2021, Harries *et al.*, 2019, Maestrini *et al*., 2017). Moreover, focal myocardial fibrosis detected by LGE is considered to be one of the characteristics of anthracycline-induced cardiomyopathy (Harries *et al*., 2019). Data on the prevalence of LGE in survivors receiving platinum-based chemotherapy is scarce. Therefore, the clinical significance of LGE and its incidence in relation to platinum-based chemotherapy needs further investigation.

Survivors showed declined global native T1 compared with healthy controls. Decreased native T1 usually occurs in iron or lipid overload (Radenkovic *et al.*, 2017). It is still not clear whether the decline in native T1 is associated with abnormal lipid deposition in this study. An early decrease of native myocardial T1 after the first administration of anthracycline is linked to subsequent development of anthracycline-induced cardiomyopathy (Muehlberg *et al.*, 2018). Attenuation in biventricular systolic function can be regarded as the functional consequences of alteration in myocardial tissue.

Platinum-induced cardiotoxicity may occur through both direct and indirect pathways. Cisplatin directly damages cardiomyocytes due to endothelial activation and apoptosis (Nuver *et al*., 2010), or through mitochondrial damage and oxidative stress (Dugbartey *et al.*, 2016). This direct damage of cardiomyocytes can be mirrored by increase in troponin and N-terminal pro-brain natriuretic peptide (NT-proBNP), directly indicating the cardiomyocyte loss. However, as our findings show, this early preclinical cardiotoxicity manifested by elevated biomarkers cannot be observed in long-term survivors (Omersa *et al*., 2017). Furthermore, platinum-based chemotherapy affects the heart also through indirect damage by a secondary toxic effect through nephrotoxicity (Oun *et al.*, 2018). The pathophysiology behind this observed platinum-related cardiotoxicity is still not completely understood, but the cardiac impairment detected by CMR might provide more evidence.

In summary, the observed deterioration in biventricular systolic function, myocardial deformation and tissue alterations may suggest the existence of platinum-related cardiomyopathy. The application of CMR imaging can help to understand the underlying mechanisms behind the chemotherapy-induced cardiotoxicity and to monitor the resulting cardiac impairment in long-term cancer survivors.

6.5 Concluding remarks

CMR imaging is widely regarded as the gold standard for assessing cardiac morphology and function. In this thesis, we applied a vast array of CMR techniques to evaluate different cardiac alterations, including athlete's heart, myocardial impairment in resistant hypertension, and platinum-related cardiotoxicity. The application of FT-CMR allows an improved characterization of cardiac function at rest and after race, and helps understand the mechanisms of cardiac adaptation in endurance athletes. Furthermore, the combined use of FT- and LGE-CMR provides tools to explore the extent of myocardial impairment. Time-volume analysis by CMR provides a better characterization of LV diastolic filling patterns in endurance athletes, which has important implications for differentiating physiologic and pathologic cardiac phenotypes induced by physical activity. Lastly, the application of multiparametric CMR imaging helps to comprehend the underlying mechanisms of chemotherapy-induced cardiotoxicity and to monitor the corresponding cardiac impairment in long-term cancer survivors. This thesis highlights the vital role of CMR imaging in assessing different cardiac alterations in terms of cardiac function, myocardial deformation, and tissue characterization.

7 Summary

Cardiac magnetic resonance (CMR) imaging as the gold standard for functional and morphological assessment of the heart offers further insights into cardiac alterations. While recent research has shed light on cardiac alterations in athlete's heart, resistant hypertension, and platinum-related cardiotoxicity, the mechanisms of cardiac alterations still need further elucidation, and quantitative analysis of myocardial deformation and tissue impairment remains limited. To address the aforementioned question, the overarching purpose of this thesis is applying a range of CMR techniques to assess the above representative cardiac alterations.

In the first project, we investigated the subtle alterations in myocardial deformation in triathletes with and without myocardial fibrosis after an endurance race using the feature-tracking (FT) technique. Our results indicate that diverse post-race alterations in myocardial strain suggest a compensatory mechanism following an acute bout of endurance exercise. Triathletes with focal myocardial fibrosis did not manifest any acute changes in strain, potentially due to increased myocardial stiffness.

In the second project, we identified adaptive changes of left ventricular (LV) diastolic function in triathletes and analyzed the influence of myocardial fibrosis on diastolic filling patterns using time-volume analysis. This work suggests that a “supernormal” diastolic filling pattern in triathletes is possibly induced by endurance exercise due to increased LV flexibility and elasticity. It also proposes a “pseudo-normalization” of diastolic filling patterns characterized by a compensatory increase in atrial contraction in triathletes with focal myocardial fibrosis, potentially resulting from reduced passive elasticity.

In the third project, we performed the FT technique to evaluate the alterations of LV myocardial deformation in patients with resistant hypertension. This work reveals that varying attenuation of LV myocardial strain might be associated with the adaptive changes responding to long-standing pressure overload. This project advances our understanding of the influence of myocardial fibrosis on the impairment of myocardial layers according to the alterations in different components of myocardial deformation.

In the fourth project, we applied multiparametric CMR to explore the long-term effect of platinum-based chemotherapy on cardiac impairment in germ cell cancer survivors. Our findings indicate that platinum-based chemotherapy has a long-term negative impact on systolic function, deformation, and myocardial tissue. This work emphasizes the need to further investigate the mechanisms of platinum-related cardiotoxicity and points to the importance of long-term cardiovascular follow-up in this particular group of cancer survivors.

Overall, the FT technique allows a more thorough characterization of myocardial deformation in endurance athletes at rest and after race, and offers deep insights into the influence of prolonged pressure overload and myocardial fibrotic process on cardiac deformation. Furthermore, CMR imaging helps to elucidate the effects of myocardial fibrosis on LV diastolic filling patterns and platinum-induced cardiotoxicity. This thesis emphasizes the crucial role of CMR imaging in assessing different cardiac alterations in terms of cardiac function, myocardial deformation, and tissue characterization.

8 Zusammenfassung

Die kardiale Magnetresonanztomographie (CMR) gilt als Goldstandard für die funktionelle und morphologische Beurteilung des Herzens. Während die jüngste Forschung die kardialen Veränderungen bei Sportlern, bei Patienten mit resistenter arterieller Hypertonie und die Platin-assoziierte Kardiotoxizität thematisiert, sind die Mechanismen dieser kardialen Veränderungen nicht endgültig verstanden. Zudem sind quantitative Analysen der myokardialen Deformation und der Gewebeschädigung eher begrenzt. Um diese Themenbereiche weiter aufzuleuchten, werden in dieser Arbeit eine Reihe von CMR-Techniken angewandt.

Im ersten Projekt untersuchten wir subtile Veränderungen der Myokardverformung bei Triathleten mit und ohne Myokardfibrose nach einem Ausdauerwettkampf mithilfe der Feature-Tracking-Technik (FT). Unsere Ergebnisse deuten darauf hin, dass kompensatorische Veränderungen der Myokardverformung nach einem Wettkampf induziert werden. Die Subgruppe von Triathleten mit fokaler Myokardfibrose zeigten dagegen keine akuten Veränderungen nach dem Wettkampf, was möglicherweise auf eine erhöhte Myokardsteifigkeit zurückzuführen ist.

Im zweiten Projekt haben wir adaptive Veränderungen der diastolischen Funktion des linken Ventrikels (LV) bei Triathleten und den Einfluss der Myokardfibrose auf das diastolische Füllungsmuster mit Hilfe von Zeit-Volumen-Analysen untersucht. Diese Arbeit zeigt, dass ein "supernormales" diastolisches Füllungsmuster bei Triathleten möglicherweise durch Ausdauertraining aufgrund erhöhter LV-Flexibilität und -Elastizität induziert wird. Zudem beobachtet man eine "Pseudonormalisierung" des diastolischen Füllungsmusters bei Triathleten mit fokaler Myokardfibrose, die durch eine kompensatorische Zunahme der Vorhofkontraktion charakterisiert ist, welche möglicherweise auf eine verminderte passive LV-Elastizität zurückzuführen ist.

Im dritten Projekt verwendeten wir die FT-Technik, um die Veränderungen der LV-Myokarddeformation bei Patienten mit resistenter arterieller Hypertonie zu untersuchen. Diese Arbeit zeigt, dass eine Abnahme der LV-Myokarddeformierung als adaptive Veränderung auf eine langanhaltende Drucküberlastung resultieren könnte. Dieses Projekt weitet unser Wissen über den Einfluss einer fokalen Myokardfibrose

auf die Veränderungen der Myokardverformung bei Patienten mit resistenter Hypertonie aus.

Im vierten Projekt untersuchten wir mit Hilfe der multiparametrischen CMR die langfristigen Auswirkungen einer Platin-basierten Chemotherapie auf die kardiale Funktion und Morphologie bei Langzeitüberlebenden von Keimzellkrebs. Unsere Ergebnisse deuten darauf hin, dass eine Platin-haltige Chemotherapie eine langfristige negative Auswirkung auf die biventrikuläre systolische Funktion, die Myokarddeformation und das Herzmuskelgewebe bei männlichen Langzeitüberlebenden hat. Diese Arbeit unterstreicht die Notwendigkeit, die Mechanismen der Platin-bedingten Kardiotoxizität genauer zu untersuchen, und weist auf die Bedeutung einer langfristigen kardiovaskulären Nachsorge bei den Krebsüberlebenden hin.

Insgesamt ermöglicht die FT-Technik eine genauere Quantifizierung der Herzmuskelverformung bei Ausdauersportlern in Ruhe und nach Wettkampf und hilft den Einfluss von anhaltender Drucküberlastung und Myokardfibrose auf die Herzverformung besser zu verstehen. Darüber hinaus trägt die CMR-Bildgebung dazu bei, die Auswirkungen der Myokardfibrose auf das diastolische LV-Füllungsmuster bei Triathleten und die Platin-induzierte Kardiotoxizität aufzuklären. Diese Arbeit unterstreicht die entscheidende Rolle der CMR-Bildgebung bei der Beurteilung verschiedener kardialer Veränderungen in Bezug auf die Herzfunktion, die Myokarddeformation und die Gewebecharakteristika.

9 Abbreviations

APFR	atrial peak-filling rate
bSSFP	balanced-steady state-free precession
CMR	cardiac magnetic resonance
ECG	electrocardiogram
ECG gating	electrocardiographic gating
ECV	extracellular volume
EF	ejection fraction
EPFR	early peak-filling rate
EPI	echo-planar-imaging
FID	free-induction decay
FT	feature-tracking
FW	free wall
GBCA	gadolinium-based contrast agent
GCS	global circumferential strain
GLS	global longitudinal strain
GraSE	gradient-spin-echo
GRE	gradient-echo
GRS	global radial stain
IR	inversion recovery
LA	left atrial
LGE	late gadolinium enhancement
LV	left ventricular
MOLLI	modified Look-Locker inversion

MRI	magnetic resonance imaging
M_{xy}	transverse magnetic vector
M_z	longitudinal magnetic vector
NMR	nuclear magnetic resonance
NT-proBNP	N-terminal pro-brain natriuretic peptide
PFRR	peak-filling rate ratio
PSIR	phase-sensitive inversion-recovery
T1	longitudinal relaxation time
T2	transverse relaxation time
T2w	T2-weighted
TE	echo time
TI	inversion time
TR	repetition time
RA	right atrial
RF	radiofrequency
RV	right ventricular
SAPPHIRE	saturation pulse prepared heart rate independent inversion recovery
SASHA	saturation recovery single-shot acquisition
SCMR	Society for Cardiovascular Magnetic Resonance
SE	spin-echo
shMOLLI	shortened modified Look-Locker inversion
TSE	turbo-spin-echo

10 References

ALSHARARI, R., OXBOROUGH, D., LIP, G. Y. H. & SHANTSILA, A. 2021. Myocardial Strain Imaging in Resistant Hypertension. *Curr Hypertens Rep,* 23**,** 24.

ALTENA, R., HUMMEL, Y. M., NUVER, J., SMIT, A. J., LEFRANDT, J. D., DE BOER, R. A., VOORS, A. A., VAN DEN BERG, M. P., DE VRIES, E. G., BOEZEN, H. M. & GIETEMA, J. A. 2011. Longitudinal changes in cardiac function after cisplatin-based chemotherapy for testicular cancer. *Ann Oncol,* 22**,** 2286-93.

ALTIN, C., SADE, L. E., DEMIRTAS, S., KARACAGLAR, E., KANYILMAZ, S., SIMSEK, V., AYHAN, A. & MUDERRISOGLU, H. 2015. Effects of Paclitaxel and Carboplatin combination on mechanical myocardial and microvascular functions: a transthoracic Doppler echocardiography and two-dimensional strain imaging study. *Echocardiography,* 32**,** 238-47.

AMBALE-VENKATESH, B. & LIMA, J. A. 2015. Cardiac MRI: a central prognostic tool in myocardial fibrosis. *Nat Rev Cardiol,* 12**,** 18-29.

BALTABAEVA, A., MARCINIAK, M., BIJNENS, B., MOGGRIDGE, J., HE, F. J., ANTONIOS, T. F., MACGREGOR, G. A. & SUTHERLAND, G. R. 2008. Regional left ventricular deformation and geometry analysis provides insights in myocardial remodelling in mild to moderate hypertension. *Eur J Echocardiogr,* 9**,** 501-8.

BHELLA, P. S., HASTINGS, J. L., FUJIMOTO, N., SHIBATA, S., CARRICK-RANSON, G., PALMER, M. D., BOYD, K. N., ADAMS-HUET, B. & LEVINE, B. D. 2014. Impact of lifelong exercise "dose" on left ventricular compliance and distensibility. *J Am Coll Cardiol,* 64**,** 1257-66.

BITAR, R., LEUNG, G., PERNG, R., TADROS, S., MOODY, A. R., SARRAZIN, J., MCGREGOR, C., CHRISTAKIS, M., SYMONS, S., NELSON, A. & ROBERTS, T. P. 2006. MR pulse sequences: what every radiologist wants to know but is afraid to ask. *Radiographics,* 26**,** 513-37.

BJERRING, A. W., FOSSA, S. D., HAUGNES, H. S., NOME, R., STOKKE, T. M., HAUGAA, K. H., KISERUD, C. E., EDVARDSEN, T. & SARVARI, S. I. 2021. The cardiac impact of cisplatin-based chemotherapy in survivors of testicular cancer: a 30-year follow-up. *Eur Heart J Cardiovasc Imaging,* 22**,** 443-450.

BLOCH, F. 1946. Nuclear Induction. *Physical Review,* 70**,** 460-474.

BOHM, P., SCHNEIDER, G., LINNEWEBER, L., RENTZSCH, A., KRAMER, N., ABDUL-KHALIQ, H., KINDERMANN, W., MEYER, T. & SCHARHAG, J. 2016. Right and Left Ventricular Function and Mass in Male Elite Master Athletes: A Controlled Contrast-Enhanced Cardiovascular Magnetic Resonance Study. *Circulation,* 133**,** 1927-35.

BOHNEN, S., RADUNSKI, U. K., LUND, G. K., TAHIR, E., AVANESOV, M., STEHNING, C., SCHNACKENBURG, B., ADAM, G., BLANKENBERG, S. & MUELLERLEILE, K. 2017. T1 mapping cardiovascular magnetic resonance imaging to detect myocarditis-Impact of slice orientation on the diagnostic performance. *Eur J Radiol,* 86**,** 6-12.

BONNER, F., JANZARIK, N., JACOBY, C., SPIEKER, M., SCHNACKENBURG, B., RANGE, F., BUTZBACH, B., HABERKORN, S., WESTENFELD, R., NEIZEL-WITTKE, M., FLOGEL, U. & KELM, M. 2015. Myocardial T2 mapping reveals age- and sex-related differences in volunteers. *J Cardiovasc Magn Reson,* 17**,** 9.

BREUCKMANN, F., MÖHLENKAMP, S., NASSENSTEIN, K., LEHMANN, N., LADD, S., SCHMERMUND, A., SIEVERS, B., SCHLOSSER, T., JÖCKEL, K. H.,

HEUSCH, G., ERBEL, R. & BARKHAUSEN, J. 2009. Myocardial late gadolinium enhancement: prevalence, pattern, and prognostic relevance in marathon runners. *Radiology,* 251**,** 50-7.

BROWN, M. A. & SEMELKA, R. C. 1999. MR imaging abbreviations, definitions, and descriptions: a review. *Radiology,* 213**,** 647-62.

BULL, S., WHITE, S. K., PIECHNIK, S. K., FLETT, A. S., FERREIRA, V. M., LOUDON, M., FRANCIS, J. M., KARAMITSOS, T. D., PRENDERGAST, B. D., ROBSON, M. D., NEUBAUER, S., MOON, J. C. & MYERSON, S. G. 2013. Human non-contrast T1 values and correlation with histology in diffuse fibrosis. *Heart,* 99**,** 932-7.

BURGESS, M. L., BUGGY, J., PRICE, R. L., ABEL, F. L., TERRACIO, L., SAMAREL, A. M. & BORG, T. K. 1996. Exercise- and hypertension-induced collagen changes are related to left ventricular function in rat hearts. *Am J Physiol,* 270**,** H151-9.

BYDDER, G. M. & YOUNG, I. R. 1985. MR imaging: clinical use of the inversion recovery sequence. *J Comput Assist Tomogr,* 9**,** 659-75.

CAMERON, A. C., MCMAHON, K., HALL, M., NEVES, K. B., RIOS, F. J., MONTEZANO, A. C., WELSH, P., WATERSTON, A., WHITE, J., MARK, P. B., TOUYZ, R. M. & LANG, N. N. 2020. Comprehensive Characterization of the Vascular Effects of Cisplatin-Based Chemotherapy in Patients With Testicular Cancer. *JACC CardioOncol,* 2**,** 443-455.

CAVIGLI, L., ZORZI, A., SPADOTTO, V., GISMONDI, A., SISTI, N., VALENTINI, F., ANSELMI, F., MANDOLI, G. E., SPERA, L., DI FLORIO, A., BACCANI, B., CAMELI, M. & D'ASCENZI, F. 2022. The acute effects of an ultramarathon on biventricular function and ventricular arrhythmias in master athletes. *Eur Heart J Cardiovasc Imaging,* 23**,** 423-430.

CHAVHAN, G. B., BABYN, P. S., JANKHARIA, B. G., CHENG, H. L. & SHROFF, M. M. 2008. Steady-state MR imaging sequences: physics, classification, and clinical applications. *Radiographics,* 28**,** 1147-60.

CHENG, L., ALBERS, P., BERNEY, D. M., FELDMAN, D. R., DAUGAARD, G., GILLIGAN, T. & LOOIJENGA, L. H. J. 2018. Testicular cancer. *Nat Rev Dis Primers,* 4**,** 29.

CHIA, J. M., FISCHER, S. E., WICKLINE, S. A. & LORENZ, C. H. 2000. Performance of QRS detection for cardiac magnetic resonance imaging with a novel vectorcardiographic triggering method. *J Magn Reson Imaging,* 12**,** 678-88.

CHITIBOI, T. & AXEL, L. 2017. Magnetic resonance imaging of myocardial strain: A review of current approaches. *J Magn Reson Imaging,* 46**,** 1263-1280.

CLAESSENS, P. J., CLAESSENS, C. W., CLAESSENS, M. M., CLAESSENS, M. C. & CLAESSENS, J. E. 2001. Supernormal left ventricular diastolic function in triathletes. *Tex Heart Inst J,* 28**,** 102-10.

CLAUS, P., OMAR, A. M. S., PEDRIZZETTI, G., SENGUPTA, P. P. & NAGEL, E. 2015. Tissue Tracking Technology for Assessing Cardiac Mechanics: Principles, Normal Values, and Clinical Applications. *JACC Cardiovasc Imaging,* 8**,** 1444-1460.

CROUSER, E. D., ONO, C., TRAN, T., HE, X. & RAMAN, S. V. 2014. Improved detection of cardiac sarcoidosis using magnetic resonance with myocardial T2 mapping. *Am J Respir Crit Care Med,* 189**,** 109-12.

D'ASCENZI, F., CAMELI, M., ZACA, V., LISI, M., SANTORO, A., CAUSARANO, A. & MONDILLO, S. 2011. Supernormal diastolic function and role of left atrial myocardial deformation analysis by 2D speckle tracking echocardiography in elite soccer players. *Echocardiography,* 28**,** 320-6.

DABIR, D., CHILD, N., KALRA, A., ROGERS, T., GEBKER, R., JABBOUR, A., PLEIN, S., YU, C. Y., OTTON, J., KIDAMBI, A., MCDIARMID, A., BROADBENT, D., HIGGINS, D. M., SCHNACKENBURG, B., FOOTE, L., CUMMINS, C., NAGEL, E. & PUNTMANN, V. O. 2014. Reference values for healthy human myocardium using a T1 mapping methodology: results from the International T1 Multicenter cardiovascular magnetic resonance study. *J Cardiovasc Magn Reson,* 16**,** 69.

DAUGHERTY, S. L., POWERS, J. D., MAGID, D. J., TAVEL, H. M., MASOUDI, F. A., MARGOLIS, K. L., O'CONNOR, P. J., SELBY, J. V. & HO, P. M. 2012. Incidence and prognosis of resistant hypertension in hypertensive patients. *Circulation,* 125**,** 1635-42.

DIXON, R. L. & EKSTRAND, K. E. 1982. The physics of proton NMR. *Med Phys,* 9**,** 807-18.

DOMENECH-XIMENOS, B., SANZ-DE LA GARZA, M., PRAT-GONZALEZ, S., SEPULVEDA-MARTINEZ, A., CRISPI, F., DURAN-FERNANDEZ, K., PEREA, R. J., BIJNENS, B. & SITGES, M. 2020. Prevalence and pattern of cardiovascular magnetic resonance late gadolinium enhancement in highly trained endurance athletes. *J Cardiovasc Magn Reson,* 22**,** 62.

DONAL, E., BERGEROT, C., THIBAULT, H., ERNANDE, L., LOUFOUA, J., AUGEUL, L., OVIZE, M. & DERUMEAUX, G. 2009. Influence of afterload on left ventricular radial and longitudinal systolic functions: a two-dimensional strain imaging study. *Eur J Echocardiogr,* 10**,** 914-21.

DOUGLAS, P. S. 1989. Cardiac considerations in the triathlete. *Med Sci Sports Exerc,* 21**,** S214-8.

DUGBARTEY, G. J., PEPPONE, L. J. & DE GRAAF, I. A. 2016. An integrative view of cisplatin-induced renal and cardiac toxicities: Molecular mechanisms, current treatment challenges and potential protective measures. *Toxicology,* 371**,** 58-66.

DUMOULIN, C. L. & HART, H. R., JR. 1986. Magnetic resonance angiography. *Radiology,* 161**,** 717-20.

ECTOR, J., GANAME, J., VAN DER MERWE, N., ADRIAENSSENS, B., PISON, L., WILLEMS, R., GEWILLIG, M. & HEIDBUCHEL, H. 2007. Reduced right ventricular ejection fraction in endurance athletes presenting with ventricular arrhythmias: a quantitative angiographic assessment. *Eur Heart J,* 28**,** 345-53.

EDELMAN, R. R., CHIEN, D. & KIM, D. 1991. Fast selective black blood MR imaging. *Radiology,* 181**,** 655-60.

FERFERIEVA, V., VAN DEN BERGH, A., CLAUS, P., JASAITYTE, R., VEULEMANS, P., PELLENS, M., LA GERCHE, A., RADEMAKERS, F., HERIJGERS, P. & D'HOOGE, J. 2012. The relative value of strain and strain rate for defining intrinsic myocardial function. *Am J Physiol Heart Circ Physiol,* 302**,** H188-95.

FERNANDEZ-JIMENEZ, R., SANCHEZ-GONZALEZ, J., AGUERO, J., DEL TRIGO, M., GALAN-ARRIOLA, C., FUSTER, V. & IBANEZ, B. 2015. Fast T2 gradient-spin-echo (T2-GraSE) mapping for myocardial edema quantification: first in vivo validation in a porcine model of ischemia/reperfusion. *J Cardiovasc Magn Reson,* 17**,** 92.

FERREIRA, V. M., PIECHNIK, S. K., DALL'ARMELLINA, E., KARAMITSOS, T. D., FRANCIS, J. M., CHOUDHURY, R. P., FRIEDRICH, M. G., ROBSON, M. D. & NEUBAUER, S. 2012. Non-contrast T1-mapping detects acute myocardial edema with high diagnostic accuracy: a comparison to T2-weighted cardiovascular magnetic resonance. *J Cardiovasc Magn Reson,* 14**,** 42.

FROHLICH, E. D., APSTEIN, C., CHOBANIAN, A. V., DEVEREUX, R. B., DUSTAN, H. P., DZAU, V., FAUAD-TARAZI, F., HORAN, M. J., MARCUS, M., MASSIE, B. & ET AL. 1992. The heart in hypertension. *N Engl J Med,* 327**,** 998-1008.

GALLICHAN, D., COCOSCO, C. A., DEWDNEY, A., SCHULTZ, G., WELZ, A., HENNIG, J. & ZAITSEV, M. 2011. Simultaneously driven linear and nonlinear spatial encoding fields in MRI. *Magn Reson Med,* 65**,** 702-14.

GEORGE, K., WHYTE, G. P., GREEN, D. J., OXBOROUGH, D., SHAVE, R. E., GAZE, D. & SOMAUROO, J. 2012. The endurance athletes heart: acute stress and chronic adaptation. *Br J Sports Med,* 46 Suppl 1**,** i29-36.

GERBER, B. L., RAMAN, S. V., NAYAK, K., EPSTEIN, F. H., FERREIRA, P., AXEL, L. & KRAITCHMAN, D. L. 2008. Myocardial first-pass perfusion cardiovascular magnetic resonance: history, theory, and current state of the art. *J Cardiovasc Magn Reson,* 10**,** 18.

GINAT, D. T., FONG, M. W., TUTTLE, D. J., HOBBS, S. K. & VYAS, R. C. 2011. Cardiac imaging: Part 1, MR pulse sequences, imaging planes, and basic anatomy. *AJR Am J Roentgenol,* 197**,** 808-15.

GIRI, S., CHUNG, Y. C., MERCHANT, A., MIHAI, G., RAJAGOPALAN, S., RAMAN, S. V. & SIMONETTI, O. P. 2009. T2 quantification for improved detection of myocardial edema. *J Cardiovasc Magn Reson,* 11**,** 56.

GROSSMAN, W., JONES, D. & MCLAURIN, L. P. 1975. Wall stress and patterns of hypertrophy in the human left ventricle. *J Clin Invest,* 56**,** 56-64.

HAAF, P., GARG, P., MESSROGHLI, D. R., BROADBENT, D. A., GREENWOOD, J. P. & PLEIN, S. 2016. Cardiac T1 Mapping and Extracellular Volume (ECV) in clinical practice: a comprehensive review. *J Cardiovasc Magn Reson,* 18**,** 89.

HANNA, N. & EINHORN, L. H. 2014. Testicular cancer: a reflection on 50 years of discovery. *J Clin Oncol,* 32**,** 3085-92.

HARRIES, I., BIGLINO, G., BARITUSSIO, A., DE GARATE, E., DASTIDAR, A., PLANA, J. C. & BUCCIARELLI-DUCCI, C. 2019. Long term cardiovascular magnetic resonance phenotyping of anthracycline cardiomyopathy. *Int J Cardiol,* 292**,** 248-252.

HARRIES, I., LIANG, K., WILLIAMS, M., BERLOT, B., BIGLINO, G., LANCELLOTTI, P., PLANA, J. C. & BUCCIARELLI-DUCCI, C. 2020. Magnetic Resonance Imaging to Detect Cardiovascular Effects of Cancer Therapy: JACC CardioOncology State-of-the-Art Review. *JACC CardioOncol,* 2**,** 270-292.

HENDEL, R. C., FRIEDRICH, M. G., SCHULZ-MENGER, J., ZEMMRICH, C., BENGEL, F., BERMAN, D. S., CAMICI, P. G., FLAMM, S. D., LE GULUDEC, D., KIM, R., LOMBARDI, M., MAHMARIAN, J., SECHTEM, U. & NAGEL, E. 2016. CMR First-Pass Perfusion for Suspected Inducible Myocardial Ischemia. *JACC Cardiovasc Imaging,* 9**,** 1338-1348.

HILL, J. A. & OLSON, E. N. 2008. Cardiac plasticity. *N Engl J Med,* 358**,** 1370-80.

HOFFMANN, F., MOESTL, S., WOOTEN, S. V., STRAY-GUNDERSEN, S., TOMCZAK, C. R., TANK, J., TANAKA, H., RITTWEGER, J. & CHILIBECK, P. D. 2021. Left Ventricular Dimensions and Diastolic Function Are Different in Throwers, Endurance Athletes, and Sprinters From the World Masters Athletics Championships. *Front Physiol,* 12**,** 643764.

HOLTACKERS, R. J., EMRICH, T., BOTNAR, R. M., KOOI, M. E., WILDBERGER, J. E. & KREITNER, K. F. 2022. Late Gadolinium Enhancement Cardiac Magnetic Resonance Imaging: From Basic Concepts to Emerging Methods. *Rofo,* 194**,** 491-504.

HUDDART, R. A., NORMAN, A., SHAHIDI, M., HORWICH, A., COWARD, D., NICHOLLS, J. & DEARNALEY, D. P. 2003. Cardiovascular disease as a long-term complication of treatment for testicular cancer. *J Clin Oncol,* 21**,** 1513-23.

IMBALZANO, E., ZITO, C., CARERJ, S., ORETO, G., MANDRAFFINO, G., CUSMA-PICCIONE, M., DI BELLA, G., SAITTA, C. & SAITTA, A. 2011. Left ventricular function in hypertension: new insight by speckle tracking echocardiography. *Echocardiography,* 28**,** 649-57.

IYER, N. R., LE, T. T., KUI, M. S. L., TANG, H. C., CHIN, C. T., PHUA, S. K., BRYANT, J. A., PUA, C. J., ANG, B., TOH, D. F., AW, T. C., LEE, C. H., COOK, S. A., UGANDER, M. & CHIN, C. W. L. 2022. Markers of Focal and Diffuse Nonischemic Myocardial Fibrosis Are Associated With Adverse Cardiac Remodeling and Prognosis in Patients With Hypertension: The REMODEL Study. *Hypertension,* 79**,** 1804-1813.

JEROSCH-HEROLD, M. 2010. Quantification of myocardial perfusion by cardiovascular magnetic resonance. *J Cardiovasc Magn Reson,* 12**,** 57.

JUDD, R. M., ATALAY, M. K., ROTTMAN, G. A. & ZERHOUNI, E. A. 1995. Effects of myocardial water exchange on T1 enhancement during bolus administration of MR contrast agents. *Magn Reson Med,* 33**,** 215-23.

KALAM, K., OTAHAL, P. & MARWICK, T. H. 2014. Prognostic implications of global LV dysfunction: a systematic review and meta-analysis of global longitudinal strain and ejection fraction. *Heart,* 100**,** 1673-80.

KANG, S. J., LIM, H. S., CHOI, B. J., CHOI, S. Y., HWANG, G. S., YOON, M. H., TAHK, S. J. & SHIN, J. H. 2008. Longitudinal strain and torsion assessed by two-dimensional speckle tracking correlate with the serum level of tissue inhibitor of matrix metalloproteinase-1, a marker of myocardial fibrosis, in patients with hypertension. *J Am Soc Echocardiogr,* 21**,** 907-11.

KELLMAN, P. & ARAI, A. E. 2012. Cardiac imaging techniques for physicians: late enhancement. *J Magn Reson Imaging,* 36**,** 529-42.

KELLMAN, P., ARAI, A. E., MCVEIGH, E. R. & ALETRAS, A. H. 2002. Phase-sensitive inversion recovery for detecting myocardial infarction using gadolinium-delayed hyperenhancement. *Magn Reson Med,* 47**,** 372-83.

KELLMAN, P. & HANSEN, M. S. 2014. T1-mapping in the heart: accuracy and precision. *J Cardiovasc Magn Reson,* 16**,** 2.

KELLMAN, P., WILSON, J. R., XUE, H., BANDETTINI, W. P., SHANBHAG, S. M., DRUEY, K. M., UGANDER, M. & ARAI, A. E. 2012a. Extracellular volume fraction mapping in the myocardium, part 2: initial clinical experience. *J Cardiovasc Magn Reson,* 14**,** 64.

KELLMAN, P., WILSON, J. R., XUE, H., UGANDER, M. & ARAI, A. E. 2012b. Extracellular volume fraction mapping in the myocardium, part 1: evaluation of an automated method. *J Cardiovasc Magn Reson,* 14**,** 63.

KIM, P. K., HONG, Y. J., IM, D. J., SUH, Y. J., PARK, C. H., KIM, J. Y., CHANG, S., LEE, H. J., HUR, J., KIM, Y. J. & CHOI, B. W. 2017. Myocardial T1 and T2 Mapping: Techniques and Clinical Applications. *Korean J Radiol,* 18**,** 113-131.

KIM, R. J., FIENO, D. S., PARRISH, T. B., HARRIS, K., CHEN, E. L., SIMONETTI, O., BUNDY, J., FINN, J. P., KLOCKE, F. J. & JUDD, R. M. 1999. Relationship of MRI delayed contrast enhancement to irreversible injury, infarct age, and contractile function. *Circulation,* 100**,** 1992-2002.

KIM, R. J., SHAH, D. J. & JUDD, R. M. 2003. How we perform delayed enhancement imaging. *J Cardiovasc Magn Reson,* 5**,** 505-14.

KING, G. J., MURPHY, R. T., ALMUNTASER, I., BENNETT, K., HO, E. & BROWN, A. S. 2008. Alterations in myocardial stiffness in elite athletes assessed by a new Doppler index. *Heart,* 94**,** 1323-5.

KOREN, M. J., DEVEREUX, R. B., CASALE, P. N., SAVAGE, D. D. & LARAGH, J. H. 1991. Relation of left ventricular mass and geometry to morbidity and mortality in uncomplicated essential hypertension. *Ann Intern Med,* 114**,** 345-52.

KRAMER, U., MANGOLD, S., KRUMM, P., SEEGER, A., FRANZEN, E., NIESS, A. M., CLAUSSEN, C. D. & BURGSTAHLER, C. 2013. Determination of Morphological and Functional Adaptations in Top Level Female Handball Players Using Cardiac MR Imaging. *Deutsche Zeitschrift für Sportmedizin,* 2013.

KRITTAYAPHONG, R., ZHANG, S., SAIVIROONPORN, P., VIPRAKASIT, V., TANAPIBUNPON, P., KOMOLTRI, C. & WANGWORATRAKUL, W. 2017. Detection of cardiac iron overload with native magnetic resonance T1 and T2 mapping in patients with thalassemia. *Int J Cardiol,* 248**,** 421-426.

KUBLER, J., BURGSTAHLER, C., BRENDEL, J. M., GASSENMAIER, S., HAGEN, F., KLINGEL, K., OLTHOF, S. C., BLUME, K., WOLFARTH, B., MUELLER, K. A. L., GREULICH, S. & KRUMM, P. 2021. Cardiac MRI findings to differentiate athlete's heart from hypertrophic (HCM), arrhythmogenic right ventricular (ARVC) and dilated (DCM) cardiomyopathy. *Int J Cardiovasc Imaging,* 37**,** 2501-2515.

KURT, M., WANG, J., TORRE-AMIONE, G. & NAGUEH, S. F. 2009. Left atrial function in diastolic heart failure. *Circ Cardiovasc Imaging,* 2**,** 10-5.

KURUVILLA, S., JANARDHANAN, R., ANTKOWIAK, P., KEELEY, E. C., ADENAW, N., BROOKS, J., EPSTEIN, F. H., KRAMER, C. M. & SALERNO, M. 2015. Increased extracellular volume and altered mechanics are associated with LVH in hypertensive heart disease, not hypertension alone. *JACC Cardiovasc Imaging,* 8**,** 172-80.

LA GERCHE, A., BURNS, A. T., MOONEY, D. J., INDER, W. J., TAYLOR, A. J., BOGAERT, J., MACISAAC, A. I., HEIDBUCHEL, H. & PRIOR, D. L. 2012. Exercise-induced right ventricular dysfunction and structural remodelling in endurance athletes. *Eur Heart J,* 33**,** 998-1006.

LA GERCHE, A., JURCUT, R. & VOIGT, J. U. 2010. Right ventricular function by strain echocardiography. *Curr Opin Cardiol,* 25**,** 430-6.

LAM, H. V., GROTH, M., MIR, T., BANNAS, P., LUND, G. K., JAHNKE, C. M., WARNCKE, M., MAAS, K. J., ADAM, G., HERRMANN, J. & TAHIR, E. 2021. Impact of chest wall deformity on cardiac function by CMR and feature-tracking strain analysis in paediatric patients with Marfan syndrome. *Eur Radiol,* 31**,** 3973-3982.

LEE, H. J., LEE, H., KIM, S. M., PARK, J. B., KIM, E. K., CHANG, S. A., PARK, E., KIM, H. K., LEE, W., KIM, Y. J., LEE, S. C., PARK, S. W., SOHN, D. W., OH, J. K., PARK, S. J. & LEE, S. P. 2020. Diffuse Myocardial Fibrosis and Diastolic Function in Aortic Stenosis. *JACC Cardiovasc Imaging,* 13**,** 2561-2572.

LENG, S., TAN, R. S., ZHAO, X., ALLEN, J. C., KOH, A. S. & ZHONG, L. 2018. Validation of a rapid semi-automated method to assess left atrial longitudinal phasic strains on cine cardiovascular magnetic resonance imaging. *J Cardiovasc Magn Reson,* 20**,** 71.

LOOK, D. C. & LOCKER, D. R. 1970. Time Saving in Measurement of NMR and EPR Relaxation Times. *Review of Scientific Instruments,* 41**,** 250-251.

MAESTRINI, V., CHEANG, M. H., KOTWINSKI, P., ROSMINI, S., LLOYD, G., KELLMAN, P., PENNELL, D. J., MONTGOMERY, H., MOON, J. C. &

MANISTY, C. 2017. Late Anthracycline-Related Cardiotoxicity in Low-Risk Breast Cancer Patients. *J Am Coll Cardiol,* 69**,** 2573-2575.
MANGION, K., MCCOMB, C., AUGER, D. A., EPSTEIN, F. H. & BERRY, C. 2017. Magnetic Resonance Imaging of Myocardial Strain After Acute ST-Segment-Elevation Myocardial Infarction: A Systematic Review. *Circ Cardiovasc Imaging,* 10.
MARET, E., TODT, T., BRUDIN, L., NYLANDER, E., SWAHN, E., OHLSSON, J. L. & ENGVALL, J. E. 2009. Functional measurements based on feature tracking of cine magnetic resonance images identify left ventricular segments with myocardial scar. *Cardiovasc Ultrasound,* 7**,** 53.
MARKL, M. & LEUPOLD, J. 2012. Gradient echo imaging. *J Magn Reson Imaging,* 35**,** 1274-89.
MARON, B. J., DOERER, J. J., HAAS, T. S., TIERNEY, D. M. & MUELLER, F. O. 2009. Sudden deaths in young competitive athletes: analysis of 1866 deaths in the United States, 1980-2006. *Circulation,* 119**,** 1085-92.
MEINARDI, M. T., GIETEMA, J. A., VAN DER GRAAF, W. T., VAN VELDHUISEN, D. J., RUNNE, M. A., SLUITER, W. J., DE VRIES, E. G., WILLEMSE, P. B., MULDER, N. H., VAN DEN BERG, M. P., KOOPS, H. S. & SLEIJFER, D. T. 2000. Cardiovascular morbidity in long-term survivors of metastatic testicular cancer. *J Clin Oncol,* 18**,** 1725-32.
MESSROGHLI, D. R., MOON, J. C., FERREIRA, V. M., GROSSE-WORTMANN, L., HE, T., KELLMAN, P., MASCHERBAUER, J., NEZAFAT, R., SALERNO, M., SCHELBERT, E. B., TAYLOR, A. J., THOMPSON, R., UGANDER, M., VAN HEESWIJK, R. B. & FRIEDRICH, M. G. 2017. Clinical recommendations for cardiovascular magnetic resonance mapping of T1, T2, T2* and extracellular volume: A consensus statement by the Society for Cardiovascular Magnetic Resonance (SCMR) endorsed by the European Association for Cardiovascular Imaging (EACVI). *J Cardiovasc Magn Reson,* 19**,** 75.
MESSROGHLI, D. R., RADJENOVIC, A., KOZERKE, S., HIGGINS, D. M., SIVANANTHAN, M. U. & RIDGWAY, J. P. 2004. Modified Look-Locker inversion recovery (MOLLI) for high-resolution T1 mapping of the heart. *Magn Reson Med,* 52**,** 141-6.
MODI, K., JOPPA, S., CHEN, K. A., ATHWAL, P. S. S., OKASHA, O., VELANGI, P. S., HOOKS, M., NIJJAR, P. S., BLAES, A. H. & SHENOY, C. 2021. Myocardial damage assessed by late gadolinium enhancement on cardiovascular magnetic resonance imaging in cancer patients treated with anthracyclines and/or trastuzumab. *Eur Heart J Cardiovasc Imaging,* 22**,** 427-434.
MOON, J. C., MESSROGHLI, D. R., KELLMAN, P., PIECHNIK, S. K., ROBSON, M. D., UGANDER, M., GATEHOUSE, P. D., ARAI, A. E., FRIEDRICH, M. G., NEUBAUER, S., SCHULZ-MENGER, J., SCHELBERT, E. B., SOCIETY FOR CARDIOVASCULAR MAGNETIC RESONANCE, I. & CARDIOVASCULAR MAGNETIC RESONANCE WORKING GROUP OF THE EUROPEAN SOCIETY OF, C. 2013. Myocardial T1 mapping and extracellular volume quantification: a Society for Cardiovascular Magnetic Resonance (SCMR) and CMR Working Group of the European Society of Cardiology consensus statement. *J Cardiovasc Magn Reson,* 15**,** 92.
MORGANROTH, J., MARON, B. J., HENRY, W. L. & EPSTEIN, S. E. 1975. Comparative left ventricular dimensions in trained athletes. *Ann Intern Med,* 82**,** 521-4.
MUEHLBERG, F., FUNK, S., ZANGE, L., VON KNOBELSDORFF-BRENKENHOFF, F., BLASZCZYK, E., SCHULZ, A., GHANI, S., REICHARDT, A., REICHARDT,

P. & SCHULZ-MENGER, J. 2018. Native myocardial T1 time can predict development of subsequent anthracycline-induced cardiomyopathy. *ESC Heart Fail,* 5**,** 620-629.
MURBRAECH, K., SOLHEIM, O., AULIE, H. M., FOSSA, S. D. & AAKHUS, S. 2015. The impact of cisplatinum-based chemotherapy on ventricular function and cardiovascular risk factors in female survivors after malignant germ cell cancer. *ESC Heart Fail,* 2**,** 142-149.
NEILAN, T. G., JANUZZI, J. L., LEE-LEWANDROWSKI, E., TON-NU, T. T., YOERGER, D. M., JASSAL, D. S., LEWANDROWSKI, K. B., SIEGEL, A. J., MARSHALL, J. E., DOUGLAS, P. S., LAWLOR, D., PICARD, M. H. & WOOD, M. J. 2006. Myocardial injury and ventricular dysfunction related to training levels among nonelite participants in the Boston marathon. *Circulation,* 114**,** 2325-33.
NUVER, J., DE HAAS, E. C., VAN ZWEEDEN, M., GIETEMA, J. A. & MEIJER, C. 2010. Vascular damage in testicular cancer patients: a study on endothelial activation by bleomycin and cisplatin in vitro. *Oncol Rep,* 23**,** 247-53.
O'BRIEN, A. T., GIL, K. E., VARGHESE, J., SIMONETTI, O. P. & ZAREBA, K. M. 2022. T2 mapping in myocardial disease: a comprehensive review. *J Cardiovasc Magn Reson,* 24**,** 33.
OMERSA, D., CUFER, T., MARCUN, R. & LAINSCAK, M. 2017. Echocardiography and cardiac biomarkers in patients with non-small cell lung cancer treated with platinum-based chemotherapy. *Radiol Oncol,* 51**,** 15-22.
OUN, R., MOUSSA, Y. E. & WHEATE, N. J. 2018. The side effects of platinum-based chemotherapy drugs: a review for chemists. *Dalton Trans,* 47**,** 6645-6653.
OXBOROUGH, D., WHYTE, G., WILSON, M., O'HANLON, R., BIRCH, K., SHAVE, R., SMITH, G., GODFREY, R., PRASAD, S. & GEORGE, K. 2010. A depression in left ventricular diastolic filling following prolonged strenuous exercise is associated with changes in left atrial mechanics. *J Am Soc Echocardiogr,* 23**,** 968-76.
PASCHAL, C. B. & MORRIS, H. D. 2004. K-space in the clinic. *J Magn Reson Imaging,* 19**,** 145-59.
PICHLER, G., REDON, J., MARTINEZ, F., SOLAZ, E., CALAFORRA, O., ANDRES, M. S., LOPEZ, B., DIEZ, J., OBERBAUER, R., ADLBRECHT, C., KARTH, G. D. & MACEIRA, A. 2020. Cardiac magnetic resonance-derived fibrosis, strain and molecular biomarkers of fibrosis in hypertensive heart disease. *J Hypertens,* 38**,** 2036-2042.
POOLEY, R. A. 2005. AAPM/RSNA physics tutorial for residents: fundamental physics of MR imaging. *Radiographics,* 25**,** 1087-99.
PYKETT, I. L., NEWHOUSE, J. H., BUONANNO, F. S., BRADY, T. J., GOLDMAN, M. R., KISTLER, J. P. & POHOST, G. M. 1982. Principles of nuclear magnetic resonance imaging. *Radiology,* 143**,** 157-68.
RADENKOVIC, D., WEINGARTNER, S., RICKETTS, L., MOON, J. C. & CAPTUR, G. 2017. T1 mapping in cardiac MRI. *Heart Fail Rev,* 22**,** 415-430.
RADUNSKI, U. K., LUND, G. K., SARING, D., BOHNEN, S., STEHNING, C., SCHNACKENBURG, B., AVANESOV, M., TAHIR, E., ADAM, G., BLANKENBERG, S. & MUELLERLEILE, K. 2017. T1 and T2 mapping cardiovascular magnetic resonance imaging techniques reveal unapparent myocardial injury in patients with myocarditis. *Clin Res Cardiol,* 106**,** 10-17.
RIDGWAY, J. P. 2010. Cardiovascular magnetic resonance physics for clinicians: part I. *J Cardiovasc Magn Reson,* 12**,** 71.

RODRIGUES, J. C., AMADU, A. M., GHOSH DASTIDAR, A., MCINTYRE, B., SZANTHO, G. V., LYEN, S., GODSAVE, C., RATCLIFFE, L. E., BURCHELL, A. E., HART, E. C., HAMILTON, M. C., NIGHTINGALE, A. K., PATON, J. F., MANGHAT, N. E. & BUCCIARELLI-DUCCI, C. 2017. ECG strain pattern in hypertension is associated with myocardial cellular expansion and diffuse interstitial fibrosis: a multi-parametric cardiac magnetic resonance study. *Eur Heart J Cardiovasc Imaging,* 18**,** 441-450.

ROMANO, S., DELL'ATTI, D., JUDD, R. M., KIM, R. J., WEINSAFT, J. W., KIM, J., HEITNER, J. F., HAHN, R. T. & FARZANEH-FAR, A. 2021. Prognostic Value of Feature-Tracking Right Ventricular Longitudinal Strain in Severe Functional Tricuspid Regurgitation: A Multicenter Study. *JACC Cardiovasc Imaging,* 14**,** 1561-1568.

ROTH, G. A., MENSAH, G. A., JOHNSON, C. O., ADDOLORATO, G., AMMIRATI, E., BADDOUR, L. M., BARENGO, N. C., BEATON, A. Z., BENJAMIN, E. J., BENZIGER, C. P., BONNY, A., BRAUER, M., BRODMANN, M., CAHILL, T. J., CARAPETIS, J., CATAPANO, A. L., CHUGH, S. S., COOPER, L. T., CORESH, J., CRIQUI, M., DECLEENE, N., EAGLE, K. A., EMMONS-BELL, S., FEIGIN, V. L., FERNANDEZ-SOLA, J., FOWKES, G., GAKIDOU, E., GRUNDY, S. M., HE, F. J., HOWARD, G., HU, F., INKER, L., KARTHIKEYAN, G., KASSEBAUM, N., KOROSHETZ, W., LAVIE, C., LLOYD-JONES, D., LU, H. S., MIRIJELLO, A., TEMESGEN, A. M., MOKDAD, A., MORAN, A. E., MUNTNER, P., NARULA, J., NEAL, B., NTSEKHE, M., MORAES DE OLIVEIRA, G., OTTO, C., OWOLABI, M., PRATT, M., RAJAGOPALAN, S., REITSMA, M., RIBEIRO, A. L. P., RIGOTTI, N., RODGERS, A., SABLE, C., SHAKIL, S., SLIWA-HAHNLE, K., STARK, B., SUNDSTROM, J., TIMPEL, P., TLEYJEH, I. M., VALGIMIGLI, M., VOS, T., WHELTON, P. K., YACOUB, M., ZUHLKE, L., MURRAY, C., FUSTER, V. & GROUP, G.-N.-J. G. B. O. C. D. W. 2020. Global Burden of Cardiovascular Diseases and Risk Factors, 1990-2019: Update From the GBD 2019 Study. *J Am Coll Cardiol,* 76**,** 2982-3021.

ROUJOL, S., WEINGÄRTNER, S., FOPPA, M., CHOW, K., KAWAJI, K., NGO, L. H., KELLMAN, P., MANNING, W. J., THOMPSON, R. B. & NEZAFAT, R. 2014. Accuracy, precision, and reproducibility of four T1 mapping sequences: a head-to-head comparison of MOLLI, ShMOLLI, SASHA, and SAPPHIRE. *Radiology,* 272**,** 683-9.

ROY, C., SLIMANI, A., DE MEESTER, C., AMZULESCU, M., PASQUET, A., VANCRAEYNEST, D., VANOVERSCHELDE, J. L., POULEUR, A. C. & GERBER, B. L. 2017. Age and sex corrected normal reference values of T1, T2 T2* and ECV in healthy subjects at 3T CMR. *J Cardiovasc Magn Reson,* 19**,** 72.

SACHDEV, V., SHIZUKUDA, Y., BRENNEMAN, C. L., BIRDSALL, C. W., WACLAWIW, M. A., ARAI, A. E., MOHIDDIN, S. A., TRIPODI, D., FANANAPAZIR, L. & PLEHN, J. F. 2005. Left atrial volumetric remodeling is predictive of functional capacity in nonobstructive hypertrophic cardiomyopathy. *Am Heart J,* 149**,** 730-6.

SADLER, D. B., AURIGEMMA, G. P., WILLIAMS, D. W., REDA, D. J., MATERSON, B. J. & GOTTDIENER, J. S. 1997. Systolic function in hypertensive men with concentric remodeling. *Hypertension,* 30**,** 777-81.

SADO, D. M., WHITE, S. K., PIECHNIK, S. K., BANYPERSAD, S. M., TREIBEL, T., CAPTUR, G., FONTANA, M., MAESTRINI, V., FLETT, A. S., ROBSON, M. D., LACHMANN, R. H., MURPHY, E., MEHTA, A., HUGHES, D., NEUBAUER, S., ELLIOTT, P. M. & MOON, J. C. 2013. Identification and assessment of

Anderson-Fabry disease by cardiovascular magnetic resonance noncontrast myocardial T1 mapping. *Circ Cardiovasc Imaging,* 6**,** 392-8.
SALERNO, M., SHARIF, B., ARHEDEN, H., KUMAR, A., AXEL, L., LI, D. & NEUBAUER, S. 2017. Recent Advances in Cardiovascular Magnetic Resonance: Techniques and Applications. *Circ Cardiovasc Imaging,* 10.
SANTORO, A., ALVINO, F., ANTONELLI, G., MOLLE, R. & MONDILLO, S. 2016. Left atrial strain after maximal exercise in competitive waterpolo players. *Int J Cardiovasc Imaging,* 32**,** 399-405.
SANZ-DE LA GARZA, M., GRAZIOLI, G., BIJNENS, B. H., SARVARI, S. I., GUASCH, E., PAJUELO, C., BROTONS, D., SUBIRATS, E., BRUGADA, R., ROCA, E. & SITGES, M. 2016. Acute, Exercise Dose-Dependent Impairment in Atrial Performance During an Endurance Race: 2D Ultrasound Speckle-Tracking Strain Analysis. *JACC Cardiovasc Imaging,* 9**,** 1380-1388.
SCHARF, M., BREM, M. H., WILHELM, M., SCHOEPF, U. J., UDER, M. & LELL, M. M. 2010. Atrial and ventricular functional and structural adaptations of the heart in elite triathletes assessed with cardiac MR imaging. *Radiology,* 257**,** 71-9.
SCHEFFLER, K. & LEHNHARDT, S. 2003. Principles and applications of balanced SSFP techniques. *Eur Radiol,* 13**,** 2409-18.
SCOTT, A. D., KEEGAN, J. & FIRMIN, D. N. 2009. Motion in cardiovascular MR imaging. *Radiology,* 250**,** 331-51.
SMITH, B. M., DORFMAN, A. L., YU, S., RUSSELL, M. W., AGARWAL, P. P., GHADIMI MAHANI, M. & LU, J. C. 2014. Relation of strain by feature tracking and clinical outcome in children, adolescents, and young adults with hypertrophic cardiomyopathy. *Am J Cardiol,* 114**,** 1275-80.
SPRINKART, A. M., LUETKENS, J. A., TRABER, F., DOERNER, J., GIESEKE, J., SCHNACKENBURG, B., SCHMITZ, G., THOMAS, D., HOMSI, R., BLOCK, W., SCHILD, H. & NAEHLE, C. P. 2015. Gradient Spin Echo (GraSE) imaging for fast myocardial T2 mapping. *J Cardiovasc Magn Reson,* 17**,** 12.
STEWART, G. M., CHAN, J., YAMADA, A., KAVANAGH, J. J., HASELER, L. J., SHIINO, K. & SABAPATHY, S. 2017. Impact of high-intensity endurance exercise on regional left and right ventricular myocardial mechanics. *Eur Heart J Cardiovasc Imaging,* 18**,** 688-696.
STEWART, G. M., YAMADA, A., HASELER, L. J., KAVANAGH, J. J., CHAN, J., KOERBIN, G., WOOD, C. & SABAPATHY, S. 2016. Influence of exercise intensity and duration on functional and biochemical perturbations in the human heart. *J Physiol,* 594**,** 3031-44.
SZABO, D., NAGY, D., MELCZER, C., ACS, P., RATGEBER, L., SZOKODI, I., TOTH, M., CZIRAKI, A., EKLICS, K. & SARSZEGI, Z. 2021. Influencing Factors of Cardiac Adaptation in Adolescent Athletes. *Int J Sports Med,* 42**,** 1209-1221.
TAHIR, E., SCHERZ, B., STAREKOVA, J., MUELLERLEILE, K., FISCHER, R., SCHOENNAGEL, B., WARNCKE, M., STEHNING, C., CAVUS, E., BOHNEN, S., RADUNSKI, U. K., BLANKENBERG, S., SIMON, P., PRESSLER, A., ADAM, G., PATTEN, M. & LUND, G. K. 2020. Acute impact of an endurance race on cardiac function and biomarkers of myocardial injury in triathletes with and without myocardial fibrosis. *Eur J Prev Cardiol,* 27**,** 94-104.
TAHIR, E., SINN, M., BOHNEN, S., AVANESOV, M., SARING, D., STEHNING, C., SCHNACKENBURG, B., EULENBURG, C., WIEN, J., RADUNSKI, U. K., BLANKENBERG, S., ADAM, G., HIGGINS, C. B., SAEED, M., MUELLERLEILE, K. & LUND, G. K. 2017. Acute versus Chronic Myocardial Infarction: Diagnostic Accuracy of Quantitative Native T1 and T2 Mapping

versus Assessment of Edema on Standard T2-weighted Cardiovascular MR Images for Differentiation. *Radiology,* 285**,** 83-91.

TAHIR, E., STAREKOVA, J., MUELLERLEILE, K., FREIWALD, E., VON STRITZKY, A., MUNCH, J., AVANESOV, M., WEINRICH, J. M., STEHNING, C., CAVUS, E., BOHNEN, S., RADUNSKI, U. K., BLANKENBERG, S., ADAM, G., SIMON, P., PRESSLER, A., PATTEN, M. & LUND, G. K. 2019. Impact of Myocardial Fibrosis on Left Ventricular Function Evaluated by Feature-Tracking Myocardial Strain Cardiac Magnetic Resonance in Competitive Male Triathletes With Normal Ejection Fraction. *Circ J,* 83**,** 1553-1562.

TAHIR, E., STAREKOVA, J., MUELLERLEILE, K., VON STRITZKY, A., MUNCH, J., AVANESOV, M., WEINRICH, J. M., STEHNING, C., BOHNEN, S., RADUNSKI, U. K., FREIWALD, E., BLANKENBERG, S., ADAM, G., PRESSLER, A., PATTEN, M. & LUND, G. K. 2018. Myocardial Fibrosis in Competitive Triathletes Detected by Contrast-Enhanced CMR Correlates With Exercise-Induced Hypertension and Competition History. *JACC Cardiovasc Imaging,* 11**,** 1260-1270.

TAYLOR, A. J., SALERNO, M., DHARMAKUMAR, R. & JEROSCH-HEROLD, M. 2016. T1 Mapping: Basic Techniques and Clinical Applications. *JACC Cardiovasc Imaging,* 9**,** 67-81.

TAYLOR, R. J., MOODY, W. E., UMAR, F., EDWARDS, N. C., TAYLOR, T. J., STEGEMANN, B., TOWNEND, J. N., HOR, K. N., STEEDS, R. P., MAZUR, W. & LEYVA, F. 2015. Myocardial strain measurement with feature-tracking cardiovascular magnetic resonance: normal values. *Eur Heart J Cardiovasc Imaging,* 16**,** 871-81.

TESKE, A. J., PRAKKEN, N. H., DE BOECK, B. W., VELTHUIS, B. K., DOEVENDANS, P. A. & CRAMER, M. J. 2009. Effect of long term and intensive endurance training in athletes on the age related decline in left and right ventricular diastolic function as assessed by Doppler echocardiography. *Am J Cardiol,* 104**,** 1145-51.

THAVENDIRANATHAN, P., WALLS, M., GIRI, S., VERHAERT, D., RAJAGOPALAN, S., MOORE, S., SIMONETTI, O. P. & RAMAN, S. V. 2012. Improved detection of myocardial involvement in acute inflammatory cardiomyopathies using T2 mapping. *Circ Cardiovasc Imaging,* 5**,** 102-10.

VAN DE SCHOOR, F. R., AENGEVAEREN, V. L., HOPMAN, M. T., OXBOROUGH, D. L., GEORGE, K. P., THOMPSON, P. D. & EIJSVOGELS, T. M. 2016. Myocardial Fibrosis in Athletes. *Mayo Clin Proc,* 91**,** 1617-1631.

VAN DEN BELT-DUSEBOUT, A. W., DE WIT, R., GIETEMA, J. A., HORENBLAS, S., LOUWMAN, M. W., RIBOT, J. G., HOEKSTRA, H. J., OUWENS, G. M., ALEMAN, B. M. & VAN LEEUWEN, F. E. 2007. Treatment-specific risks of second malignancies and cardiovascular disease in 5-year survivors of testicular cancer. *J Clin Oncol,* 25**,** 4370-8.

VAN GEUNS, R. J., WIELOPOLSKI, P. A., DE BRUIN, H. G., RENSING, B. J., VAN OOIJEN, P. M., HULSHOFF, M., OUDKERK, M. & DE FEYTER, P. J. 1999. Basic principles of magnetic resonance imaging. *Prog Cardiovasc Dis,* 42**,** 149-56.

VAN SCHINKEL, L. D., WILLEMSE, P. M., VAN DER MEER, R. W., BURGGRAAF, J., VAN ELDEREN, S. G., SMIT, J. W., DE ROOS, A., OSANTO, S. & LAMB, H. J. 2013. Chemotherapy for testicular cancer induces acute alterations in diastolic heart function. *Br J Cancer,* 109**,** 891-6.

VITIELLO, D., CASSIRAME, J., MENETRIER, A., RUPP, T., SCHUSTER, I., REBOUL, C., OBERT, P., TORDI, N. & NOTTIN, S. 2013. Depressed systolic

function after a prolonged and strenuous exercise. *Med Sci Sports Exerc,* 45**,** 2072-9.

WANG, J., KHOURY, D. S., YUE, Y., TORRE-AMIONE, G. & NAGUEH, S. F. 2008. Preserved left ventricular twist and circumferential deformation, but depressed longitudinal and radial deformation in patients with diastolic heart failure. *Eur Heart J,* 29**,** 1283-9.

WANG, S., HU, H., LU, M., SIRAJUDDIN, A., LI, J., AN, J., CHEN, X., YIN, G., LAN, T., DAI, L., ZHANG, Y., YIN, X., SONG, L., DANG, A., KELLMAN, P., ARAI, A. E. & ZHAO, S. 2017. Myocardial extracellular volume fraction quantified by cardiovascular magnetic resonance is increased in hypertension and associated with left ventricular remodeling. *Eur Radiol,* 27**,** 4620-4630.

WATERHOUSE, D. F., ISMAIL, T. F., PRASAD, S. K., WILSON, M. G. & O'HANLON, R. 2012. Imaging focal and interstitial fibrosis with cardiovascular magnetic resonance in athletes with left ventricular hypertrophy: implications for sporting participation. *Br J Sports Med,* 46 Suppl 1**,** i69-77.

WATERTON, J. C., JENKINS, J. P., ZHU, X. P., LOVE, H. G., ISHERWOOD, I. & ROWLANDS, D. J. 1985. Magnetic resonance (MR) cine imaging of the human heart. *Br J Radiol,* 58**,** 711-6.

WILLIAMS, B., MANCIA, G., SPIERING, W., AGABITI ROSEI, E., AZIZI, M., BURNIER, M., CLEMENT, D. L., COCA, A., DE SIMONE, G., DOMINICZAK, A., KAHAN, T., MAHFOUD, F., REDON, J., RUILOPE, L., ZANCHETTI, A., KERINS, M., KJELDSEN, S. E., KREUTZ, R., LAURENT, S., LIP, G. Y. H., MCMANUS, R., NARKIEWICZ, K., RUSCHITZKA, F., SCHMIEDER, R. E., SHLYAKHTO, E., TSIOUFIS, C., ABOYANS, V., DESORMAIS, I. & GROUP, E. S. C. S. D. 2018. 2018 ESC/ESH Guidelines for the management of arterial hypertension. *Eur Heart J,* 39**,** 3021-3104.

WILSON, M., O'HANLON, R., PRASAD, S., DEIGHAN, A., MACMILLAN, P., OXBOROUGH, D., GODFREY, R., SMITH, G., MACEIRA, A., SHARMA, S., GEORGE, K. & WHYTE, G. 2011a. Diverse patterns of myocardial fibrosis in lifelong, veteran endurance athletes. *J Appl Physiol (1985),* 110**,** 1622-6.

WILSON, M., O'HANLON, R., PRASAD, S., OXBOROUGH, D., GODFREY, R., ALPENDURADA, F., SMITH, G., WONG, J., BASAVARAJAIAH, S., SHARMA, S., NEVILL, A., GAZE, D., GEORGE, K. & WHYTE, G. 2011b. Biological markers of cardiac damage are not related to measures of cardiac systolic and diastolic function using cardiovascular magnetic resonance and echocardiography after an acute bout of prolonged endurance exercise. *Br J Sports Med,* 45**,** 780-4.

YOUNG, A. A., IMAI, H., CHANG, C. N. & AXEL, L. 1994. Two-dimensional left ventricular deformation during systole using magnetic resonance imaging with spatial modulation of magnetization. *Circulation,* 89**,** 740-52.

11 Acknowledgements

I would like to take this chance to express my deep appreciation to all those who supported me all along the way. Without your encouragement and help, I would not have been able to accomplish this challenge.

First, I am deeply grateful to Prof. Dr. Gerhard Adam for giving me the opportunity to conduct my doctoral research at the Department of Diagnostic and Interventional Radiology and Nuclear Medicine. Thank you indeed for providing me with the necessary resources and infrastructure for research. Thanks for providing me with financial support to attend academic conferences.

In particular, I would like to express my sincere appreciation to my supervisor, PD Dr. Enver Tahir, for your patient guidance and unwavering support throughout my entire doctoral journey. Your expertise has been instrumental in shaping my scientific thinking and questions in many research projects. I am also grateful for you providing constructive feedback and suggestions in my academic writing and each presentation. Thanks for creating every opportunity for me to attend academic conferences. These unforgettable experiences have been helping me to network with other scholars, and gain exposure to frontier research ideas and imaging techniques. Thanks for your unselfish help in my life in Hamburg, renting apartment, extending visa, etc. It must be a precious memory that I will never forget.

I feel incredibly fortunate to have the opportunity to work alongside such talented colleagues who have shared many scientific moments with me. I would like to extend my sincere gratitude to all co-authors for your contributions to my publications.

I would like to express my heartfelt appreciation to the China Scholarship Council for offering me with the financial support. This allows me to focus on my research without worrying about financial burdens, and gives me the opportunity to broaden my horizons.

Love stays oceans apart, oceans an easy reach. To my family and friends, thanks for your unwavering support and encouragement. Despite being separated by thousands

of miles, I can still feel the endless love and care from my brother and aunt. Thanks to my boyfriend's company, which makes my journey more brilliant.

Finally, I dedicate this thesis to the memory of my beloved mother. Your love has been a constant source of my motivation and persistence, and I am forever thankful for the time we had together.

12 Curriculum Vitae

Personal Information

Name: Hang Chen

Gender: Female

Date and Place of Birth: March 31, 1994 in Sichuan, China

Nationality: Chinese

Email address: hang.chen@stud.uke.uni-hamburg.de; hang.chen331@gmail.com

Education

10/2020 - present	University Hospital Hamburg Eppendorf, Hamburg, Germany • Ph.D. student
10/2017 - 06/2020	Chongqing Medical University, Chongqing, China • Master of Medicine
09/2012 - 07/2017	Chongqing Medical University, Chongqing, China • Bachelor of Medicine

Research Experience

10/2020 - present	Study on "Assessment of cardiac impairment in long-term survivors of testicular cancer following platinum-based chemotherapy by CMR imaging"
08/2022 - 02/2023	Study on "Predictive performance of CMR parameters for left ventricular adverse remodeling after AMI"
07/2022 - 12/2022	Study on "Left ventricular myocardial strain in patients with resistant hypertension evaluated by FT-CMR"
11/2021 - 06/2022	Study on "Left ventricular diastolic filling patterns in competitive triathletes by CMR time-volume analysis"
10/2020 - 10/2021	Study on "Acute impact of an endurance race on myocardial strain in triathletes by FT-CMR"

Publications

1. **Chen H**, Brunner FJ, Özden C, et al. Left ventricular myocardial strain responding to chronic pressure overload in patients with resistant hypertension evaluated by feature-tracking CMR [published online ahead of print, 2023 Apr 10]. *Eur Radiol*.
2. **Chen H**, Warncke ML, Muellerleile K, et al. Acute impact of an endurance race on biventricular and biatrial myocardial strain in competitive male and female triathletes evaluated by feature-tracking CMR. *Eur Radiol.* 2022;32(5):3423-3435.
3. **Chen H**, Jungesblut J, Saering D, et al. Left ventricular diastolic filling patterns in competitive triathletes with and without myocardial fibrosis by cardiac magnetic resonance time-volume analysis [published online ahead of print, 2022 Nov 19]. *Eur J Radiol.* 2022;158:110615.
4. Erley J, Starekova J, Sinn M, Muellerleile K, **Chen H**, et al. Cardiac magnetic resonance feature tracking global and segmental strain in acute and chronic ST-elevation myocardial infarction. *Sci Rep.* 2022;12(1):22644.
5. **Chen H**, Zeng M, Wang X, et al. A CT-based radiomics nomogram for predicting prognosis of coronavirus disease 2019 (COVID-19) radiomics nomogram predicting COVID-19. *Br J Radiol.* 2021;94(1117):20200634.
6. **Chen H**, Xiang B, Zeng J, Luo H, Yang Q. The feasibility in estimating pulmonary vascular resistance by cardiovascular magnetic resonance in pulmonary hypertension: A systematic review and meta-analysis. *Eur J Radiol*. 2019;114:137-145.
7. **Chen H**, Zeng J, Liu D, Yang Q. Prognostic value of late gadolinium enhancement on CMR in patients with severe aortic valve disease: a systematic review and meta-analysis. *Clin Radiol.* 2018;73(11):983.e7-983.e14.

13 Eidesstattliche Versicherung

Ich versichere ausdrücklich, dass ich die Arbeit selbständig und ohne fremde Hilfe verfasst, andere als die von mir angegebenen Quellen und Hilfsmittel nicht benutzt und die aus den benutzten Werken wörtlich oder inhaltlich entnommenen Stellen einzeln nach Ausgabe (Auflage und Jahr des Erscheinens), Band und Seite des benutzten Werkes kenntlich gemacht habe.
Ferner versichere ich, dass ich die Dissertation bisher nicht einem Fachvertreter an einer anderen Hochschule zur Überprüfung vorgelegt oder mich anderweitig um Zulassung zur Promotion beworben habe.
Ich erkläre mich einverstanden, dass meine Dissertation vom Dekanat der Medizinischen Fakultät mit einer gängigen Software zur Erkennung von Plagiaten überprüft werden kann.

Unterschrift: .....Hang Chen.....